UNIVERSIDADE DE LISBOA
FACULDADE DE CIÊNCIAS
DEPARTAMENTO DE BIOLOGIA ANIMAL

The role of Cadherin11 (Cdh11) in the establishment of laterality in the zebrafish

José Maria Lage de Sousa Leitão

Mestrado em Biologia Evolutiva e do Desenvolvimento

Dissertação orientada por:

Leonor Saúde
Solveig Thorsteinsdóttir

2018

Acknowledgements

Queria agradecer a todos os que me acompanharam ao longo deste ano pelo apoio e por todo o tipo ajuda que ofereceram. Desde aqueles que me motivaram com palavras de incentivo, até aos que acompanharam o avançar desta tese diariamente. Todos foram uma ajuda e espero ter a oportunidade de agradecer pessoalmente a cada um, mas é especialmente àqueles que estiveram lá todos os dias que gostava de agradecer aqui.

Tenho de agradecer acima de tudo e muito especialmente à **Leonor**. Obrigado por me ter recebido no estágio e depois para fazer a tese. Nunca poderia imaginar um ano tão bom como este. Já é um privilégio poder trabalhar num local onde posso aprender com investigadores de alto nível, e ao mesmo tempo ser tão bem recebido e com este ambiente fantástico. É um privilégio ainda maior ter uma chefe com estas mesmas qualidades. Obrigado por me levar a ser um melhor investigador, tanto pelo seu exemplo como pelas suas orientações e desculpe lá qualquer coisinha.

Muito obrigado à professora **Solveig** pela preocupação e atenção que teve comigo e com todos nós no mestrado. Obrigado por estar sempre disponível ao longo do primeiro ano para aturar com os nossos falhanços e desesperos, e por toda a ajuda neste ano. Obrigado à professora **Gabriela** por todo o entusiasmo e atenção ao longo destes anos, e pelas primeiras aulas de desenvolvimento no 3º ano, que me mostraram como o desenvolvimento é extraordinário. Obrigado ao professor **Élio** por sempre se preocupar com a exigência e qualidade do mestrado, nas suas aulas e nos testes. Agora olhando para trás vejo como isso foi importante.

Dalila, não sei o que posso escrever que seja suficiente para agradecer tudo o que fizeste por mim este ano. Obrigado por me ensinares praticamente tudo o que sei, pelas dicas e ajudas, e pelo teu trabalho incansável no ministério da propaganda. Tive a sorte enorme de ter um exemplo de uma grande cientista que pude seguir de perto todo este tempo. Obrigado pelas luzes e motivação nos momentos mais caóticos desta tese. Queria agradecer também muito especialmente a **Sara** porque sem ela este projecto não aconteceria, literalmente. Obrigado por estares sempre disponível para qualquer dúvida, mesmo quando já estavas a escrever a tua tese, e também pelo teu exemplo como investigadora.

Guida, obrigado por seres a mãe deste grupo, sempre preocupada com os teus filhos desorientados. Ajudaste-me em tantas coisas ao longo da tese que seria preciso um capítulo só para agradecer cada uma dessas coisas. Os nossos projectos no laboratório não seriam possíveis sem ti, não só pelo teu trabalho mas também pela alegria e atenção que tens com cada um. Boa sorte para o teu mestrado! Queria agradecer a **Fish Facility** e obviamente a quem a faz! À **Lara,** por todo o trabalho em tornar a facility de alta qualidade, e o cuidado com cada um de nós. Obrigado pelo ânimo quando as experiências encravavam, ou quando os peixes não estavam interessados no progresso científico. Obrigado **Aida** por trazeres um entusiasmo contagiante em todos os momentos, e pelas caixas de cruzamentos personalizadas. Obrigado também por te preocupares em ajudar o mais possível sempre que precisei. Queria agradecer às duas por irem além dos aspectos técnicos e se preocuparem a fundo com cada pessoa e pela união do grupo todo. Obrigado à **Isaura** por toda a alegria e entusiasmo no laboratório, e o bocadinho de loucura saudável nos tempos mais críticos. Obrigado pelo teu exemplo de alguém que verdadeiramente gosta de fazer ciência, por estares sempre disponível para ajudar e pelo teu relógio biológico apuradíssimo.

Obrigado à **Ana** e à **Rita** por toda a ajuda que me deram ao longo deste ano, sempre disponíveis para responder a dúvidas e grandes exemplo de investigadoras que pude acompanhar. Obrigado ao **Diogo** pela companhia e pela ajuda em equilibrar a balança para o lado masculino neste grupo. Força! Obrigado à **Mariana Ferreira,** pela caridade de me relembrar em todos os momentos que devia estar a trabalhar e à **Mariana Costa** pelo croissant (a vingança serve-se fresca). Queria gradecer ao **Domingos**, ao **João** e ao **Gonçalo** pela companhia neste ano, por me ajudarem seja com reagentes ou com dúvidas, e muito especialmente pelos bolos e queijos.

Queria agradecer à **Bioimaging**, **Flow**, **Histology Facilities** pela ajuda ao longo do projecto e por toda a atenção que recebi de cada um dos técnicos sempre que precisei.
Obrigado à **Susana Lopes** e todo ao seu grupo pela ajuda com protocolos, reagentes e dúvidas no geral. Obrigado à **Catarina Certal** e especialmente à **Joana Monteiro** por todo o trabalho com os gRNA, e pela ajuda técnica que ofereceram

Obrigado muito especialmente aos meus pais por me terem recebido como o seu primeiro projecto de desenvolvimento e por tudo, mesmo. Aos meus irmãos, à minha família e a todos os amigos que sempre se perguntaram sobre o que era exactamente a minha tese, "para que serve isso?", e "peixes fluorescentes? Fixe!". Para aqueles que ainda estão confusos, boas leituras.

Non nobis Domine

Resumo

O plano corporal aparentemente simétrico dos vertebrados esconde assimetrias no seu interior. O estabelecimento consiste em 4 momentos conservado nos vertebrados: começa com a quebra de simetria no organizador de Esquerda-Direita (ED), que é transmitida para Placa Lateral Mesodérmica (PLM). Aqui desencadeia a cascata de Nodal, restrita ao lado esquerdo deste tecido que finalmente informa a formação dos órgãos.
Neste trabalho identificámos uma molécula de adesão celular, a caderina11 (Cdh11) que aparentemente influencia o estabelecimento da ED no peixe zebra.
Através de ensaios de perda de função deste gene, usando Morpholinos (MO), observámos que a lateralidade do coração e do tracto digestivo se alteravam. No entanto, enquanto no tracto digestivo a simetria era invertida, a maior parte dos embriões afectados tinham o coração simétrico. Esta observação indica que há um desemparelhamento do estabelecimento da simetria na formação destes dois órgãos. Para além disso, após injecção com MO, a expressão dos dois genes da cascata de Nodal na PLM (spaw e pitx2), inverte-se e fica restrito ao lado direito da PLM. Consequentemente, a expressão anormal destes genes pode explicar a inversão do tracto digestivo mas não a simetria do coração.

A expressão de *cdh11* foi detectada na endoderme e na Mesoderme Intermédia (MI) nos estadios em que o sinal de ED passa do organizador, chamado Vesícula de Kupffer (VK) no peixe-zebra, para a PLM, entre os estadios de 8 e 12 somitos. Este resultado sugere que a Cadh11 pode estar envolvida na passagem do sinal da VK para PLM. Por um lado, no rato e no *Xenopus* a endoderme tem um papel nesta transmissão, e por outro lado podemos observar que a MI localiza-se entre a VK e a PLM.

A cdh11 também foi detectada nos Pronefros (PN), que deriva da MI, nos estadios em que o tracto digestivo adquire a sua torção., entre as 24 e 30 horas pós-fertilização (hpf). Nós observámos que a porção anterior dos PN coincide dorso-ventralmente com a região de migração da PLM que provoca a torção do tracto digestivo. Deste modo é possível que os PN sirvam como estrutura de suporte para esta migração.

Cdh11 também foi observado na PLM anterior ao estadio de 20 sómitos. Esta expressão coincide espacial e temporalmente com a migração dos percursores do coração.
Tendo em conta estes resultados, sugerimos que a Cdh11 tem um papel no desenvolvimento do coração e tracto digestivo. Quanto ao desenvolvimento do tracto digestivo, a Cdh11 nos PN pode ser importante para a estabilidade desta estrutura e consequentemente da migração assimétrica da PLM. Por outro lado, a Cdh11 na endoderme e na MI podem afectar a passagem do sinal assimétrico da VK para PLM. A Cdh11 pode estar presente nas junções comunicantes da endoderme atravessadas pela onda de cálcio que transporta a informação assimétrica para PLM, ou nas junções aderentes da IM quando o próprio Nodal passar da VK para a PLM. Quanto ao coração, a Cdh11 pode afectar a migração dos percursores do coração e consequentemente a formação deste órgão.

Como uma abordagem complementar analisámos um mutante para *cdh11* que no entanto não reproduziu os fenótipos obervados com o MO. Para entender melhor os efeitos da inactivação deste gene produzimos um novo mutante através da técnica de CRISPR-Cas9.

Palavras Chave: Cdh11, Esquerda-Direita, Placa Lateral Mesodérmica, Peixe zebra, Mutante

Abstract

Symmetric body plans in vertebrates hide asymmetrical organs on the inside. The establishment of this asymmetry is generally conserved in vertebrates. It starts in the Left-Right Organizer (LRO), is then translated to the left Lateral Plate Mesoderm (LPM) and ultimately informs organogenesis.

Using a morpholino (MO) loss-of-function approach for the cell adhesion molecule, Cadherin 11 (Cdh11), we observed that the establishment of LR in organogenesis was disrupted. However, while the majority of the affected embryos exhibited reversed laterality phenotypes in the gut, the predominant disorder of the heart was the absence of asymmetric looping. This is an indication of some kind of uncoupling of laterality between these organs. Additionally, in a high number of the *cdh11*^{MO} injected embryos the conserved LR genes (*spaw* and *pitx2*) were expressed on the right LPM instead of the left LPM. Thus, we proposed that the abnormal expression of the conserved LR genes in the right LPM might underlie the reversed gut loop phenotype but not of the heart.

Transcript of *cdh11* was found to be present in the Endoderm at 8-somite stage (ss), and in the Intermediate Mesoderm (IM) from 8ss to 12ss. These stages coincide with the transfer of the laterality signal from the zebrafish LRO, the Kupffer's Vesicle (KV) to the LPM. Recent findings in other model vertebrates suggested a model for this relay: the LR information might be transferred either by calcium waves going from the LRO to the LPM through gap junctions in the endoderm, or Nodal itself might cross the extracellular matrix towards the LPM, or a combination of both. This suggests that, in the zebrafish, Cdh11 could play a role in the relay of the LR signal. Calcium waves starting from the KV have been described. These might travel from the KV through gap junctions composed of Ca2+ sensitive Cdh11 molecules, in the endoderm towards the LPM. Alternatively, the Nodal protein (Spaw) might travel directly along the extracellular matrix, crossing the IM, which is located between the KV and the LPM.

cdh11 was also detected in the Pronephros (PN), an IM derivative, at the same stages when the looping of the gut occurs, between 24 and 30 hours-post-fertilization (hpf). We confirmed that the anterior portion of the PN coincides dorsoventrally with the gut looping region at the level of the third somite pair. This supports the hypothesis that the PN could affect the asymmetric migration of the LPM that is essential to promote the displacement of the gut.

Furthermore, *cdh11* was also detected at 20ss in the anterior LPM. This region is located anteriorly to the LPM asymmetric migration area, however, it coincides both spatially and temporally with the migrating heart primordia territory.

Taken together, these results suggest that Cdh11 might play a role in the LR development of both the gut and heart:

Gut - Cdh11 in the PN might be important for the stability of this structure, and consequently to the asymmetric migration of the LPM; Alternatively, Cdh11 might affect the transfer of the asymmetric signal from the KV to the LPM, between 8ss and 12ss, upstream of the Nodal cascade in the LPM. It participates either through the gap junctions in the endoderm relaying a calcium wave, or at the adherens junctions of the cells of the IM, affecting the passage of Spaw in the extracellular matrix. Absence of Cdh11 disrupts the Nodal cascade in the LPM and the asymmetric migration of this tissue over the gut endoderm that ultimately leads to the displacement of the gut.

Heart: At 20ss, in the anterior LPM, Cdh11 might affect the migration of the heart primordia and consequently the LR development of the heart.

As a complementary approach, we analysed a *cdh11* mutant, which, however, did not reproduce the phenotypes observed in the MO-injected embryos. This discrepancy raised questions about the specificity of our MO and the quality of the null *cdh11* mutant. To better understand the effect of a *cdh11* knockout, we produced a new *cdh11* mutant, resorting to the CRISPR-Cas9 genome editing system.

In this work, we have detected the expression of *cdh11* in tissues where it had not been observed before. This raised new hypotheses for the function of Cdh11 in the establishment of LR more in line with what has been described in other vertebrate models. Nevertheless, the specific mechanism of action of Cdh11 during the establishment is still not clear and needs further investigation.

Keywords: Cdh11, Left-Right, Lateral Plate Mesoderm, Zebrafish, Morpholino, Mutant

Abbreviations

AP – Anterior-Posterior;
DV – Dorsal-Ventral;
LR – Left-Right;
LRO – Left-Right Organizer;
KV – Kupffer's vesicle;
DFC – Dorsal Forerunner Cells;
hpf - hours post-fertilization;
TGF- β - transforming growth factor-β;
Spaw – Southpaw;
LPM - lateral plate mesoderm;
aPKC - atypical protein kinase C;
ZO-1 - zonula occludens 1;
IM - Intermediate Mesoderm;
PN – Pronephros;
i.e – That is;
Cdh – Cadherin;
EC – Extracellular Domain;
TM - Transmembrane Domain;
IC – Intracellular Domain;
Cdh2 – N-cadherin;
HH - Hamburger and Hamilton;
DM – Dorsal Mesentery;
Cdh11 – Cadherin-11;
WT – Wild Type;
EZRC - European Zebrafish Resource Center;
gDNA – genomic Deoxyribonucleic acid;
PK – Proteinase K;
RT – room temperature;
PCR – Polymerase Chain Reaction;
Fw – Forward;
Rv – Reverse;
MO - Morpholino oligonucleotides;
cdh11^{MO} - *cdh11 splice blocking MO;*
Control^{MO} - Standard Control MO;
DIG – Dioxigenin;
WISH - Whole mount *in situ* hybridization;
s – seconds;
h – hours;
Pre-Hybmix - pre-Hybridization Mix;
PBS - Phosphate-buffered saline;
PFA – Paraformaldehyde;
MetOH – Methanol;
BSA - Bovine Serum Albumin;
qPCR – quantitative PCR;
CRISPR - Clustered Regularly Interspaced Short Palindromic Repeat;
gRNA - single-guide RNA;
Cas9 - CRISPR associated protein 9;
NTR – Nitroreductase;
Mtz – Metronidazole.
gRNA – guide Ribonucleic acid

Index

Chapter 1 - Introduction

1.1 – Left Right Development

The external bilateral symmetry in vertebrates hides internal organ asymmetries. Organs such as the heart, liver, spleen, gall bladder, among others, are consistently asymmetrically distributed regarding the Left-Right (LR) body plan. This normal distribution of the internal organs is referred to as *situs solitus* and is largely conserved among a population of a given species (Grimes & Burdine, 2017).

Of all of the organs, the asymmetry of the digestive tract was probably the first to evolve. In all vertebrates, its length is greater than the main body axis and in all kinds of species we can observe the functional specialization of each module: mouth, oesophagus, stomach and gut. On the other hand, in evolutionary terms, a primitive heart was nothing more than a linear contractile muscle that facilitated the distribution of nutrients throughout the body (Blum et al., 2014). This morphology can be seen in the Drosophila. Additionally, the asymmetries of the lungs might reflect spatial constraints in the thorax resulting from asymmetric heart placement rather than a specific function (Blum et al., 2014).

For human individuals it is crucial to understand how consistent LR asymmetry is established in embryogenesis. These patients might face difficulties due to the lack of proper connections between the heart and the different organs. Disorders of the organization of the LR axis include the complete reversal of the internal organs *(situs inversus totalis)*, partial asymmetries (*situs inversus abdominalis* or *thoracalis*) and symmetry, leading to duplication or complete loss of single organs such as the spleen (isomerism) (Figure 1) (Vandenberg & Levin, 2013). *Situs inversus totalis* occurs in 1 of 20.000 cases in humans and is the only non-life-threatening condition (Vandenberg & Levin, 2013).

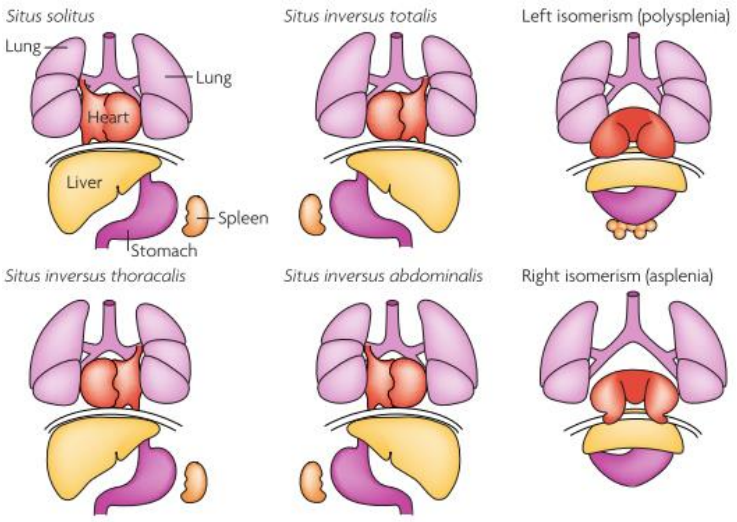

Figure 1 – **Human Laterality disorders** - Schematic illustration of normal left–right body asymmetry (*situs solitus*) and five laterality defects that affect the lungs, heart, liver, stomach and spleen. Taken from Fliegauf *et al*. 2007.

The mechanisms that direct the establishment of LR asymmetry are highly conserved across the different vertebrate model organisms (Blum et al., 2014). In zebrafish, the process of establishment of asymmetry throughout development can be divided in four phases: **1** - Breaking of symmetry; **2** - *Nodal* expression in the KV and transfer of the asymmetric signal to the left lateral plate mesoderm (LPM); **3** - Nodal Cascade in the LPM; **4** - Left-right asymmetric organ morphogenesis (Collins & Ryan, 2014; Hamada et al., 2002; Shiratori, 2006).

1.1.1 – Phase 1: Breaking of symmetry

The establishment of LR asymmetries results from a series of molecular and morphogenetic events. It has been shown that, before gastrulation, ion transporters that are asymmetrically distributed in the embryo, generate differences in pH and membrane voltage potential between the left and right sides (Kawakami et al., 2003). It is believed that this asymmetric membrane polarization promotes the accumulation of LR determinants, such as serotonin, through directional transport involving gap-junction channels (Fukumoto et al., 2005a; Fukumoto et al., 2005b). LR asymmetry is further established during early somite stages in the conserved ciliated organ of asymmetry, the LR organizer (LRO), known as the Kupffer's vesicle (KV) in zebrafish (Matsui et al., 2015).

The KV originates from a cluster of 20-30 cells, the dorsal forerunner cells (DFCs), which is maintained by cadherin- based adherens junctions (D'Amico & Cooper, 1997; Matsui et al., 2015; Oteiza et al., 2010). These cells are formed via a Nodal signalling-dependent ingression of surface enveloping layer cells from the dorsal blastoderm margin. The initial group migrates ahead of the dorsal margin and proliferates during epiboly stage. At the end of epiboly, by 10hpf, these cells undergo a mesenchymal- to-epithelial transition (MET) to form the KV in a vesicle-like structure with a mono-ciliated epithelium (Essner et al., 2005; Gokey et al., 2017; Oteiza et al., 2008). KV cells create a fluid filled lumen arising from the apical membrane that rapidly expands during early somite stages (G. Wang et al., 2011). At the same time, a single cilium forms and elongates from the apical surface of each KV cell to extend into the lumen (Oteiza et al., 2008; Smith et al., 2014; Wang et al., 2012) Directional ciliary beating in the LRO generates leftward flow of extraembryonic fluid which is essential to LR development. (Kramer-Zucker, 2005; Nonaka et al., 1998; Okabe et al., 2008). This directional fluid flow is induced by a combination of planar cell polarity (PCP) and rotational movement of cilia in the organizer (Shinohara & Hamada, 2017). In order for the KV to produce a robust fluid flow it requires a minimum of 30 motile cilia and an anterior-dorsal cluster of motile cilia (Sampaio et al., 2014; Smith et al., 2014). The number of motile cilia in the KV seems to be modulated by Notch signalling, through a mechanism that involves the activity of Her12 (hairy- related 12) (Sampaio et al., 2014; Tavares et al., 2017). Changes in the ratio of motile to immotile cilia mediated by Her12 impacts both the intensity of the flow and the distribution of cilia (Tavares et al., 2017).

Two alternative and nonexclusive theories have been proposed to explain how the LR flow is translated to asymmetric information:
1 – The chemosensing hypothesis states that asymmetric flow creates a LR concentration gradient of morphogens that is detected by receptors on the left side, triggering LR asymmetric gene expression; (Okada et al., 2005; Tanaka et al., 2005).
2 – The mechanosensing (or two-cilia) hypothesis states that cells of the KV can mechanically sense flow due to a particular type of non-motile sensory cilia, activating an asymmetric response on the periphery of the KV.(McGrath et al., 2003; Sampaio et al., 2014; Tabin & Vogan, 2003, Yoshiba et al., 2012).

A recent study has showed that in the mechanosensing mechanism the number of immotile cilia in the KV is insufficient, however, motile cilia could sense their own motion. Additionally they showed that a chemosensory mechanism could explain the observed robust LR asymmetry establishment, provided that the particle size is above the lower limit of about 2 nm (Ferreira et al., 2017)

The LR information of the flow has been shown to lead to the activation of cation channel PKD2 (Yoshiba et al., 2012). This in turn is necessary for the asymmetric release of calcium around the KV, which is initiated within the cilia (Yuan et al., 2015). This leads to an increase in cytoplasmic calcium at the left side of the KV (McGrath et al., 2003; Yoshiba et al., 2012; Yuan et al., 2015).

1.1.2 – Phase 2: *nodal* expression in the KV and transfer of the asymmetric signal to the left lateral plate mesoderm (LPM)

The Nodal related gene *spaw* is expressed bilaterally in the cells surrounding the KV at the 4ss to 6ss (Long et al., 2003). Dand5 (member of the Cerberus/Dan family) is a negative regulator of Nodal related genes. Dand5 binds to Spaw, a Nodal related gene, inhibiting its binding to receptors in adjacent region on the right side of the KV (Hashimoto et al., 2004). The expression of *dand5* in the KV is initially symmetric but by the 8ss it has become restricted to right-side. It has been shown that the transcription of *dand5* in zebrafish is sensitive to fluid flow, given that in the absence of flow in the KV its expression is no longer biased (Lopes et al., 2010). The LR information of the flow leads to the activation of cation channel PKD2 (Yoshiba et al., 2012). This activates an asymmetric calcium release, initiated within the cilia, which in turn leads to repression of Dand5 on the left side of the KV (Yoshiba et al., 2012; Yuan et al., 2015). How calcium affects Dand5 is, therefore, the next challenge to understand mechanisms of symmetry breakage driven by flow (Blum & Vick, 2015).

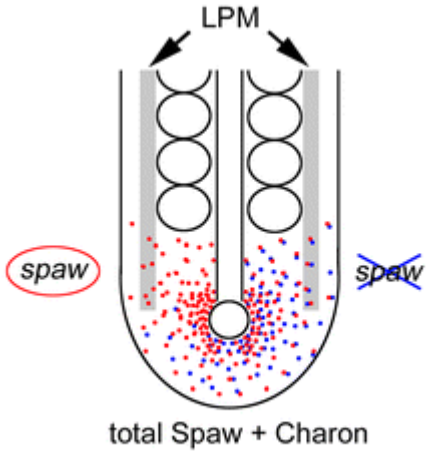

Figure 2 – Dand5 antagonism of Spaw – Dand5 antagonizes Spaw by attaching to it. Spaw signal reaches the left LPM after repression of Dand5 on this side. Taken from Matsui & Bessho 2012.

Consequently, due to the repression of Dand5, a left-sided *spaw* restricted signal starts from the KV towards the left LPM, becoming delimited to this tissue at the 10 to 12-somite stage (Figure 2). Here the Nodal Cascade is activated on the left but not on the right side. (Marques et al., 2004; Matsui & Bessho, 2012).

The mechanism of transfer of information from the LR organizer to the LPM in vertebrates is still relatively unknown but previous findings in mouse and frog development have raised two complementing hypotheses for this process (Grimes & Burdine, 2017; Norris, 2012; Saijoh et al., 2014). In mouse embryos, Ca2+ signals have been observed to spread laterally beyond the node and reaching as far as the LPM (McGrath et al., 2003). Previous experiments in *Xenopus* (Beyer et al., 2012) and mouse, (Saund et al., 2012; Viotti et al., 2012), have described that this Ca2+, or other signals, might travel intracellularly through endodermal cells, which are connected by gap junctions, towards the LPM. The expression of *spaw* would then be activated in the LPM by this Ca2+ signal (Figure 3) (Viotti et al., 2012; Saund et al., 2012; Beyer et al., 2012).

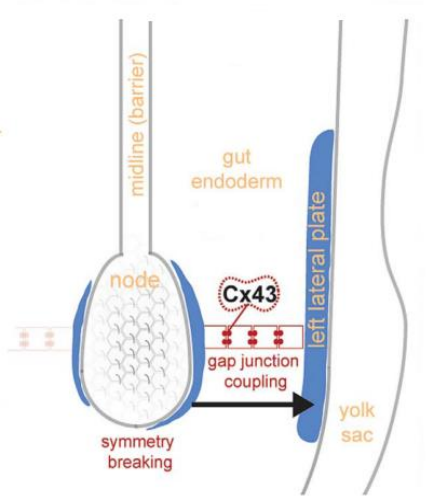

Figure 3- Model for the transfer of LR information in the mouse. After LR symmetry is broken in the node by rotating cilia, the resulting nodal flow induces left-biased asymmetries around the node. These asymmetries are transmitted via gap junctions comprised of Cx43 within the gut endoderm to the left LPM, where the Nodal cascade is activated. Adapted from Viotti 2012

Conversely, Nodal itself, which is produced in greater amounts at the left side of LROs, might directly travel to the LPM through the extracellular matrix, and activate its own expression (Figure 4). In mouse embryos, sulfated glycosaminoglycans (sGAGs) are located in the basement membrane between the endoderm and the mesoderm (Oki et al., 2007). In fact, Nodal expression at the LRO is required for Nodal activation in the LPM (Brennan et al., 2002; Saijoh et al., 2003) and Nodal is able to activate its own expression (Adachi et al., 1999; Norris & Robertson, 1999). However, this may not be the case in zebrafish since mutants lacking either expression of *spaw* in the KV, or *spaw* mutants themselves still express *spaw* in the LPM (Burdine et al., 2016; Noel et al., 2013). Some experiments have proposed that Dvr1/Gdf3 (a member of the TGFβ family) facilitates the transfer of the LR signal from KV to the LPM (Peterson et al., 2013). Knockdown of *gdf3* prevents the expression of *spaw* from occurring in the LPM even in the absence of Nodal inhibitors Dand5 and Lefty1 (Pelliccia et al., 2017).

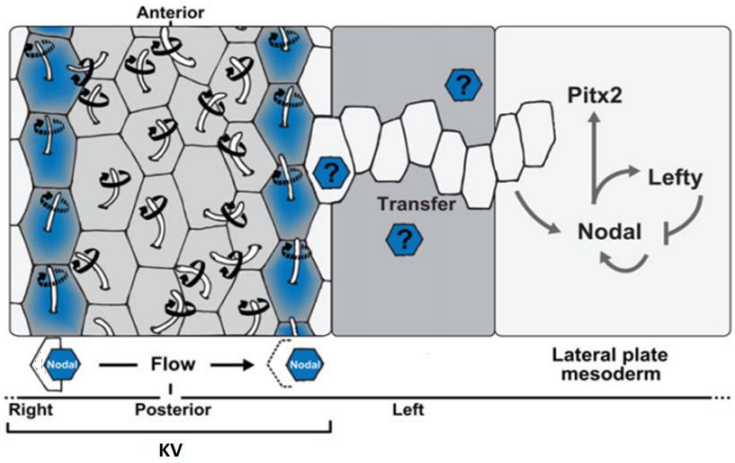

Figure 4- Representation of the left sided flow in the KV and later relay of the LR signal to the LPM. Motile and polarized cilia (positioned at the posterior pole of cells) rotate in a clockwise fashion to produce a leftward fluid flow in the extracellular space. Dand5is repressed on the right side, freeing Spaw (Nodal) on the left side. Spaw crosses across the paraxial and intermediate mesoderm towards the left LPM triggering the Nodal cascade. Adapted from Blum 2014

A combination of these two hypotheses suggests that Ca2+ spreading through gap junctions in endodermal cells may enhance the secretion of sGAGs, assisting the transfer of Nodal protein from the organizer to the LPM (Beyer et al., 2012; Norris, 2012).

1.1.3 - Intermediate Mesoderm and Pronephros

In zebrafish, between the KV and the LPM stands a stretch of mesodermal cells called the Intermediate Mesoderm (IM), which could play a role in the transfer of Spaw to the LPM. Shortly after epiboly, these IM cells emerge as a band of tissue at the ventrolateral edge of the paraxial mesoderm (Figure 5A) (Drummond et al., 2016). In zebrafish the IM gives rise to both kidney and blood cells, and, as development proceeds, the nephrogenic component of the IM is determined by the expression of renal markers such as the transcription factors *hnf1ba, pax2a, pax8,* and *lhx1a*. Later, this tissue develops into the Pronephros (PN). In teleost fish, such as the zebrafish, the PN is the functional kidney of early larval life (Drummond et al., 2016). This structure is composed by three segments: anteriorly the glomerulus, then the tubule and posteriorly the duct(Figure 5B). Each of these segments is determined by the anterior to posterior interaction of *wt1, pax2a* and *sim1*.Anteriorly the domain expressing only *wt1* will give rise to the glomerulus, the region expressing *wt1* and *pax2a* will originate the tubule and the tissue expressing *pax2a* and *sim1* will develop into the duct. (Drummond et al., 2016; Serluca & Fishman, 2001).

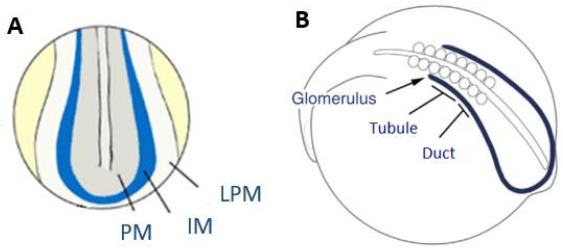

F**igure 5 – Development of the Intermediate Mesoderm and the Pronephros**. **A** – At 10 hpf, the Intermediate Mesoderm (IM) is located between the Paraxial Mesoderm (PM) and the Lateral Pate Mesoderm (LPM). Adapted from Marra and Wingert et al., 2014. **B** –The IM later gives rise to the Pronephros (PN) with its three distinct segments: Glomerulus, Tubule and Duct. Adapted from Drummond et al., 2016

1.1.4 –Phase 3: Nodal Cascade in the LPM

Expression of *spaw* in the left LPM can be seen by 10ss. In the LPM Spaw activates itself and *pitx2*, and the expression of both spreads from the posterior to the anterior end of the LPM, eventually covering the whole left side of the LPM (Shiratori et al., 2006). The left-sided expression of *pitx2* remains for many hours after Nodal signalling has stopped (Shiratori et al., 2006). Before reaching the LPM, Spaw from the KV activates *lefty1* expression in the posterior notochord (Grimes et al., 2016). It has been proposed that *lefty1* acts to repress Spaw signalling to the LPM, preventing the activation of Nodal target genes in the LPM before the asymmetric signal from the KV (Grimes et al., 2016). The expression of *lefty1* in the notochord is driven by Spaw as it propagates anteriorly within the LPM (X. Wang & Yost, 2008) and acts as a molecular midline barrier preventing *spaw* activation on the right LPM (Lenhart et al., 2011). The expression of *lefty2* is induced within the left side of the heart field once Spaw reaches the anterior left and also prevents Spaw from spreading to the right LPM (Lenhart et al., 2011). Therefore, both *lefty1* and *lefty2* play a critical role in confining the expression of *spaw* to the left side of the LPM (Zinski et al., 2017).

1.1.5 – Phase 4: Left-right asymmetric organ morphogenesis

The asymmetric information in the LPM is interpreted by individual organ primordia, resulting in the asymmetric morphogenesis of several organs. The heart is the first organ to form and function during vertebrate embryo development (Bakkers et al., 2009). At 12 hpf (15ss), myocardial progenitors are found in the anterior LPM, with ventricular progenitors more medial than atrial progenitors. Endocardial progenitors lie anteriorly. Then, myocardial and endocardial progenitors migrate to the midline and fuse by 19 hpf (20ss) to create the cardiac cone. The endocardium covers the inner lining of the myocardial tube forming the linear heart tube by 24 hpf (Bakkers, 2011; Grimes & Burdine, 2017; Staudt & Stainier, 2012).

The first asymmetric displacement is called the heart jogging. It occurs when the cells on the left side of the cone migrate anteriorly more quickly than cells on the right side, resulting in a clockwise rotation and the movement of the cone to the left. It then involutes and extends to produce a leftward pointing cardiac tube by 24–26 hpf. At 36 hpf, the second asymmetric displacement, called cardiac looping, starts with a shift of the ventricle towards the mid-line, and the constriction at the position of the atrioventricular canal is first visible. The heart tube continuous to loop and by 48 hpf, it has formed a right-sided ventricle and left-sided atrium in a D-loop shape (Figure 6) (Bakkers, 2011; Grimes & Burdine, 2017; Staudt & Stainier, 2012).

Asymmetric heart morphogenesis seems to be directed by Spaw asymmetrically expressed in the anterior LPM (Bakkers et al., 2011). However, it has been observed that after loss of *spaw*, normal looping is reduced but still occurs in most of the embryos (Baker et al., 2008). Additionally, zebrafish heart tubes, isolated and cultivated cultured ex vivo, still undergo D-looping most of the times (Noel et al., 2013). This movement could be prevented by blocking actin polymerization, or the activity of non-muscle myosin II (Noel et al., 2013). Altogether, these data indicate that emerging cardiomyocytes have an intrinsic bias to laterality, requiring actomyosin activity, which could be amplified by the action of the Nodal pathway (Campione & Franco, 2016)

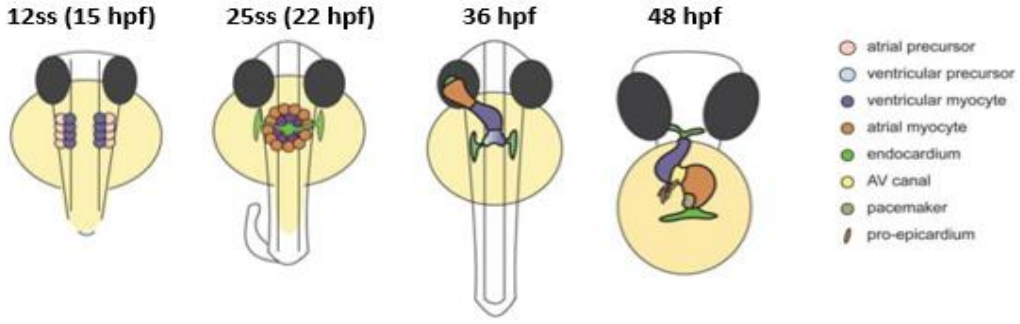

Figure 6 - Stages of heart development. At the **12-somite stage (ss)** cardiogenic differentiation starts by the expression of cardiac myosins (purple). By **25ss**, the cardiac disc is formed, with the endocardial cells within the hole at the centre, ventricular myocytes at the circumference and atrial myocytes at the periphery of the disc. Cardiac jogging then forms the cardiac tube with the endocardium forming the inner lining of the myocardial tube. At **36 hpf**, cardiac looping has started, with a displacement of the ventricle towards the mid-line. The heart tube continuous to loop and forms an S-shaped loop by 48 hpf. Adapted from Bakkers et al., 2011

It is assumed that the establishment of laterality of the heart, gut, liver and pancreas is a consequence of the events that happen in the LPM (Davis et al., 2008). However, while the heart derives from the LPM tissue, the digestive tract organs originate from the underlying solid rod of endodermal cells that forms at the ventral midline between 24 and 30 hpf (Davis et al., 2008). Their development starts at a particular position along the anterior–posterior axis by a process known as gut looping. This displacement is mediated by the asymmetric migration of the LPM. It occurs specifically within the gut looping region and requires functional LR gene expression and establishment of epithelial polarity within the LPM (Horne-Badovinac et al., 2003). At 20 hpf the endodermal rod lies in the midline and epithelial cells of the LPM flank the endoderm at the same dorsoventral level (Figure 7 A, E, E'). Starting at 26 hpf, both sides of the LPM migrate towards the midline. The left LPM migrates dorsally to gut and the right LPM migrates ventrolaterally (Figure 7 F, F'). At 30 hpf the developing gut has shifted to the left and the LR position of the LPM is highly asymmetric (Figure G-I'). (Horne-Badovinac et al., 2003). It has been shown that bidirectional signalling between EphrinB1, in the liver progenitors, and EphB3b, in the LPM, coordinates the movements of the hepatic endoderm and adjacent LPM, resulting in asymmetric positioning of the zebrafish liver (Cayuso et al., 2016). Remodelling of the extracellular matrix (ECM) is also required. During gut looping, Laminin is reduced by the activity of matrix metalloproteinases (MMP) along the LPM/gut boundary, and the activity of the MMP is regulated by transcription factor Hand2. In *hand2* mutants there is no asymmetric migration of the LPM nor gut looping, showing that Laminin depletion is necessary for LPM migration (Hochgreb-Hägele et al., 2013; Yin et al., 2010).

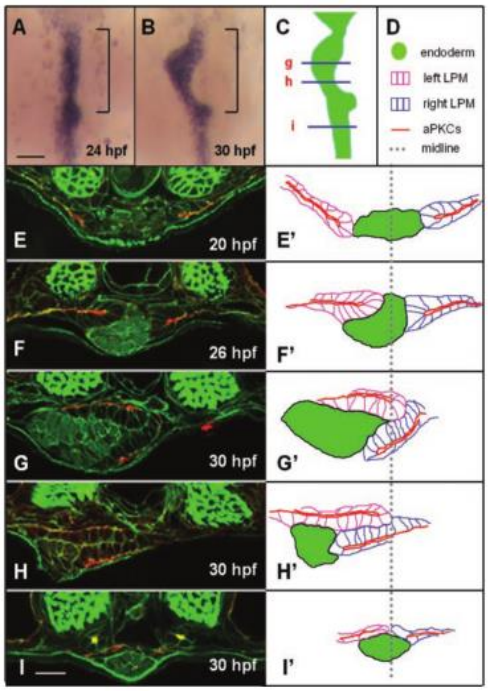

Figure 7 - The LPM undergoes asymmetric migration in the gut-looping region – (A/B) Whole mount in situ hybridization reveals digestive tract morphology. **(C to I)** – Transverse section of the endoderm and LPM and respective diagrams **(E' to I').** Taken from Horne-Badovinac *et al* 2003.

Interestingly, Noel et al. observed that heart looping was mostly normal in *spaw* mutants, where asymmetric *pitx2* expression is lost in the LPM (Noel et al., 2013). However, Ji et al. described that gut laterality was completely randomized after loss of *spaw*, but was normal in *pitx2* mutants. This indicates

that LR signalling downstream of Spaw is mediated by molecules other than Pitx2 during zebrafish gut LR development (Ji et al., 2015).

1.2 - Cadherins in development

We have seen so far that during embryonic development, individual cells participate in multicellular processes to co-ordinately remodel tissue (Oteiza et al., 2008; Bakkers et al., 2011; Horne-Badovinac et al., 2003). This means that cells sense and adapt to each other via physical contacts between them. A principal intercellular structure that links cells together is the adherens junction. These junctions consist of cadherin adhesion receptors that can interact with the actin cytoskeleton via catenin adaptor proteins that link cadherins to the actin cytoskeleton, cell signalling and regulatory proteins. They regulate the adhesive interaction between adjacent cells in a polarized epithelium (Takeichi et al., 2014, Malinova et al., 2017).

Cadherins, a key component in adherens junctions, represent one class of CAMs (cell adhesion molecules) that mediate Ca2+ dependent interactions between cells. In general, classical cadherins are transmembrane glycoproteins that have a common cytoplasmic domain and an extracellular domain containing five tandem extracellular cadherin domains (Figure 8). These domains are highly homologous to each other and hold Ca2+ binding sites. (Alimperti et al., 2015). Cadherin-mediated cell–cell homophilic junctions are formed as a result of interaction between extracellular domains of identical cadherins, located on the membranes of the neighbouring cells (Ivanov et al., 2001). Even though some cadherins can mediate weak heterophilic interactions, highly specific homophilic adhesions play a key role in tissue and organ development during embryogenesis and in maintenance of normal tissue structure in the adult organism. (Ivanov et al. 2001; Alimperti et al., 2015; Collins et al., 2014)

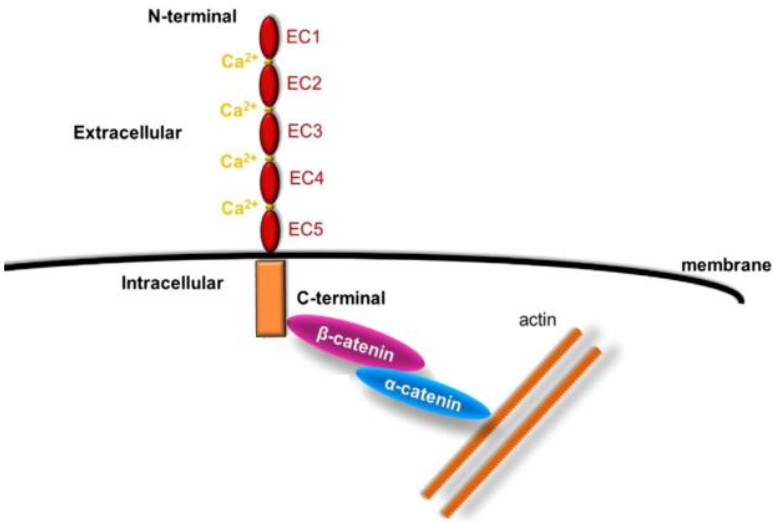

Figure 8 - **Structure of classical cadherins and their interaction with cytoplasmic proteins**. Adapted from Alimperti *et al*. 2015.

Experiments with chick embryos have shown that cadherins, especially N-Cadherin (Cdh2), have been implicated in the establishment of LR asymmetry both early and later in development (Davis et al., 2008; García-Castro et al., 2000; Mendes et al., 2014; Plageman, et al., 2011, Gonzalez-Morales et al., 2015). Some have established a link between actin dynamics and cadherin-based junctions, which culminate in the asymmetric cell behaviours seen during gut morphogenesis (Davis et al., 2008; Kurpios et al., 2008; Welsh et al., 2013). Work from our lab showed that N-cadherin plays a role in LR patterning in the chick

(Mendes et al., 2014). It is a key molecule responsible for finishing the leftward cell movements at the node. Stopping these movements at the right time is crucial to stabilize the molecular asymmetries generated in the node, so that the correct asymmetric information is conveyed to the LPM and the proper looping of the heart is achieved (Mendes et al., 2014)

1.2.1 – Cadherin 11

In zebrafish, Cadherins are required to maintain the adhesive interactions of the dorsal forerunner cells (DFC) during their migration and subsequently for lumen formation when they differentiate to form the KV (Matsui et al., 2011; Oteiza et al., 2008; Tay et al., 2013). One specific cadherin, Cadherin-11 (Cdh11) cadherin has been studied in the mouse and *Xenopus*. It is involved in the cell differentiation and migration of neural crest (Pegoraro et al., 2013; Simonneau et al., 1995; Vallin et al., 1998) and metastatic tumour cells (Chu et al., 2009; Huang et al., 2011). In zebrafish, this cadherin was initially detected during epiboly, later in the neural keel, and at 20ss in the ventral neural tube, otic vesicle, midbrain and diencephalon (Franklin & Sargent, 1996). Experiments have found that Cdh11 is present in membrane structures important for otolith formation (Clendenon et al., 2009), and that it is also required for the development of the visual system of the zebrafish (Clendenon et al., 2012). However, Cdh11 had not been described in the establishment of LR asymmetry.

At the start of this project, in order to understand the role of Cdh11 we injected embryos with a *cdh11* morpholino. We saw that at 48 hpf both the heart and the gut had laterality defects (Figures 9 and 10). By injecting into a *sox17*:EGFP transgenic line, we observed that approximately 20% of the embryos showed an inverted gut conformation. In some cases we also saw bilateral disturbances, such as an extra liver (Figure 9). Using a *myl7* probe, we saw that *cdh11* morphants often showed reversed or symmetric hearts (50%) (Figure 10).

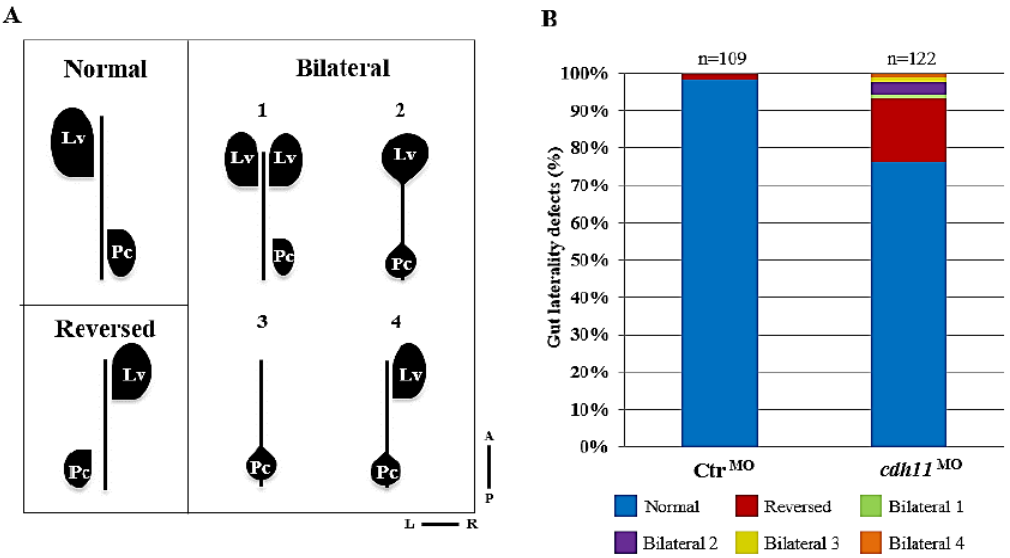

Figure 9 – **Cdh11 knockdown causes gut laterality defects at 50 hpf. A-** Schematic representation of normal gut loop (Normal) and five gut laterality defects (Reversed, Bilateral 1, 2, 3 and 4); **B-** Percentages of normal (blue), reversed (red), bilateral 1 (green), bilateral 2 (purple), bilateral 3 (yellow) and bilateral 4 (Orange) in Ctr MO (n=109) and *cdh11* MO (n=122) injected embryos analyzed at 50 hpf. Lv-liver, Pc-Pancreas, L-Left, R-Right, A-Anterior, P-Posterior. Unpublished data from Sara Fernandes

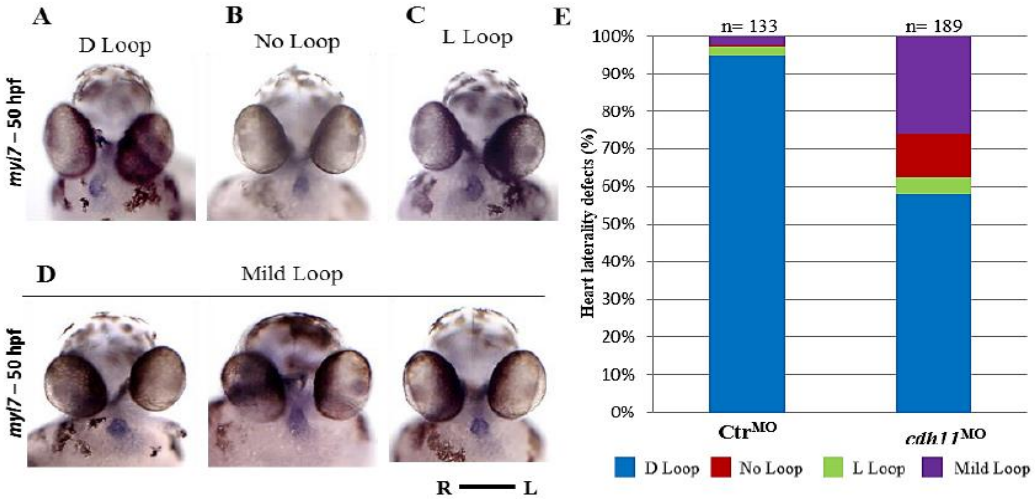

Figure 10 – Morphants embryos exhibit heart laterality defects at 50 hpf. A-D - Ventral view of a Control^{MO} or *cdh11*^{MO}injected embryos at 50 hpf after *myl7* hybridization (**A-** embryo with a WT conformation (D-loop); **B-** Embryo with a symmetric heart (No-Loop); **C-** embryo with inverted heart (L-loop); **D–** Example of three embryos with Mild heart loops); **E –** Percentages of D loop (blue), No loop (red), L loop (green) and Mild loop hearts (purple) in Control^{MO} (n=133) and *cdh11*^{MO} (n=189) injected embryos. R-Right, L-Left. Data from Silva 2017.

Furthermore, after *cdh11* knockdown, the expression patterns of the LR markers *spaw* and *pitx2* were altered in the LPM. For both genes around 60% of the embryos displayed an alternative pattern, in which 30% of the morphant embryos showed *spaw* and *pitx2* expression restricted to the right LPM (Figure 11).

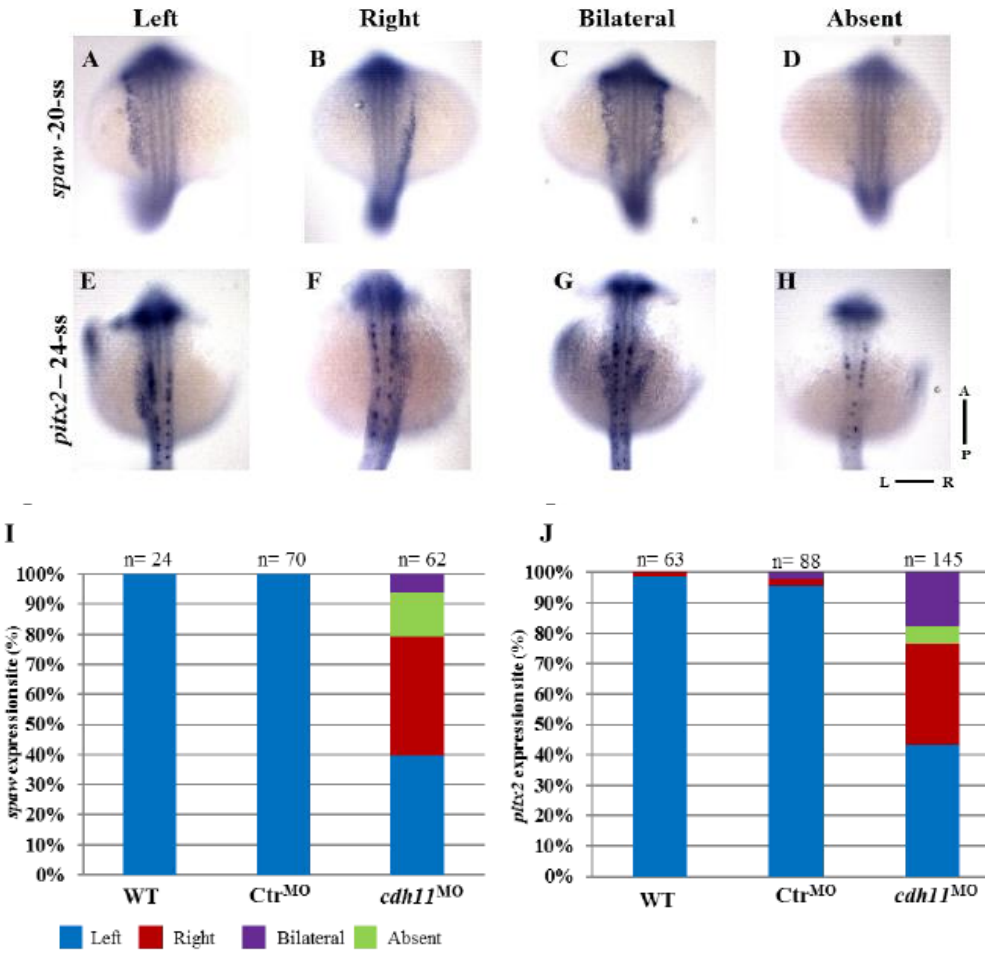

Figure 11 – Left-Right markers *spaw* and *pitx2* are affected in morphants at late somite stages. A to H - Whole-mount *in situ* hybridization in Control^{MO} or *cdh11*^{MO} injected embryo using *spaw* probe at 20-somite stage (**A** to **D**) and *pitx2* probe at 24-somite stage (**E** to **H**) (*spaw* and *pitx2* expression on the left side (WT) (**A**, **E**), right (**B**, **F**), bilateral (**C**, **G**) or absent (**D**, **H**); **I-J -** Percentages of Left (blue), Right (red), Bilateral (purple) and Absent (green) expression of *spaw* (**I**) and *pitx2* (**J**) in WT (*spaw* n=24; *pitx2* n=63), Ctr MO (*spaw* n=70; *pitx2* n=88) and *cdh11*^{MO} (*spaw* n=62; *pitx2* n=145) injected embryos analyzed at 20- and 24-somite stage respectively. L-Left, R-Right, A-Anterior, P-Posterior, ss- somite stage. Data from Silva 2017

Interestingly, the laterality phenotypes of the heart and gut were not concordant after *cdh11*^{MO} injection. The predominant heart defect was absence of loop, but the majority of the affected embryos showed a reversed gut (Figures 9 and 10). This indicates an uncoupling in the development of these organs, which had been observed before (Lopes et al., 2010; Noel et al., 2013; Ji et al., 2015). Additionally, we noticed that the percentage of bilateral expression of *spaw* and *pitx2* after MO injection also showed a lack of concordance (Figure 11). Therefore, we proposed that the abnormal expression of the conserved LR genes in the right LPM might account for the reversed gut loop phenotype, and the absence of these genes in the prospective heart territory would prevent the breakage of symmetry in the heart.

In order to understand what role Cdh11 might play throughout development, we searched for *cdh11* transcripts and we detected *cdh11* mRNA in the IM at 8ss (Figure 12A). Curiously, this corresponds to the stage where the laterality signal (*spaw*) is being relayed to the LPM (Shiratori et al., 2006). Additionally, Cdh11 had been detected in the PN (which derives from the IM) at 48 hpf (Figure 12B) (Clark et al., 2011). We know that by 24 hpf the PN has developed (Drummond et al., 2016), and at this stage the LPM begins its asymmetric migration to the midline (Horne-Badovinac et al., 2003). This led

us to suggest a new, not previously described role for these tissues in the establishment of symmetry in zebrafish. We proposed that that the IM could be used as mediator of the transfer of Spaw from the KV towards the LPM at the 10 to 12-somite stages, and that the PN can provide a stable structure for the LPM asymmetric migration between 26-30 hpf, that ultimately leads to the shift of the gut to the left.

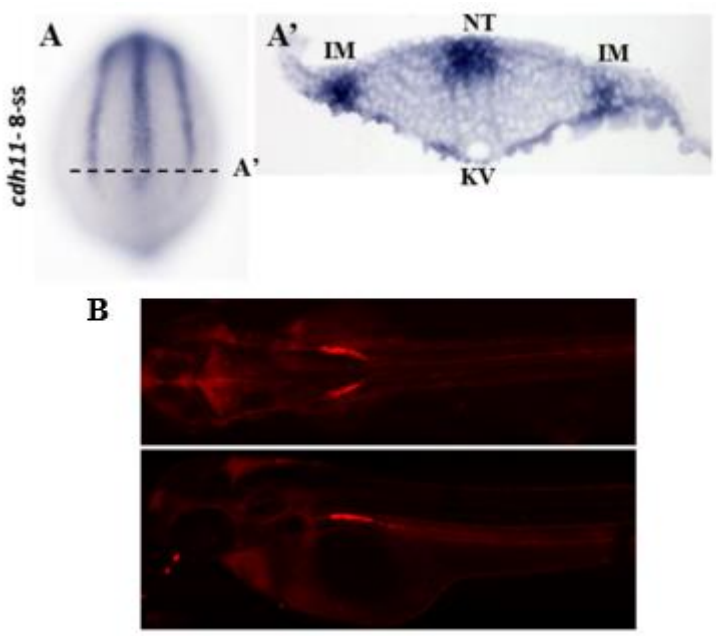

Figure 12 - *cdh11* expression pattern in WT embryos. A - WISH for *cdh11* in 8-somite stage (**A-** whole-mount embryo (dorsal view), **A'-** transversal section through KV)
WISH done by Sara Fernandes, Photos taken by Dalila and Sara. **B** – *cdh11* expression at 48 hpf using a protein-trap system. This produces a RFP transcript where and when the *cdh11* mRNA is transcribed. Adapted from Clark 2011

Additionally, we also analysed a mutant line for *cdh11*, which displayed a premature stop codon in one of its Cdh-Cdh interaction domains, producing presumably a truncated protein **(**Supplementary Figure 1). In contrast to what happened the morphants, the *cdh11* mutant did not show any of the heart and gut phenotypes that we previously characterized (Figure 9). This means that the *cdh11*^{MO} is not specific and we are observing off-target effects, that the mutant might not be functioning as a null mutation or that a genetic compensation mechanism is activated in the mutant.

1.3 – Objectives

In this project we propose to investigate the role of Cdh11 in the establishment of LR. We propose that Cdh11 could be affecting LR asymmetries either at 10-12ss during the transfer of the Nodal signal from the KV to the LPM, and also at 24 hpf during the asymmetric migration of the LPM. Additionally we want to understand how this dual role of Cdh11 might explain the lack of concordance between the heart and gut phenotypes after *cdh11* knockdown.

In this project we aim to:
- Test the specificity of the *cdh11*^{MO}
- Confirm whether *cdh11* is expressed in LR associated tissues
- Understand the role of Cdh11 in the transfer of asymmetric signal from the KV to the LPM
- Evaluate the putative role of the PN during the migration of the LPM and looping of the gut

Chapter 2 – Experimental procedures

2.1. Zebrafish maintenance

Adult zebrafish (*Danio rerio*) and embryos used in this project were maintained and bred under standard laboratory conditions **(**Westerfield et al. 2000). During this project, the embryonic stages were confirmed according to Kimmel et al., 1995.

The *cadherin-11* (*cdh11)* knockdown characterization was performed using embryos from wild-type (WT) AB strains and transgenic Tg(*sox17*:EGFP) line, maintained at Instituto de Medicina Molecular (IMM) (Sakaguchi et al., 2006). The mutant line *cdh11*^{sa14413} was obtained from the European Zebrafish Resource Center (EZRC)[1] that was generated within the TILLING project context (Moens, Donn, Wolf-Saxon, & Ma, 2008).
This line produces a truncated protein in the Cdh-Cdh interaction domain (fourth EC) due to a single nucleotide nonsense mutation (T to A) in the 454th amino acid (aa). This change leads to the formation of a premature STOP codon (TTA) instead of a Leucine (Leu) aa (TTT).

2.2. *cdh11* Knockdown

To knockdown the *cdh11*, we used a *cdh11* specific splice blocking MO, the MO3-*cdh11* (5' - TGTCACGCACCTCTGTTGTCCTTGA - 3') (*cdh11*MO) **(**Clendenon et al., 2009**)**, and a Standard Control MO (CtrMO) as a negative control (5' - CCTCTTACCTCAgTTACAATTTATA - 3') (GeneTools).
Stock solution of 3mM (Control MO) and 2,5mM (*cdh11* MO) was stored at -20°C. Injection mixture was prepared by diluting the MOs in RNase-Free water to reach a 0,2mM injection concentration.

2.2.1 - Embryo microinjections

Adult zebrafish of interest (lines WT AB) were kept overnight in a breeding cage. In the morning, a loaded injection needle was clipped using forceps, using a micrometer and mineral oil, and calibrated each time to produce a consistent injection volume. The embryos were then collected, aligned to a microscope slide in a Petri dish with a pipette
Each one-cell stage embryo was injected in the cell cytoplasm with 1,4nL of 0,2mM MO solution (0,23ng).
For each experiment, both conditions (control and *cdh11* MO) were injected into sibling embryos from two to three independent batches, and incubated in 1x Embryo Medium at 28°C until the desired developmental stage was reached.

2.2.2 - Cdh11 mRNA synthesis

cdh11 sense and anti-sense transcripts were obtained through the respective DNA plasmids, PCS2+ cdh11 sense and PCS2+ cdh11 anti-sense, available in our lab. The linearization reaction was composed of 5µg of DNA plasmid, 1µL of NotI restriction enzyme, 5µL of the respective buffer (10x) and water mixed together for a final volume of 50µL. The reaction mixture was incubated 1h at 37°C.
After 1% agarose gel electrophoresis the corresponding linearized fragments were extracted and purified with the Gel DNA Recovery kit (Zymo Research).

[1] http://www.sanger.ac.uk/sanger/Zebrafish_Zmpgene/ENSDARG00000021442#sa14413

The anti-sense transcripts were produced through the mMessage mMachine kit (Thermo Fisher) by adding approximately 1µg of the purified linearized plasmid DNA with the SP6 RNA Polymerase and following the provided protocol. 1µL of TURBO DNAse was also added. This produces the capped mRNA.
The sample was purified according to the manufacturer's instructions of the illustra™ Probe Quant™G-50 Micro Columns (GE Healthcare Life Sciences). The resulting mixture was observed in a denaturing gel and its concentration measured in the Nanodrop 2000 Spectrophotometer (Thermo Fisher).

2.3. CRISPR/Cas9

2.3.1 - gRNA design

Three different gRNAs were designed to target three regions of the Cdh11 protein: signal peptide, extracellular domain and transmembrane domain (gRNA 1, 2 and 3 respectively).
- **gRNA1** was designed to recognize the signal peptide, at the N-terminal, which directs the newly synthesized protein to its destination. Targeting this region should prevent the protein from localizing to the membrane.
- **gRNA2** targets the extracellular domain of the cadherin, downstream of the signal peptide. While mutations in this region will not prevent alternative ATG usage, if a frameshifting mutation occurs, it will give rise to two outcomes: on the one hand, transcripts using the correct ATG will produce a truncated or altered protein, thus lacking the appropriate transmembrane domain. On the other hand, transcripts that use an in frame alternative ATG, located downstream of the mutation site, will produce proteins lacking both the signal peptide and the upstream extracellular domain. This means that they probably won't localize to the membrane, but if they do, they won't be functional.
- **gRNA3** targets the transmembrane domain, stopping the protein from attaching to the membrane.

The gRNAs were genearated as described in Talbot et al., 2014. The gRNA synthesis was done as described in Ribeiro et al., 2017.
Cas9 protein was produced by the Weizmann Institute of Science, Israel as a purified batch at 1mg/mL in 20 mM Tris pH 8.0, 10mM MgCl2, 0.2M KCl.

2.3.2 – gRNA/Cas9 microinjections

All gRNA combinations were tested, from injecting each single guide, two at the time and also all three of them together. Several gRNA and Cas9 concentrations were analysed, from 107 ng/µL to 880 ng/µL of gRNA and either 666,7 ng/µL or 800 ng/µL of Cas9 protein (Table 1). The analyses present in this work derives from injecting gRNAs 1 and 2 combined, both at 293,3 ng/µL, with the Cas9 protein at 800 ng/µL. The mixture was incubated at R.T. for 5 minutes to allow for the gRNA/Cas9 complexes to form. Embryos at one-cell stage were injected with 1.4nL of this solution, as described above.

Table 1

Conditions	Attempts	Analysed
gRNA combinations	1, 2 1+2, 1+3, 2+3 1+2+3	1+2
gRNA concentration (ng/uL)	107 to 880	293,3 each
Cas9 concentration (ng/uL)	667,7 to 800	800

Table 1 – Different concentrations and combinations of *cdh11* gRNAs and Cas9 protein were injected in 1-cell stage embryos.

2.3.3 - DNA extraction

At 24 hours, embryos were collected and placed into microcentrifuge tubes in pairs (two embryos per tube). Following the protocol as described in Meeker et al., 2007.The Embryo Medium was replaced with 100µL of 50 mM NaOH and incubated at 95°C for 20 minutes. The tubes were cooled to 4°C, and then 10µL of 1 M Tris-HCl, pH 7.5, was added. The sample was centrifuged at 670g for 10 minutes at R.T., and the supernatant transferred to a new tube. The resulting mixture was purified through the DNA clean & concentrator™- 5 kit (Zymo Research)

2.3.4 - T7 endonuclease

Forward (Fw) and reverse (Rv) primers for each gRNA were designed using NCBI primer blast[2] and synthesized by STABVida. The annealing temperature was calculated using Tm Calculator by ThermoFisher Scientific™[3].

The samples were amplified by PCR and then 200ng of the purified PCR product was added to 2µL of NEBuffer 2 (adjusting with water up to 19µL) and denatured and reannealed using a thermocycler with the respective protocol (Supplementary Table 5).

After this, 1µL was added to the samples and incubated at 37 ºC for 90 minutes in the thermocycler. The samples were then run in a 2.5% agarose gel electrophoresis and gene modification levels were estimated using the ImageJ software.

2.4. Fluorescence activated cell sorting (FACS)

Approximately 100 embryos at 8-somite stage, i.e. 13 hour-post-fertilization (hpf). were dechorionated and washed in Daniaeu's buffer These cells were transferred to a CO2 independent medium (Gibco) complemented with 0.5 mM EDTA. These cells were then dissociated through pipetting. After this, the embryos were centrifuged at 700g and re-suspended in 5 mL of the same medium (this step repeated

[2] https://www.ncbi.nlm.nih.gov/tools/primer-blast/

[3] https://www.thermofisher.com/pt/en/home/brands/thermo-scientific/molecular-biology/molecular-biology-learning-center/molecular-biology-resource-library/thermo-scientific-web-tools/tm-calculator.html

three times). Afterwards, the cells were re-suspended in 1 mL of medium and filtered with a 70µm filter (Falcon) directly into a 5mL round bottom tube (Falcon).

FACS was performed with a FACSAria bench top High Speed Cell Sorter (Becton Dickinson), with the 100µm nozzle with 0-16-0 mask, and the sheath fluid pressure at 20psi.
GFP excitation was made through a 488nm (Blue) laser and the detection using 502LP e 530/30nm filtres. GFP positive cells in WT and and in *sox17*:GFP transgenic embryos were selected and collected into TRIzol buffer.

2.4.1 - RNA extraction (DNAse I)

After sorting, TRIzol was added up to 1 mL. The cells were vortexed for 30 seconds and incubated 5 minutes at room temperature. 200µL of chloroform was added and the tubes were shaken vigorously by hand for 15 seconds, incubated for 5 minutes at room temperature and centrifuged at 12000g, for 15 minutes at 4ºC. The aqueous phase was collected into a new RNAse-free tube and mixed with 0.5µL of 20µg/µL RNAse-free glycogen (ROCHE). 500µL of isopropanol was also added and mixed by hand. The samples were incubated for 10 minutes at room temperature and centrifuged at 12000g, for 10 minutes, at 4ºC. The supernatant was removed, and the pellet washed with 1 mL of cold 75% Ethanol and centrifuged at 8000g for 10 minutes at 4ºC. The wash was discarded and this step repeated. After the second wash, ethanol was removed from the tubes by pipetting and for 10 minutes the tubes were left to dry to remove all traces of ethanol. The pellet was re-suspended in 14µL of RNase free water. The samples were warmed at 60ºC for 10 minutes and cooled on ice. The samples were treated with DNase I (Promega), purified with the RNA clean and concentrator kit (Zymo Research) and stored at -80 ºC.

2.4.2 - Reverse transcriptase

First strand synthesis of cDNA was carried out using ProtoScript® II Reverse Transcriptase kit (NEB), through random primers, following the manufacturer protocol. Approximately 120 ng of the total RNA was added in a 20 µl reaction. This was initially denatured through heating (65°C for 5 minutes), followed by a 5 minutes incubation at 25°C, then 1 hour at 42°C and for 20 minutes at 65°C.

2.4.3 - cDNA Purification

100µL of Phenol:Chloroform:Isoamyl alcohol (25:24:1) (Sigma) was added into each tube and the samples were then vortexed for 30 seconds and centrifuged at 13200rpm for 5 minutes at R.T. The upper phase was transferred into a new tube, and mixed with 200µL of chloroform per 100µL of supernatant. The mixture was vortexed for 30s and centrifuged at 13200rpm for 5 minutes at R.T. Once more, the upper phase was transferred to a new tube, and mixed with 1/10 of the volume transferred of ammonium acetate 4,5M, and 2,5x the volume transferred of absolute ethanol. The samples were homogenized and incubated overnight at -20°C. On the following day, the tubes were centrifuged at 14000rpm, for 45minutes, at 4°C.
The supernatant was discarded and the pellet was washed with previously cooled 70% ethanol. The tubes were centrifuged for 15 minutes at 14000rpm, at 4°C and the supernatant was discarded. The pellet was air dried and then re-suspended in 20µL of water. The samples were quantified using the NanoDrop 2000 spectrophotometer and stored at -20°C.

2.4.4 Polymerase Chain Reaction (PCR)

All the reaction specifications were performed according with Thermo Scientific Phusion High-Fidelity DNA Polymerase product information. For a final volume of 50µL, 150ng/50µL of gDNA template was added, 10µL of 5x Phusion HF Buffer (ThermoFisher Scientific™), 1µL of 10mM dNTP mix (ThermoFisher Scientific™), 2,5µL of 10µM primer mix, 0,5µL Phusion DNA polymerase

(ThermoFisher Scientific™) and water. Cycle sequencing was performed with conditions described in Supplementary Table 2 and 3. Then the samples were analysed by agarose gel electrophoresis.

In order to amplify the *cdh11* gene region, we used the primer pair previously designed for *cdh11* gRNA 1 (see above) using the corresponding thermocycler protocol (Supplementary Table 2). Then the samples were analysed in an agarose gel electrophoresis. Primer pair for amplification of *dand5* was kindly provided by Susana Lopes laboratory.

2.5. Cdh17 ablation line plasmid

In order to produce a *cdh17* specific ablation line plasmid, two plasmids were used: the Osx:mCherry-NTRO plasmid (Renn and Winkler 2009) and the pSceI-cdh17prom-eGFP-cdh17intron plasmid (Sanker et al., 2013), kindly provided by the Didier Stainier and Neil Huckriede repectively (Supplementary figures 4 and 5)

2.5.1 - Plasmid cloning

The plasmids were initially digested with KpnI initially, later replaced by Acc65I (NTRO plasmid) and XhoI (*cdh17* plasmid) restriction enzymes. To linearize each plasmid DNA, 5µg of DNA plasmid, 1µL of the appropriated restriction enzyme, 5µL of the respective buffer (10x) and water were mixed together to a final volume of 50µL. The reaction mixture was incubated for 1h at 37°C. The efficiency of digestion was visualized on an agarose gel and later purified using the DNA clean & concentrator™- 5 kit (Zymo Research).

The 5' ends of the fragments were blunted by Klenow fragment or T4 DNA polymerase filling. With the Klenow, the reaction was composed of 15µL of the DNA sample, 2µL of the respective buffer, 0,5µL of the dNTP mix (10µM), 1µL of the Klenow fragment and water up to 20µL.

The T4 polymerase reaction was composed of the purified samples, plus 1µL of T4 DNA polymerase, 3µL of the respective buffer (10x), 1.5µL of dNTPs (10µM) and water up to 30µL. The tubes were incubated at 12°C for 15 minutes.Both samples were then cut with BamHI enzyme. This was done by adding all of the sample DNA, 10µL of the respective buffer (10x), 1µL and water up to 100µL. The mixture was incubated for 1h at 37°C.The samples were analysed in an agarose gel and the required fragments extracted and purified, using the Zymoclean™ Gel DNA Recovery kit (Zymo). The fragments were ligated using the T4 DNA Ligase (NEB) protocol, with different insert:vector ratios, for 2h at R.T. or ON at 12°C.

2.5.2 - Transformation of competent *Escherichia coli* bacteria

Frozen aliquots of competent *Escherichia coli* bacteria previously prepared in our lab (DH5α strain, kept at -80°C), were thawed on ice. 5µL of the cloned plasmid was added to 100µL of cells and incubated on ice for 30 minutes. This was followed by 40s heat shock at 42°C and a 2 minutes cooldown on ice. 900µL of SOB solution was added to the mixture and left for incubation, for 45 to 90 minutes, at 37°C with agitation. After this, 100µL of this mixture was plated on LB agar medium (containing ampicillin 100µg/mL of LB agar medium) and left at 37°C overnight. This was also done for a positive control (the original Osx:mCherry-NTRO plasmid) and a negative one (the AmpR expressing fragment, after ligation protocol).

On the next day, an isolated colony was inoculated on a 15mL falcon with LB media and left overnight at 37°C with agitation. DNA was purified according to the manufacturer's instructions of the GeneJET Plasmid Miniprep Kit (ThermoFisher Scientific™). DNA concentration was determined by spectrophotometry using the NanoDrop 2000 spectrophotometer.

2.6. Whole mount *in situ* hybridization (WISH)

In these experiments, several probes were used, previously synthesized in our lab: DIG-labelled *cdh11, cmlc2, cdh6, cdh17, foxa3* and FITC labelled *myoD.*

Zebrafish embryos were collected at specific developmental stages and fixed in a 4% paraformaldehyde solution prepared in 1x Phosphate-buffered saline (1x PBS) (4% PFA) during 4 to 5 hours at R.T. or overnight at 4°C. The embryos were then stored at -20°C after dehydrate washes performed with increasing concentrations of methanol (MetOH) diluted in 0,1% Tween 20 in 1x PBS (0,1% PBT) (two washes with 0,1% PBT, 50% MetOH and 100% MetOH).

2.6.1 - WISH protocol

Day 1: The stored embryos were rehydrated by successive washes with 75%, 50%, 25% MetOH in 0,1% PBT, and four times in 0,1% PBT, for 5 minutes each. Chorions were removed using forceps. Each set of embryos was incubated with PK (Roche) (10µg/mL) in 0,1% PBT (incubation period according to embryo stage - see Table below) and immediately re-fixed in 4% PFA for 20 minutes at R.T. and washed five times with 0,1% PBT (5 minutes each). For 2 to 5 hours, the samples were incubated at 70°C in 500µL of pre-Hybmix, followed by an overnight incubation with 200µL of probe at 70°C, having this one been previously heated for 10 minutes at 70°C.

Stage	**Incubation time**
Early somitogenesis (until 8 somites)	1 minute
18 – 20 hpf (19-23 somites)	5 minutes
24 hpf	15 minutes
36-48 hpf	30 minutes

Day 2: The probe solution was recovered in the next day and the embryos washed at 70°C with pre-heated solutions of 100% pre-Hybmix for 10 minutes, 25%, 50% and 75% 2x SSC in pre-Hybmix and 100% 2x SSC for 15 minutes. After that, the embryos were washed at R.T. twice in 0,2x SSC for 15 minutes each, once in 50% 0,2x SSC in 0,1% PBT and two times in 0,1% PBT, each one lasting 10 minutes. Embryos were incubated in 500µL of blocking solution for *in situ* at least for 1 hour at R.T. and after that incubated with Anti-DIG-AP (Roche Life Science) in blocking solution (1:5000) overnight at 4°C.

Day 3: In the last day, the embryos were washed six times with 0,1% PBT for 15 minutes each, and three times in Staining Buffer for 5 minutes each. To reveal the probe, the embryos were incubated with 500µL of purple AP substrate (Roche Life Science), or 500µl of NBT/BCIP in the dark at R.T..

The colorimetric reaction was monitored with a dissecting microscope, and stopped by changing the substrate for 0,1% PBT followed by a fixation in 4% PFA for 20 minutes at R.T. and a wash in 0,1% PBT. To store the embryos at 4°C in 100% glycerol, a series of washes in glycerol and 0,1% PBT (20%, 50% glycerol in 0,1% PBT) were performed.

2.6.2- Double WISH protocol

Double ISH was done by combining each of the DIG labelled *cdh6, cdh11,* and *cdh17* probes with the FITC labelled *myoD* probe.

At the end of **Day 2**, after being incubated with blocking, the embryos were incubated with Anti-Fluo AP (Roche Life Science) in blocking solution (1:10000) overnight at 4°C.

Day 3: the embryos were washed six times with 0,1% PBT for 15 minutes each, and three times in Tris 0,1M for 10 minutes each. Fast Red substrate was prepared according to the provided protocol (SIGMAFAST™ Fast Red TR/Naphthol AS-MX Tablets) and 500µL was added to the embryos. The

revelation took place in the dark. When the revelation process was finished 0,1% PBT was added followed by a fixation in 4% PFA for 20 minutes at R.T. The embryos were one more washed with 0,1% PBT. The acid digestion took place with Glycine for 15minutes, in agitation. The embryos were then washed in tBST twice for 5 minutes, incubated in tBST at 70°C for 30 minutes and later washed with 0,1% PBT twice. Embryos were incubated in 500µL of blocking solution for at least for 1 hour at R.T. The following protocol proceeded as described in the normal ISH protocol from this step on.

2.6.3 Embryo embedding

After the ISH protocol, the embryos were washed in 1x PBS solution until the glycerol was completely removed and then transferred to a 5% sucrose in 1x PBS solution.
They were then fixed in 4% PFA at 4°C. They were washed in 1x PBS and incubated at 4°C for approximately 15 to 30 minutes in 15% sucrose in 1x PBS solution. Later, the samples were incubated for 1h at 42°C in a previously heated 7.5% gelatine and 15% sucrose in 1x PBS solution. The bottom of a plastic mould was filled with the same solution and allowed to harden at R.T. Finally, the embryos were disposed with the correct orientation for sectioning and embedded. The gelatine cubes were fast freezed using 2-Methylbutane (Isopentane) (Sigma) solution, previously cooled at -40°C, using dry ice, and stored at -80°C.

2.6.4 - Cryosectioning

20µm thick transversal sections cut with a Cryostat LEICA CM 3050S were mounted into microscope slides by the Histology and Comparative Pathology Laboratory at iMM and stored at -20°C.The frozen microscope slides were thawed for 30 minutes at R.T. and washed 4 times with a pre-heated 1x PBS in a water bath at 42°C for 5 minutes. After removing the maximum of solution as possible, 100µL of Mowiol was added to the slide and the cover slip was set on top. The slides were left to dry at R.T. The samples were sealed using nail polish. The slides were stored at 4°C.

2.7. Agarose gel electrophoresis

To access the linearization of the plasmid DNA, PCR product size and probe synthesis, gels were prepared by heating agarose dissolved in 1x TAE buffer mixed with RedSafe™ Nucleic Acid Staining Solution (Intron) (5µL per 100mL TAE 1x). The samples mixed with Orange G (Loading Buffer) at a minimum of 1µL per 5µL of DNA sample and applied to the gel. A 1Kb Plus DNA ladder (Invitrogene) was used to evaluate samples size. The electrophoresis was performed in TAE 1x buffer for 15 minutes at 100V.

For a RNA Denaturing Gel 1,25g of agarose was dissolved by heating in 37mL in water milliQ and left ON at 70°C. On the following day, in a 15mL Falcon tube, the rest of the solution was prepared by adding 5mL of MOPS 10x, 8mL of formaldehyde 37% and 2,5µL of GelRed. This was then added to the agarose solution. The electrophoresis was performed in a buffer solution composed of 50mL MOPS x10 in 450mL of water MIlliQ

Chapter 3 - Results

3.1- Independent *cdh11* knockdown assays produce similar heart laterality phenotypes

In two previous assays, two very talented researchers showed independently that Left-Right (LR) development is disrupted after injection with two different stocks of a splice-blocking Cdh11 Morpholino (*cdh11*^{MO}) (Silva 2017). As part of the learning process, we wanted to confirm my injection efficacy by comparing my results with the ones previously obtained in our lab. We injected the *cdh11*^{MO} and standard control Morpholino (Control^{MO}) at one-cell stage, using the same conditions, and analysed the heart phenotype at 50 hpf using a *myosin light chain 7 regulatory* (*myl7*) probe, which allows to score the looping conformation of the heart at this stage (Figure 13)

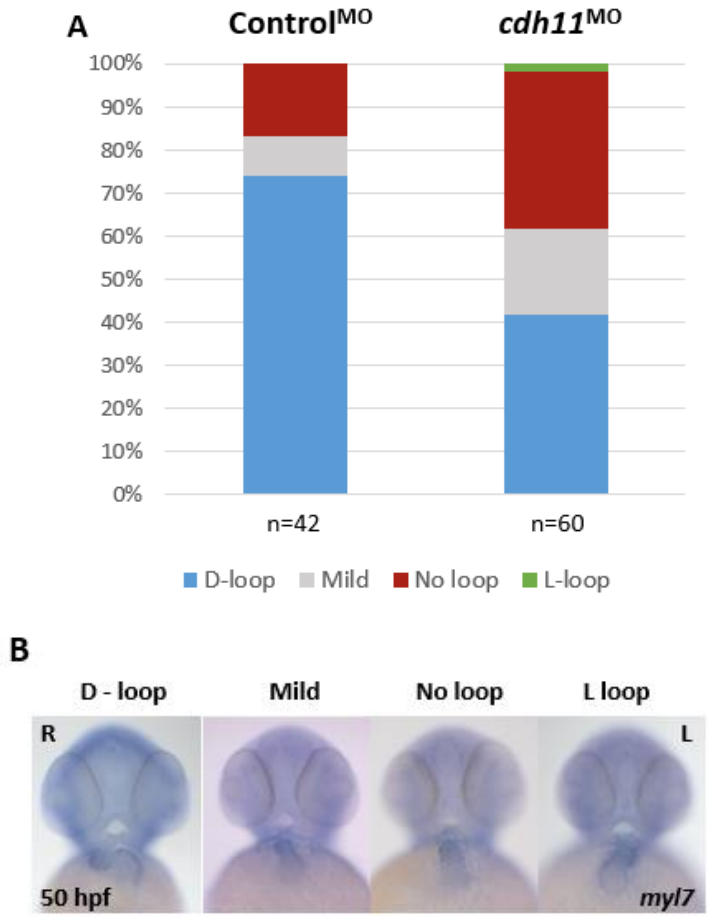

Figure 13– Independent *cdh11* knockdown experiments produce the same heart laterality phenotypes previously described. A – Percentage of D-loop (blue), Mild loop (grey), No loop (red) and L-loop (green) in Control^{MO} (n=42) and *cdh11*^{MO} (n=60) injected embryos, in two independent batches. **B –** Ventral view of embryos hybridized with *myl7* at 50 hpf showing what was considered D-loop, Mild, No-loop and L-Loop heart laterality phenotypes. R-Right, L-Left.

In the third round of injections, we could observe that "D-loop" phenotype was observed in 73,8% (n=42) of the Control^{MO} injected embryos, while with the *cdh11*^{MO} the result was of 41,7% (n=60). For the "Mild-loop", 9,5% of the controls had this phenotype and 20% of the morphants had it. "No-loop" was observed in 16,7% in the controls and 36,7% in the morphants. Lastly, 1,7% of the *cdh11*^{MO} injected embryos had an inverted, "L-loop" conformation but this was not found in controls embryos (Table 2).

Comparing the new results with the two previous assays, we can see that all phenotype categories were observed. An obvious difference is the absence of the Mild category in the first assay. It is possible that some of the embryos classified as D-loop in the first assay were more conservatively classified as Mild in the last two assays. In all the assays the "D-Loop" phenotype was the most observed and "L-loop" the least observed (Figure 13, Table 2).

Table 2

	1st Assay		**2nd Assay**		**3rd Assay**	
Phenotype	**Control MO** (%) (n=66)	***cdh11* MO** (%) (n=81)	**Control MO** (%) (n=133)	***cdh11* MO** (%) (n=189)	**Control MO** (%) (n=42)	***cdh11* MO** (%) (n=60)
D-loop	95,5	51,9	94,7	58,2	73,8	41,7
Mild-loop	-	-	2,3	25,9	9,5	20
No loop	3,0	37,0	0,8	11,6	16,7	36,7
L-loop	0	11,1	2,3	4,2	0	1,7

Table 2– Phenotype distributions after injecting *cdh11*^{MO} and Control^{MO} in three different tries.

The most noticeable differences between the three assays were a lower percentage of "D-loop" phenotypes in the third assay (41,7%) compared to the first and second ones (51,9% and 58,2% respectively) (Table 2), and a higher percentage of the "No loop" phenotype when comparing the third assay with the second one (36,7% and 11,6%, respectively) (Table 2). In conclusion, the distribution of phenotypes observed after *cdh11*^{MO} injection was similar in three independent assays, with three different researchers and two different *cdh11*^{MO} stocks. Thus, this suggests that the *cdh11*^{MO} induces a reproducible heart looping phenotype in zebrafish.

3.2 – Generation of *cdh11* mutations using the CRISPR-Cas9 genome editing system

Previous work from our laboratory has shown that the LR phenotypes observed with the splice-blocking *cdh11*^{MO} do not correspond to those found in the mutant line *cdh11*^{sa14413}. In general, the MO phenotypes were more severe than the ones found in the *cdh11*^{sa14413} mutant (Figure 9 and 10, Supplementary figures 7 and 8).
This result raises three hypotheses:
1 - The *cdh11*^{MO} is not specific and the phenotypes correspond to off-target effects (Eisen & Smith, 2008; Kok et al., 2015)
2- *cdh11*^{sa14413} is not a null mutant and the Cdh11 truncated protein still maintains some of its function (Dalila, 2015)
3- *cdh11*^{MO} is specific and the *cdh11*^{sa14413} mutant is a null mutant. In this scenario, we would argue that the absence of LR phenotypes in this mutant is due to the activation of compensatory mechanisms in the mutant embryos that are not activated in the context of the morpholino injection (Rossi et al., 2015).

Regarding the **first hypothesis**, the use of morpholinos to evaluate the putative new function of a gene has been widely debated due to the prevalence of off-target effects in embryos injected with morpholinos, leading to a discrepancy between morphant and mutant phenotypes (Kok et al., 2015). The

specificity of the morpholino can be tested either through a classic rescue experiment or by injection in a null-mutant (Blum et al. 2015; Eisen & Smith, 2008; Stainier et al., 2017). We started by preparing the rescue experiment. However, at a certain point, the embryos injected with the *cdh11*^{MO} morpholino started to show malformations that were never observed in previous assays. This probably occurred due to degradation and loss of efficacy of the morpholino (Bill, Petzold, Clark, Schimmenti, & Ekker, 2009). So, instead of pursuing this experiment by ordering a new stock of *cdh11*^{MO}, we decided to consider the other two hypotheses.

Previous work has raised the **second hypothesis**, suggesting that this *cdh11*^{sa14413} mutant line is not a null-mutant (Silva 2017). In the Cdh11 protein of these embryos, a premature STOP codon is located at EC4 and a truncated protein could still be produced and retain some functionality (Supplementary figure 1). Cdh11 domains such as Extracellular Domain 1 (EC1) are responsible for homophilic interactions (Ivanov et al., 2001) and, if unattached to the cell membrane, are free to bind with other Cdh11 molecules. Furthermore, this cell adhesion molecule can also participate in heterophilic interactions with other cadherins. One example is Cdh2 which is also expressed in the IM (Straub et al., 2003). Consequently, in this line, the Cdh11 protein may still be functional by interacting with other Cdh11 molecules or different cadherins, such as Cdh2.

The **third hypothesis** suggests that, as described in an earlier study, mutant embryos may not display the expected phenotype because they could activate a genetic compensation program (Rossi et al., 2015). In order to analyse this hypothesis, the expression pattern of *cdh6* and *cdh17* (cadherins expressed in some of the same domains as *cdh11*, such as the IM) was observed at 8-somite stage by WISH in the *cdh11*^{sa14413} mutant embryos. However, no differences were detected in their expression (Silva 2017).

Further tests are necessary in order to better understand the *cdh11*^{sa14413} mutant line: experiments can be designed to observe the function of the truncated Cdh11 protein and the role of Cdh2, especially its interaction with Cdh11. Furthermore, the compensatory program in mutant embryos can be studied by looking for upregulated genes in these embryos, through a microarray or RNA sequencing assays (Silva 2017).

When describing the function of a new gene, the results obtained by morpholino injection should be reproduced by a *cdh11* null-mutant line (Eisen & Smith, 2008). In *cdh11*^{sa14413} mutant embryos, however, a truncated Cdh11 protein might still be produced and so this mutation may not be effective in knocking out *cdh11*. Consequently, we decided to use the CRISPR-Cas9 genome editing system to produce a new *cdh11* mutant (Gagnon et al., 2014). This was done by synthesizing three small guide RNA molecules (gRNA) that target different functional domains of Cdh11: the signal peptide, the third extracellular domain and the transmembrane domain (denominated gRNA1, 2 and 3 respectively) (Figure 14). These gRNAs were designed to prevent the protein from reaching the membrane by either directly inducing mutations in the signal peptide or the transmembrane domain, or by truncating the protein, preventing the synthesis of one of these two domains.

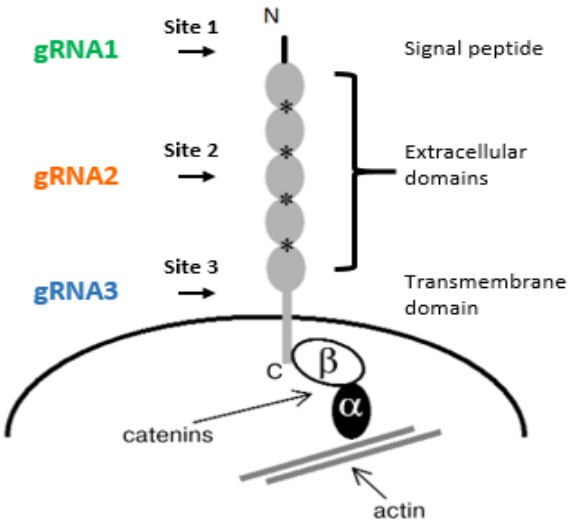

Figure 14 - Structure of classical cadherins with the functional domains. gRNA1 was designed to target the signal peptide (site1), gRNA2 the fourth extracellular domain (site 2) and gRNA3 the transmembrane domain (site 3). Adapted from Ivanov 2001

The injection mixture was prepared by adding the gRNAs and Cas9 before each injection session and then the embryos were injected at the 1-cell stage (Gagnon et al., 2014). We tested different gRNA combinations and different concentrations of gRNA and Cas9 (Table 1). The following analysis describes the results obtained from injecting gRNA1 and gRNA2 together, both at 293,3 ng/µL, with the Cas9 protein at 800 ng/µL. To access the mutagenesis efficiency, we analyzed the embryos at 24 hpf using the T7 Endonuclease assay, and observed their phenotype at 50 hpf.

3.2.1 - T7 Endonuclease I assay reveals the occurrence of mutagenesis

To analyze the mutagenesis efficiency at 24 hpf we extracted the genomic DNA from 26 of the gRNA1+2 injected embryos, in pairs (Meeker et al., 2007). For each paired sample, we amplified by PCR each gRNA binding regions (site 1 and site 2) (Figure 15). The samples were then treated with T7 Endonuclease I (T7EI) in order to observe the level of mutagenesesis. In this assay, the DNA samples are denatured and re-annealed, and heteroduplex DNA can form, resulting from the annealing of DNA strands that have been modified by the Cas9 with DNA strands without modification. T7 Endonuclease I recognizes these mismatches and cleaves the DNA (Vouillot et al., 2015). The result of this assay can be observed by agarose gel electrophoresis, through the detection of smaller, digested fragments.

In the first T7EI assays, we tested several combinations of gRNAs and Cas9, and collected the injected embryos in groups of 10, as described in previous experiments (Gagnon et al., 2014; Vouillot et al., 2015). However, the cleaved fragments were very faint in these batches (Supplementary Figure 9). We hypothesized that, by analyzing 10 embryos at the same time, the percentage of mutated strands in the sample would be too low for detection in the agarose gel, and so we decided to collect the embryos in pairs. For this assay, we used the gRNA1+2 mixture because, of all of the combinations, this one had shown the strongest mutated fragments in the first round of analyses (Supplementary Figure 9).

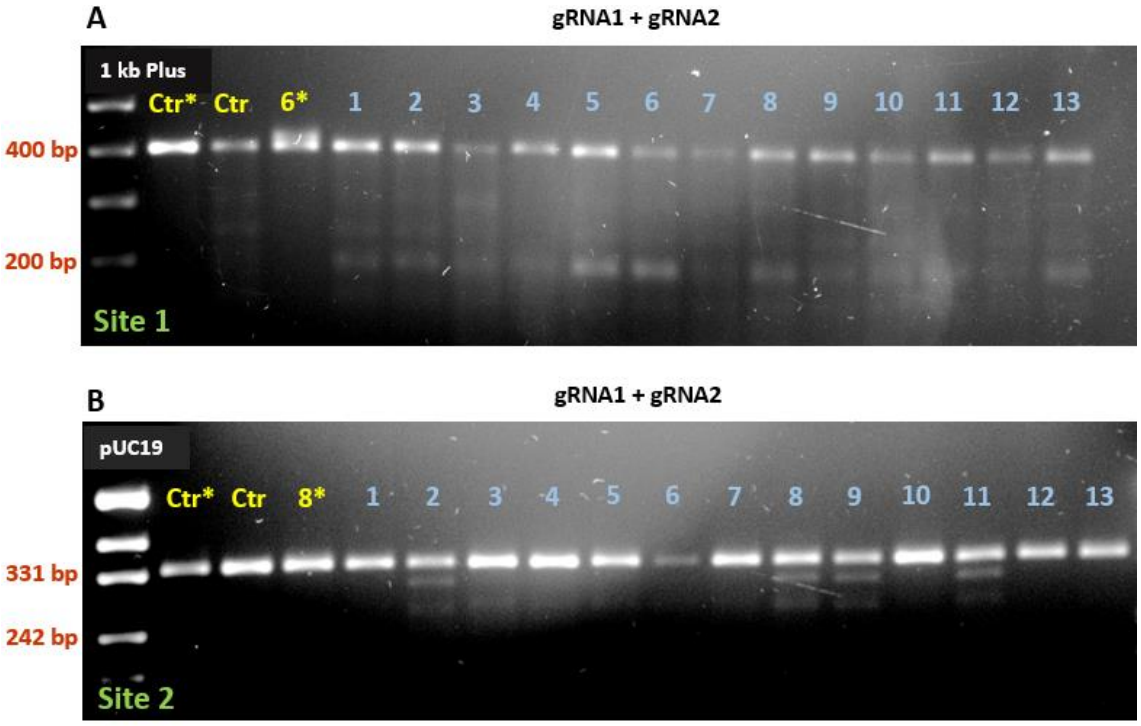

Figure 15 - T7 Endonuclease assay supports the existence of mutagenesis events in embryos injected at the 1-cell stage with a mix of gRNA1 and gRNA2. Detection of shorter fragments, digested with T7 Endonuclease I, indicates that mutations are occurring at the *cdh11* binding site 1 **(A)** and site 2 **(B)** binding site. **Lanes Ctr*, Ctr, 6*,8* and 1 to 13 –** Each lane contains DNA extracted from two embryos, collected at 24 hpf. **Lane Ctr* –** Control sample undigested with T7 Endonuclease I. **Lane Ctr –** Control sample digested with T7 Endonuclease I. **Lane 6* and 8* –** sample **6** and **8**, respectively, undigested by T7 Endonuclease I. **Lanes 1-13 –** Experimental embryos treated with T7 Endonuclease I (each sample contains 2 embryos at 24hpf).

After injections with the mixture of gRNA1 and gRNA2, we performed PCR assay for both target sites, site 1 (for gRNA1) and site 2 (for gRNA2). At site 1 we could observe one strong fragment aligning at approximately 400bp and, in most lanes, a weaker fragment at approximately 200bp (Figure 15A). From the design of the primers used in this PCR assay, we know that the amplicon from site 1 should have approximately 398bp (Supplementary Figure 6), which may correspond to the stronger fragment present on the agarose gel (Figure 15A). Furthermore, we can estimate that, if Cas9 cleavage induces a mutation, two fragments of approximately 201bp and 197bp should be detected after T7 Endonuclease digestion (Supplementary Figure 6) (Wu et al., 2015). So, the smaller fragment observed at the range of 200bp in the gel could correspond to the overlay of these two products, since they have similar sizes (Figure 15A). Furthermore, we could observe that at site 1 some of the undigested sample has migrated above the amplicon band (lane 6*). This extension might correspond to heteroduplexes, formed by the annealing of mutated and non-mutated strands of DNA (Figure 15A) (Vouillot et al., 2015).

In the PCR amplification of the DNA site 2 (i.e. gRNA2 binding site) we could observe one clear product close to the 331bp, and in some of the lanes, at least two fragments with a lower size, between the 331bp and 242bp (Figure 15B). With this pair of primers we expect an amplicon from site 2 of approximately 334bp (Supplementary Figure 6), which seems to match with the stronger PCR band in the gel (Figure 15B). Additionally, if Cas9 produces a cleavage that induces a mutation in any of the embryos injected with the gRNA1+2, the T7EI digestion will cut the original amplicon from site 2 in two fragments of

approximately 86bp and 248bp (Supplementary Figure 6) (Wu et al., 2015). However, both of the observed fragments aligned closer to the 331bp (Figure 15B).

Overall, the detection of smaller digested fragments of DNA which do not appear in our control (non-injected embryos), after treatment with T7EI, means that Cas9 has successfully cleaved the DNA strand and induced mutations in both site 1 (at least 9 out of 13 batches) and site 2 (5 out of 13 batches) even if in the latter the sizes of the fragments do not correspond to the expected sizes. This can be tested by sequencing the fragments digested by T7 to determine how they are being cleaved.

Additionally, we can estimate the level of genetic modification through the intensities of the fragments in the gel, comparing the different injected samples with the control sample. A sample with higher level of modification will have a higher percentage of cleaved fragments, and consequently a less intense original amplicon fragment (Guschin et al., 2010).
In the assays above, instead of analysing batches of 10 embryos, we grouped them in pairs. This increases the absolute amount of mutated strands in the total sample. However, since each batch contains fewer embryos, the different rates of mutagenesis will be less noticeable over the individual variation between embryos. Therefore, in order to detect the level of modification we calculated a mean value for the injected samples (13 samples) and compared to the control (Ctr lane) We calculated that the level of modification was 42,9% for site 1 and 45,3% for site 2.
This means that close to 50% of the DNA strands were mutated in both gRNA sites in this assay.

3.2.2 – Left-Right phenotypes in the heart and gut are not observed in the F0 population of *cdh11* CRISPR-Cas9 mutants

After injecting the mixture of gRNA1 and gRNA2, we not only wanted to detect the level of mutagenesis but also whether the knockdown phenotypes could be reproduced in the heart and the gut. While the CRISPR-Cas9 system is usually used to create non-mosaic knockout animals by selecting founders for germline transmission (Hwang et al., 2013), recent experiments have demonstrated that it is possible to replicate loss-of-function phenotypes in the injected population (F0) (Burger et al., 2016; Jao et al., 2013; Ribeiro et al.,, 2017).

In order to observe the laterality of the gut at 50 hpf, we injected the gRNA1+2 mixture with Cas9 in Tg(*sox17*:EGFP) embryos which, at this stage have the gut as well as the pancreas and liver labelled in green fluorescence (Sakaguchi et al., 2006; Sampaio et al., 2014). The heart could be seen live at 50 hpf.

At 50 hpf, all of the injected embryos showed the normal "D-loop" heart conformation (Figure 13B) and WT gut phenotype (Figure 9A). These phenotypes were detected after injecting the gRNA1+2 mixture, and also in all of the different gRNA and Cas9 combinations and concentrations tested (Table 1). These results mean that the knockdown phenotypes were not seen in the founder population. However, this phenotype distribution does not necessarily correspond to the mutant conformation, since injected embryos are most likely to be mosaic for the resulting genomic mutations and so we have to be cautious in establishing a phenotype-genotype correlation in this population (Schulte-Merker & Stainier, 2014). Therefore, in order to develop a new mutant line for further analysis, we injected a new batch of embryos with the gRNA1+gRNA2 mixture and Cas9 in the same conditions. The embryos are now growing in the IMM fish facility.

Is *cdh11* expressed in Left-Right associated tissues?

In this work we aimed to understand the role of Cdh11 in the establishment of Left-Right asymmetry in zebrafish. Previously in our lab, we demonstrated that the knockdown of *cdh11*, during the early stages of development, leads to laterality defects both in the heart and the gut. (Silva 2017). The *cdh11* transcript was not detected by WISH in any of the known LR patterning tissues. At 8ss, the period in which the asymmetry is being established, *cdh11* is expressed in the Neural Tube (NT) and Intermediate Mesoderm (IM), but not in LR related tissues such as the Kupffer's Vesicle (KV) or the Lateral Plate Mesoderm (LPM) (Figure 12A). Later, at 20ss and 24 hpf its expression was detected in the otic vesicles and Pronephros, but again, not in the KV or LPM (Figure 12B) (Silva 2017, Clark et al., 2011).

In order to describe the pattern of the Cdh11 protein through immunohistochemistry and Western blot assays, two custom made antibodies were synthesized. However, neither of the experiments performed showed a specific pattern of this protein, thus questioning the efficiency of these antibodies (Silva 2017).

After observing that the knockdown of *cdh11* has an effect in the establishment of LR, describing the Cdh11 expression pattern during development became even more crucial. Thus, we decided to look for new convincing evidence for the expression of *cdh11* at the most important steps in the establishment of LR in the zebrafish.

3.3 – Where is *cdh11* expressed at the breaking of symmetry?

Arguably, the first defining moment in the establishment of LR during development happens in the zebrafish Left-Right Organizer (LRO), the Kupffer's Vesicle (KV) (Yoshiba 2012, Yuan et al., 2015). At the start of organogenesis, the first detected asymmetric signal is the expression of *dand5* in the posterior end of the KV. This signal is initially expressed bilaterally from 5ss to 7ss and then becomes clearly asymmetric on the right side by 8ss (Lopes et al., 2010). Therefore, we decided to first confirm whether *cdh11* is expressed in or close to the KV during these stages.

3.3.1 – New *in situ* hybridization assays suggest that *cdh11* is expressed around the Kupffer's Vesicle.

In previous experiments, we were not able to detect the expression of the *cdh11* transcript in any of the known LR tissues through WISH. However, other WISH experiments with a *foxa3* probe, which labels the gut, pancreas and liver at 50 hpf (Warga & Nüsslein-Volhard, 1999), showed that using the chromogenic substrate NBT/BCIP instead of BM Purple highly improved the staining definition.

Given this result, we thought that the chromogenic substrate could also influence the *cdh11* detection. Therefore, we performed a new WISH experiment with the *cdh11* probe, using the chromogenic substrate NBT/BCIP in parallel with BM Purple in WT embryos at 5ss. We observed that, in both substrates, the *cdh11* seem to be expressed in the cells that surround the KV at 5ss (Figure 16 A-B) and this pattern is more explicit with NBT/BCIP, where the background staining is lower (Figure 16B). Curiously this pattern was observed at 5ss but not at 8ss. However, when sectioned, this design could not be detected in the KV or around this organ in any of the embryos (Figure 16C)

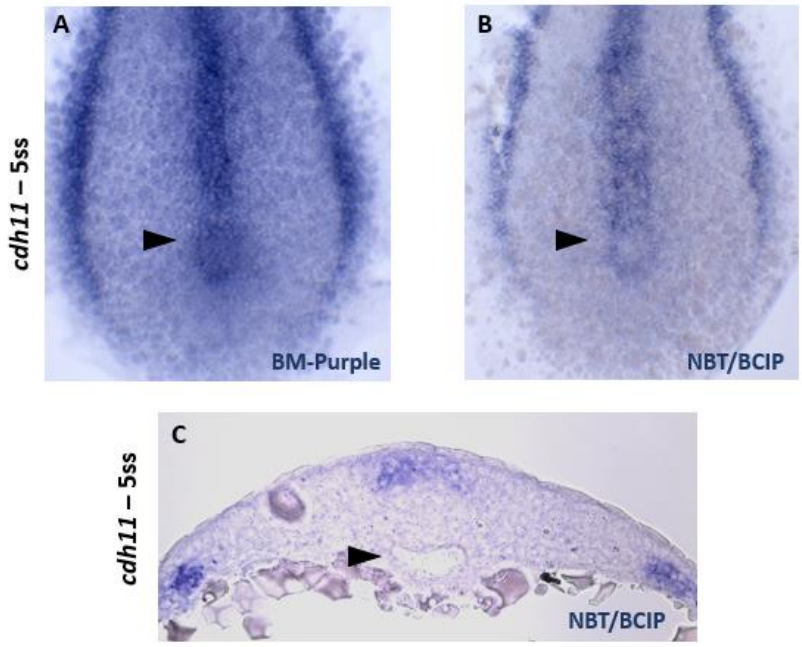

Figure 16- *cdh11* expression pattern obtained using two different chromogenic substrates BM-Purple and NBT/BCIP in WT embryos at 5ss. Caudal end of 5-somite stage embryos hybridized with *cdh11* mRNA probe, developed with two different chromogenic substrates: BM-Purple **(A)** and NBT-BCIP **(B).** Anterior to the top; Posterior to the bottom. **(C)** Embryo section at 5ss. (black arrow head indicates the Kupffer's Vesicle). Dorsal to the top; Ventral to the bottom.

This pattern apparently around the KV might in fact correspond to the underdeveloped NT. Between 4ss and 14ss the posterior neural tissue converges medially, elongates and is shaped into a ''rod-like'' structure (Harrington 2010).This means that neural tissue has migrated medially in 8ss embryos but not in some of 5ss embryos, producing a circular pattern of *cdh11* expressing cells of the NT over the KV.

This result shows that, on one hand, the chromogenic substrate does in fact affect the quality of the WISH assay. However, it also indicates that *cdh11* transcript might not be expressed in the KV or its surrounding cells at 5ss.

3.3.2 - FACS profiling identifies three GFP-expressing sub-populations of cells in *sox17*:EGFP embryos at 8ss.

The WISH assays previously suggested that *cdh11* is not expressed either in the KV cells or around it, at 5ss. However, in these embryos the staining is still not very clear and the background is still noticeable. Furthermore, WISH analysis may not be able to in identify targets that have low DNA and RNA copies, which may be our case (Jensen, 2014). Consequently we needed a new approach to evaluate the presence of *cdh11* in the KV.

We decided to isolate the KV cells from the rest of the embryo, and as a consequence from the rest of the *cdh11* expressing tissues, so that we could analyse the expression of *cdh11* in these specific cells. This assay was performed at 8ss, using the *sox17*:EGFP line, which at this stage only labels the KV and endodermal cells of the embryo (Sakaguchi et al., 2006; Sampaio et al., 2014)

First, we analysed the GFP intensity in whole *sox17*:EGFP embryos under a fluorescent dissecting stereoscope. As illustrated in Figure 17A-B, at 8ss the KV cells show a GFP level that is clearly higher than the signal of endodermal cells. This information allowed us to isolate the KV cells through fluorescence activated cell sorting (FACS). Using this technique, we could describe and collect individual cells according to characteristics such as size, granulosity or fluorescent signal (Ibrahim &

Van Den Engh, 2007). Thus, we could confidently identify and sort the KV cells from the endodermal cells and other tissues based on the intensity of the GFP signal. We collected 100 embryos from *sox17*:EGFP line at 8ss, as well as from WT embryos used as a control. The samples were prepared as described in Experimental Procedures, and then analysed in the FACS sorter (Figure 17C-D).

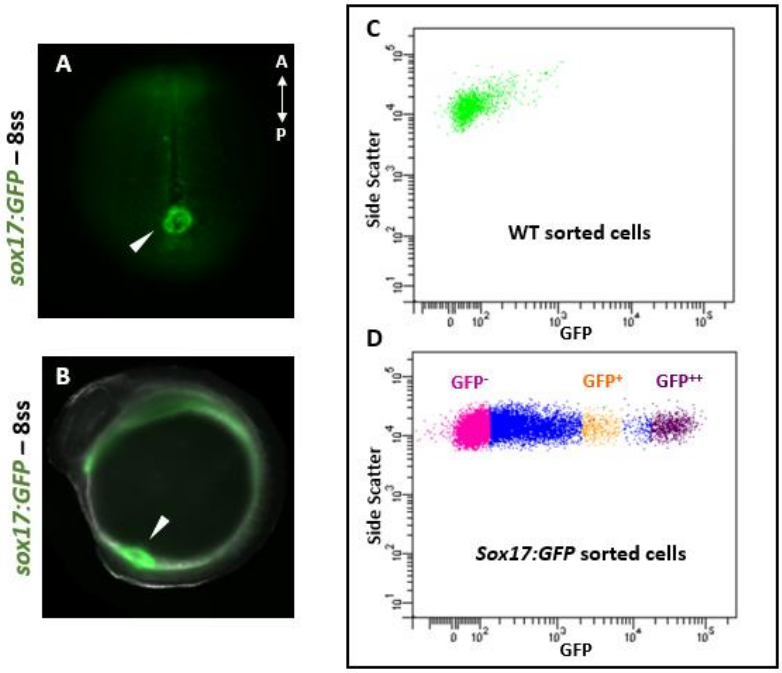

Figure 17- Three GFP-expressing populations are sorted after FACS profiling of *sox17*:EGFP transgenic embryos. A – Dorsal view, anterior to the top, of a *sox17:*EGFP embryo at 8ss. KV cells (white arrow head) strongly express GFP and endodermal cells express GFP at lower levels. **B** – Lateral view, anterior to the left, of a *sox17:*EGFP embryo at 8ss. Overly of fluorescence and dark field channels. (KV – white arrow head). **C** - FACS profile from 100 WT embryos at 8ss used to define the levels of embryo auto-fluorescence. **D** - FACS profile from 100 *sox17:*EGFP embryos at 8ss highlighting 3 GFP selected sub-populations. In growing order of GFP intensity: **GFP^{-}**: cells with GFP signal equivalent to WT embryo cells; **GFP^{+}**: cells corresponding to endodermal cells; **GFP^{++}**: cells corresponding to KV cells. (GFP- Green fluorescent protein; RFP – Red fluorescent protein)

The profile of the *sox17*:EGFP embryos showed a clear cell distribution by GFP signal intensity (horizontal axis) (Figure 17D). WT embryos cells, which do not express GFP, are used as a control for the auto fluorescence of the cells (Figure 17C). Under fluorescent microscopy we had seen that the GFP level was clearly higher in the KV cells than in the endodermal cells (Figure 17 A-B). Thus, using the FACS profile of the *sox17*:EGFP embryos, we selected and sorted three sub-populations of cells according to GFP intensity (Figure 17D):

- **GFP^{++}**, with the strongest GFP signal. This sub-population corresponds to the KV cells.
- **GFP^{-}**, with the lowest GFP signal, coinciding with the level of auto-fluorescence of the cells. This sub-population includes the cells that do not express *sox17*:EGFP, which means no KV nor endodermal cells.
- **GFP^{+}**, with a GFP level between **GFP^{-}** and **GFP^{++}**. These correspond to the endodermal cells.

Overall, FACS profiling allowed us to identify and isolated three sub-populations of cells from the *sox17*:EGFP line, at 8ss, according to GFP intensity (denominated **GFP^{-}**, **GFP^{+}** and **GFP^{++}**).

3.3.3– PCR assays indicate that *cdh11* is expressed in the endodermal cells.

Our main goal was to observe whether *cdh11* was expressed in the KV cells at 8ss. For that we used the three different sub-populations isolated using FACS and decided to analyse the expression of *cdh11* in each group.

From each sorted sub-population, we extracted the total mRNA and produced the respective cDNA in order to detect the expression of *cdh11* through a PCR assay. As a control we also performed a PCR for the *dand5* locus, because this gene is expressed exclusively in the KV by 8ss, and it was used as a control for the presence of KV cells in the collected sub-populations (Hashimoto et al., 2004). The same extraction and treatment was performed for whole WT embryos at 2 hpf and 8ss which correspond to the negative and positive controls for the expression of both genes. The samples were amplified and observed after a 2.5% agarose gel electrophoresis (Figure 18).

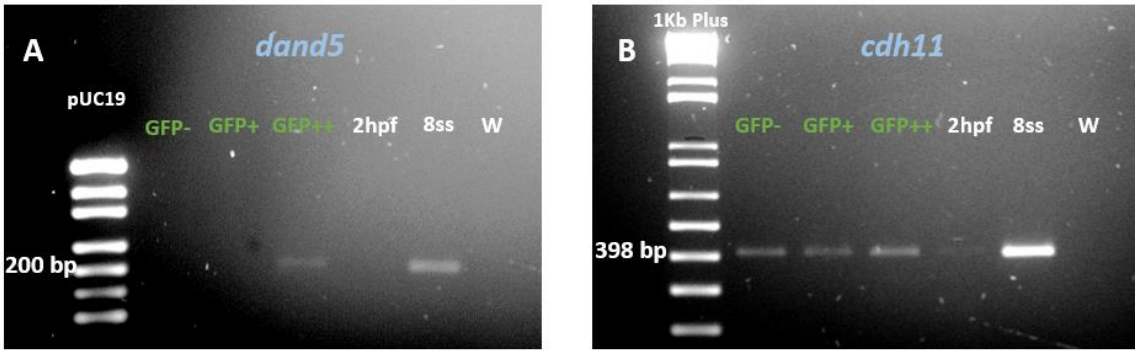

Figure 18 - Expression of *cdh11* is detected in all three GFP sub-populations. A – cDNA amplified by PCR with *dand5* specific primers. Amplicon with 200 bp. **B** – cDNA amplified by PCR with *cdh11* **site 1** primers. Amplicon with 398 bp. **GFP**$^{-}$ corresponds to cells with a GFP signal equivalent to WT cells, **GFP**$^{+}$ corresponds to endodermal cells and **GFP**$^{++}$ corresponds to KV cells sorted from the *sox17*:GFP transgenic line. Samples labelled **2 hpf** and **8ss** correspond to WT whole embryos at the stated developmental stages. Sample **W** corresponds to the PCR negative control.

In the case of *cdh11*, the transcript was present in all three sub-populations (Figure 18B), while *dand5* was detected in the **GFP**$^{++}$ population and not in the other two sub-populations (Figure 18A). As expected neither transcripts were detected in the 2 hpf negative control. In the 8ss control embryos, the expression of both genes was observed (Figure 18).

Overall, the fact that *cdh11* is present in all three sorted sub-populations suggests that, at 8ss, *cdh11* gene is not only expressed in the IM and NT, as previously demonstrated, but also in the endoderm, which had not been described so far. The expression of *dand5* indicates that we have KV cells only in the **GFP**$^{++}$ sub-population.

3.4 – Expression of *cdh11* in the Intermediate Mesoderm and Pronephros

The Intermediate Mesoderm (IM) is located at the ventrolateral edge of the paraxial mesoderm. It will give rise to blood cells and by 24 hpf it has developed into the Pronephros (PN) (Drummond et al., 2016). In our hypothesis, we described that the IM and later the PN could influence the establishment of LR asymmetry through the action of Cdh11.

3.4.1 – The Pronephros could have a role in the asymmetric migration of LPM during the displacement of the gut.

It has been shown that, between 24 and 30 hpf, the LPM asymmetrically migrates over the developing endoderm, displacing the gut to the left. This movement is required for the correct loop-sided development of the liver and pancreas and is dependent on LR signalling (Horne-Badovinac, 2003). Using a loss-of-function approach, we saw that in *cdh11* morphants the laterality of the gut is disrupted (Figure 9). Due to the proximity of the PN to the LPM at this stage (Drummond et al., 2016), the PN could have a role in organ laterality displacement. In order to test this possibility, we wanted to first characterize the position of both the PN and the gut during the looping of the gut (between 24 and 30 hpf).

Previously in this project, we tried to observe the asymmetric migration of the LPM through sections of *sox17*:EGFP transgenic embryos (labelling the endoderm) and immunostaining with a mix of ZO-1 (labelling tight-junctions, for polarity) and phalloidin 488 (labelling F-actin, for the shape of the cells). Even though we were able to reproduce the results obtained by Horne-Badovinac, this immunostaining combination does not allow us to see the PN during the displacing of the gut (Supplementary Figure 2). We could have used Cdh11 antibodies to detect the PN at this stage, but we have seen that immunohistochemistry assays were not successful with these antibodies (Silva 2017).

To overcome this problem, we did separate assays to observe the localization of the looping gut and the PN. Our first approach was to characterize the exact location of the gut looping process in the embryo. We used the Tg(*sox17*:EGFP) line which at 24-30 hpf labels the gut endoderm (Sakaguchi et al., 2006; Sampaio et al., 2014) and we overlapped this expression with the bright field channel, where we could see each pair of somites (Figure 19B-C). Using this combination, we confirm that the gut looping takes place mainly between the first and third somite pairs of the embryo, as previously described (Yin et al., 2010) (Figure 19B-C).

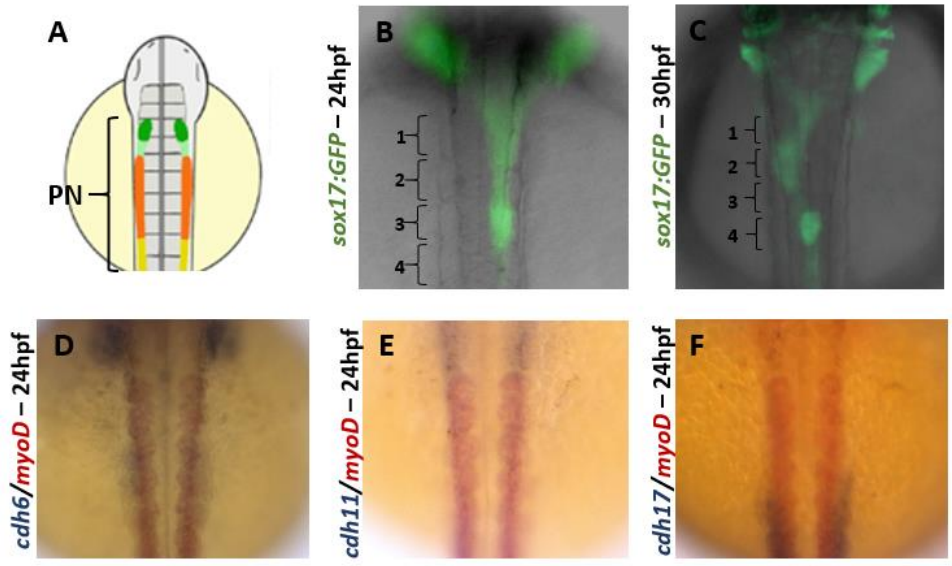

Figure 19 - Gut looping occurs at the level of the first to the third somite pair. A- Schematic representation of the positioning of the Pronephros (**PN**) relative to somite pairs (grey) at 24 hpf (adapted from Marra and Wingert 2014). **B** - Dorsal view of a *sox17*:GFP embryo at 24 hpf exhibiting the extension of the gut before looping (somite pairs numbered with brackets). **C** -Dorsal view of a *sox17*:GFP embryo at 30 hpf exhibiting the extension of the gut after looping (somite pairs numbered with brackets).**D-F** - Dorsal view of WT embryos at 24 hpf hybridized with *cdh6* (**D**), *cdh11* (**E**) and *cdh17* (**F**) in blue, and *myoD* in red.

Next, we wanted to observe which part of the PN is indeed aligned with the gut looping region, given the fact that previous studies did not always agree on the positioning of these structures (Huang et al., 2008; Wingert et al., 2007; Yin et al., 2010). This was done by observing the expression pattern of *cadherin 6* (*cdh6*) and *cadherin 17* (*cdh17*), as well as the pattern of *cdh11* at 24 hpf. Both *cdh6* and *cdh17* are expressed in the IM and PN like *cdh11* (Horsfield et al., 2002; Kubota et al., 2007). At 24 hpf *cdh6* is expressed in the anterior region of the pronephric duct and nephron primordium (Kubota et al., 2007), while *cdh17* is detected in the posterior portion of the PN (Horsfield et al., 2002). We performed a double WISH with each of these cadherins alongside *myoD*, which at 24 hpf is expressed in the somites (Weinberg et al., 1996).
We could see that that the expression of *cdh6* reaches the third somite pair (Figure 19D), while *cdh17* only reaches between the fourth and the fifth pair (figure 19E). The expression of *cdh11* is not clear enough to identify its boundaries (figure 19F).

These results show us that the gut looping region and the Pronephros overlap slightly. We have seen that the gut looping occurs between the first and third somite pairs (Figure 19B-C), while the expression of *cdh6* indicates that the anterior end of the PN, the nephron primordium, reaches the third somite pair (Figure 19D). This analysis should be complemented by observing the migration of the LPM compared with the somite pattern, but due to time constrains this was not performed. Nevertheless, this result strengthens the hypothesis that the PN could influence the asymmetric migration of LPM.

3.4.2 – Developing a new method to study the role of the Intermediate Mesoderm in Left-Right asymmetry

After being activated, Spaw is transferred from the KV to the left LPM between 10ss to 12ss, activating the Nodal cascade (Long et al., 2003). As we mentioned before, the IM is a tissue that lays between the KV and LPM and therefore, could play a role during the signal relay. In this project we demonstrated that the knockdown of *cdh11* lead to laterality phenotypes, including the randomization of the expression of *spaw* and *pitx2* in the LPM by 20ss and 24ss, respectively (Figure 11). However, we still have not been able to produce any convincing evidence that the IM plays a role in the establishment of LR asymmetry through Cdh11.

In order to test the necessity of this tissue in LR asymmetry, we intended to generate a targeted cell ablation line using the Nitroreductase (NTR)-Metronidazole (Mtz) system (Curado et al., 2008). In this technique, cells expressing the NTR enzyme are capable of converting the non-toxic prodrug Mtz into a cytotoxic compound that induces the death of these cells without affecting the neighbouring cells. NTR is under the control of a tissue-specific promoter, usually attached to a fluorescent protein, and the cytotoxic compound is only formed when Mtz is added into the water, meaning that the reaction is both spatially and temporally controlled (Curado et al., 2008). We selected *cdh17* as the promoter. This cadherin is expressed in the IM since the first stages of development and later in the PN (Horsfield et al., 2002). As we had seen, by 24 hpf, *cdh17* is only expressed in the posterior region of the PN and thus might not directly affect the gut looping region, but, as far as we know, this is the only cadherin expressed exclusively in the IM and the PN.

To produce our construct, we used the Osx:mCherry-NTRO plasmid as the vector (Renn and Winkler 2009), in which the mCherry and NTR are under control of the Osx promoter. The *cdh17* promoter was obtained from the pSceI-cdh17prom-eGFP-cdh17intron plasmid (Sanker et al., 2013)

(Supplementary Figures 4 and 5). In order to restrict the expression of this plasmid to *cdh17* expressing cells we replaced the Osx promoter with a *cdh17* promoter.

Initially we used the enzymes KpnI in the NTRO vector and XhoI in the cdh17 vector. In order for the fragments to ligate we produce blunt ends by digesting them with Klenow fragment. Then both vectors were cut with BamHI, observed in an agarose gel and the required fragment from each vector was excised (Figure 20). The new NTRO vector and the *cdh17* fragment were ligated and transformed into competent cells.

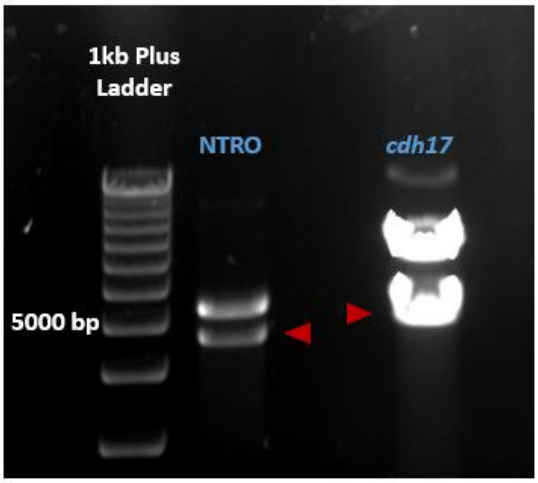

Figure 20 – Plasmid vector and insert fragments for ligation were detected and extracted from the agarose gel. Samples observed after digestion with Acc65I and BamHI (**NTRO** plasmid) and XhoI and BamHI (***cdh17*** plasmid). The new vector corresponds to the NTRO fragment and the insert to the *cdh17* fragment. Red arrow top – extracted fragments

After several attempts we were never able to grow bacteria transformed with our construct.
Initially we calculated the efficiency of the DH5α strain competent cells and used a different batch as well. We tried different ratios of vector vs fragment. We also replaced the KpnI enzyme with its isoschizomer Acc65I which has a 5' overhang and is more easily blunted by the Klenow fragment. However, only the cells transformed with the control NTRO vector grew. Alternatively we tried using the T4 DNA Polymerase as a blunting enzyme, in place of the Klenow fragment, but the result was the same.
In face of all these setbacks we should consider a different approach to produce the *cdh17* restricted ablation line construct, such as using different starting plasmids.

3.5 – Is Cdh11 expressed in the LPM?

In previous experiments, the expression of *cdh11* has not been detected in any of the LR associated tissues of the embryo, including the LPM. However, after *cdh11* knockdown both the heart and gut conformations were altered (Figures 9 and 10). The LPM is crucial for the development of both these organs: both the heart primordia and the required LR information come from the LPM, while the migration of this tissue drives the displacement of the gut (Horne-Badovinac, 2003; Staudt & Stainier, 2012). We wanted to confirm whether *cdh11* was indeed expressed in the LPM at the start of heart development and looping of the gut. Earlier in this investigation, we saw that the use of a different chromogenic substrate, such as NBT/BCIP improved the staining pattern in WISH assays (Figure 16A,B). Therefore, we hybridized WT embryos at 20ss with the *cdh11* probe and used both NBT/BCIP as chromogenic substrates. We observed a clear pattern of expression of *cdh11* in the anterior LPM at

this stage (Figure 21 A,B). After sectioning we confirmed that the expression corresponded to the LPM, albeit with slight variations along the A-P axis (Figure C1,2).

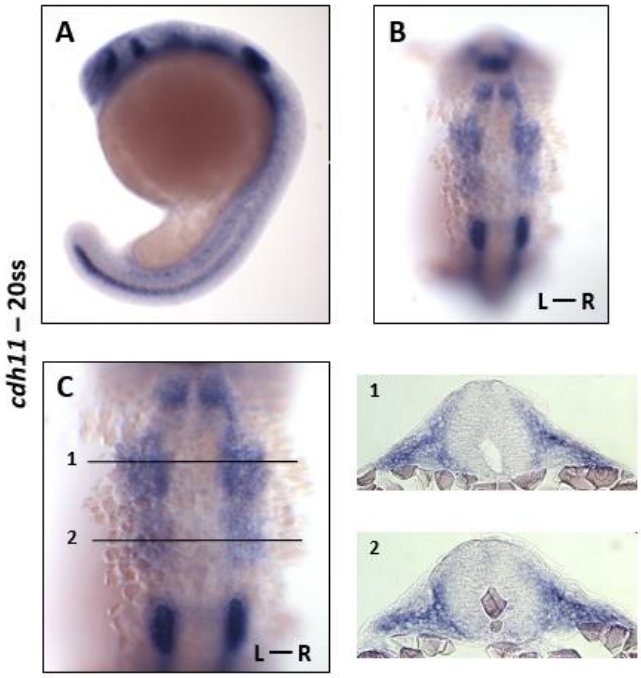

Figure 21 - *cdh11* is expressed in the anterior LPM at 20-somite stage. A 20-somite stage embryo hybridized with a *cdh11* mRNA probe and NBT/BCIP chromogenic substrate. Lateral view (**A**). Dorsal view (**B**), anterior to the top. (**C**) Magnification of (B) showing the transverse sections at the levels of the lines **1** and **2**. L – Left, R – Right.

This means that Cdh11 could be affecting the development of the heart and the gut by acting directly through the LPM. While this result should be confirmed through other techniques, the expression of this gene in the LPM raises new hypothesis for the role of Cdh11 during development.

Chapter 4 - Discussion

4.1 – Determining the specificity of the knockdown LR phenotypes

In this project, we have shown that knocking down *cdh11*, through the action of a splice-blocking morpholino (MO), induces several LR associated phenotypes (Figures 9 and 10).
To independently validate our results, we wanted to analyse a *cdh11* mutant line. As previously mentioned, we ordered a *cdh11*^{sa14413} mutant line from the EZRC. However, when analysed, this *cdh11*^{sa14413} mutant line did not show any of the phenotypes observed by us and other groups using the *cdh11*^{MO} (Clendenon et al., 2009; Clendenon et al., 2012).

The suitability of morpholino assays in development has been hotly debated throughout the years since their origin (Ekker, 2000; Heasman et al., 2000; Nasevicius & Ekker, 2000). The use of MOs has several advantages: the ability to test different dose-dependent effects of a gene; combining different MOs to target multiple gene products, and also the ability to target the maternal mRNA along with the zygotic product (Blum et al., 2015). MOs have been used as a tool to disrupt the function of the genes that were not covered by forward genetic screens, as well as a complementary approach to support the results obtained in mutants (Stainier et al., 2017).

On the other hand, the use of MOs also includes several downsides. The effect is not permanent, usually only lasting a few days, and it is difficult to determine how effectively the target protein has been knocked down (Eisen & Smith, 2008). One of the major disadvantages of using MOs is the possible occurrence of off-target effects in injected embryos. In order to guarantee the specificity of each MO, several guidelines have been proposed throughout the years. In this list, we can find suggestions such as the use of a control morpholino in parallel to the experimental one; performing rescue experiments by co-injecting a form of the targeted RNA that is not recognised by the morpholino; and designing at least two MOs for each target gene, one translation-blocking, the other splice-blocking (Blum et al., 2015; Eisen & Smith, 2008; Stainier et al., 2017).

During this project, due to technical setbacks, we were unable to follow thoroughly these guidelines. As mentioned before, we stopped using the *cdh11*^{MO} after the apparent degradation of the working stock solution. In order to confirm the specificity of the MO used in our knockdown analysis we should have performed a classic rescue experiment with a new vial of the same MO used previously (Clendenon et al., 2008). This assay would consist in the injection at the 1-cell stage embryos of a synthesized capped *cdh11* sense mRNA along with the experimental morpholino. If the *cdh11*^{MO} is specific, we expect that the phenotypic effects observed during this work to be reversed when co-injected with *cdh11* sense mRNA (Bill et al., 2009). Additionally, the specificity of this MO could be confirmed by analysing the possible LR phenotypes resulting from the injection of a different *cdh11* MO. In our case, we could use a translation-blocking MO, by opposition of the one used by us (splice-blocking MO (Clendenon et al., 2008)). Both morpholinos should be tested independently to ensure that they induce similar phenotypes, and also simultaneously to test for synergism (Eisen & Smith, 2008).

4.2 – Confirming the morpholino assays with a new mutant line

As described in the literature, the analysis of a phenotype resulting from MO injection without a genetic mutant comparison, should be viewed very critically (Schulte-Merker & Stainier, 2014; Stainier et al., 2015), and in the *cdh11*^{sa14413} mutant line we did not observe the LR phenotypes initially seen after injection of *cdh11*^{MO} (Figures 9-11, Supplemetnatery Figures 7 and 8). This discrepancy indicates that

one of the assays is not working properly, but ultimately might mean that disruption of this gene does not in fact affect LR. In one hand, the lack of concordance between mutant and morphant embryos has been observed before (Law & Sargent, 2014), and MO induced phenotypes have been found to be more severe than the corresponding mutants (Kok et al., 2015). This can occur due to the already mentioned off targets of the MO (Kok et al., 2015), phenotypic rescue of zygotic mutants by maternally provided wild-type mRNAs, the translation of which can be blocked by MOs (Stainier et al., 2017), hypomorphic nature of the mutant allele (Stainier et al., 2017) or genetic compensation in the mutant (El-Brolosy & Stainier, 2017; Rossi et al., 2015). Additionally, a recent study has revealed that mRNA processing in the mutant background often produces transcripts that escape nonsense-mediated decay, thus potentially maintaining the function of the gene (Anderson et al., 2017).
On the other hand, in the case of the *cdh11*^{sa14413} mutant line, it has been previously discussed that we were not able to reproduce any of the phenotypes observed in the morphant embryos because the *cdh11* mutants could produce a truncated protein that could still be functional (Silva 2017).

Therefore, we started to develop a new *cdh11* mutant line using the CRISPR-Cas9 genome editing system. This technology allows us to generate stable mutant lines and hence to use reverse genetics to study gene function in different model organisms such as the zebrafish (Stainier et al., 2017).

To create the new *cdh11* mutant line, we injected several combinations and concentrations of the three guide RNAs (gRNAs), targeting different functional domains of the Cdh11 protein (Figure 14, Table 1). The new mutant line that was generated after injecting both gRNA1+2 with Cas9 protein (Figure 15) and is now growing at IMM zebrafish facility. Once this line is ready we intend to analyse this mutant line in light of the phenotypes observed in the morphant embryos. If the phenotypes observed after MO injections phenocopy the mutant embryos, then we can consider the morphant embryos as suitable alternatives to the mutant (Stainier et al., 2017).

4.2.1 – Should we observe the mutant phenotype in CRISPR-Cas9 injected founder embryos?

The CRISPR-Cas9 technology is usually used to create non-mosaic knockout animals by selecting founders for germline transmission (Hwang et al., 2013). Nonetheless, several researchers have described the appearance and maintenance of loss-of-function phenotypes in founder embryos (F0 generation) (Jao et al., 2013; Ribeiro et al., 2017; Shah et al.,2015). Some have described that up to 80% of the injected embryos displayed complete phenotype expressivity (Burger et al., 2016). If the LR phenotypes obtained with the *cdh11*^{MO} are specific, we expected to observe the same phenotypes after injection with the different combinations of *cdh11* gRNA, both in the F0 generation as well as the future stable *cdh11* mutant line. However, when we analysed the founder embryos they displayed a normal LR phenotypes in all the conditions observed.

Given that LR phenotypes observed were not replicated in a mutant, we might be lead to conclude that the MO is not specific. However, even though a number of experiments have described mutant phenotypes in founder embryos (Burger et al., 2016; Jao et al., 2013; Ribeiro et al., 2017; Shah et al., 2015) there are several reasons why it may not happen. One explanation is the lack of effectiveness of the gRNAs injected with the Cas9 mRNA/protein. Previous experiments have shown that different gRNAs can have very different activity levels, and, in some studies, 50% or more of the gRNAs were ineffective (Gagnon et al., 2014; Moreno-Mateos et al., 2015; Shah et al., 2015). In our investigation, we confirmed that both gRNA1 and gRNA2 are effective. We analysed the DNA collected from injected embryos at 24 hours and observed that mutagenesis was occurring at both binding sites (Figure 15).

Additionally, we must consider that significant phenotype penetrance on a whole embryo scale requires a mutagenesis efficiency close to or reaching saturation (Burger et al., 2016). Several experiments have described that not all genomic loci are equally accessible to mutagenesis by the CRISPR-

Cas9 system (Chen et al., 2017; Gagnon et al., 2014; Hwang et al., 2013; Jao et al., 2013). This means that the efficiency of the gRNAs is depended on factors like the features of the targeting sequence and neighbouring regions (Doench et al., 2014; Wang et al., 2014; Wu et al., 2015), DNA modifications, and inhibitory effects of chromatin structure (Reyon et al., 2012). A recent study demonstrated that chromatin accessibility showed positive correlation with CRISPR/Cas9 efficiency (Chen et al., 2017). In this experiment, the authors characterized the chromatin organization as either Open Chromatin (OC) or Closed Chromatin (CC). Following the guidelines and software provided by this study[4] we found that that all gRNA binding sites in *cdh11* are characterized as Closed Chromatin (CC), especially in exons 2, 7 and 11 (which include the binding sites for gRNA1, 2 and 3 respectively). This might explain, at least in part, why we could not detect the knockdown LR phenotypes in the founder embryos even after confirming their efficiency.

Nevertheless, it should be noted that in other experiments, some of the targeted genes did not induce the expected phenotype, even when the mutagenesis rate was considerably high (Jao et al., 2013). Embryos injected with gRNA/Cas9 are mosaic for different types of mutations, with each founder individual having a unique spectrum of mutations (Shah et al., 2015). This means that we have to be cautious when inferring the genotype of the individual from its phenotype (Schulte-Merker & Stainier, 2014). Furthermore, even if an injected embryo had indels introduced to each individual cell's target site, one-third of indels would be in-frame and therefore potentially hypomorphic or silent, depending on the target site (Shah et al., 2015).

Overall, this shows that not being able to replicate knockdown phenotypes in founder embryos does not necessarily mean that the MO is non-specific or that the gRNAs are ineffective. We have to wait for the following generations to observe if the mutation is present in the germline of the founder embryos to start a new *cdh11* mutant line that we can analyse.
Additionally, we should inject the different combinations of the three Cdh11 gRNAs and analyse their efficiency. It would be most interesting to include the gRNA3 which was not studied here.

4.3 - Where is *cdh11* expressed at 8ss?

We wanted to determine using a sensitive method whether *cdh11* was expressed at the onset of LR asymmetry establishment, namely in the Kupffer's Vesicle (KV), at 8ss (Lopes et al., 2010). This was done by sorting the cells from a *sox17*:EGFP transgenic line. At this stage, GFP signal is seen in KV and endodermal cells (Sakaguchi et al., 2006; Sampaio et al., 2014). We sorted the cells by classifying the GFP signal intensity in three sub-populations: **GFP^{++}, GFP^{+}, GFP^{-},** that correspond to the KV, endodermal cells and the remaining tissues of the embryo, respectively. Then we performed a PCR for *cdh11* for each sub-population. The results obtained from the PCR show that *cdh11* is expressed in all three sub-populations (Figure 18B).

It has been described that, at 8ss, the KV is composed of 40 to 60 cells, which in our assay means that we will have around 4 000 to 6 000 cells, from 100 embryos (Gokey et al., 2017). This value is significantly less than the approximately 30 000 cells we collected in the **GFP^{++}** population. We collected a higher number of cells to guarantee that all KV cells were included, based on previous results indicating that *cdh11* was not expressed in endodermal cells (Silva 2017). Therefore, it is certain that in the **GFP^{++}** sub-population, besides the KV cells, we collected other GFP expressing cells, that is, endodermal cells.

Furthermore, as a control we used *dand5* primers to identify the KV cell population because at 8ss this gene is exclusively expressed in the posterior end of the KV (Lopes et al., 2010). After the PCR

[4] http://compbio.tongji.edu.cn/crispr

for *dand5* we are only able to detect this gene in the **GFP**$^{++}$ sub-population, meaning that we only have KV cells in the **GFP**$^{++}$ sub-population, as far as we can detect (Figure 18). Consequently, the **GFP**$^{+}$ sub-population is composed of the remaining GFP expressing cells, the endodermal cells.

We see that *cdh11* in expressed in all three sub-populations. Recall that these sub-populations were selected from a *sox17*:EGFP line, which at 8ss labels the KV and endoderm (Sakaguchi et al., 2006)
We expected that the *cdh11* transcript would be present in the **GFP**$^{-}$ subpopulation, in the *cdh11* expressing cells of the IM and NT (Figure 12). In the **GFP**$^{+}$ subpopulation, the absence of *dand5* expression indicates that KV cells are not present and the only cells in this group are endodermal cells. However, as discussed above, in the **GFP**$^{++}$ population, instead of having exclusively KV cells, we also have endodermal cells. Therefore, on one hand, we cannot confirm whether the KV cells are expressing *cdh11*. On the other hand, we can confirm that endodermal cells express *cdh11* and, if KV cells do not express *cdh11*, the *cdh11* transcript we detected in both GFP populations comes from the endodermal cells. In order to detect whether KV express *cdh11*, we have to improve this assay.

One way it could be done is by limiting the number of collected cells in the GFP++ to approximately 4 000-6 000 cells with the strongest GFP signal, which should be enough to guarantee that mostly KV cells are collected in this population (Gokey et al., 2017).

As a complementary approach, we want to perform a RT-qPCR for *cdh11* and *dand5* in these sub-populations. This is a better method than the regular PCR, since it is more effective in quantifying the levels of expression of both genes in these populations (Bonab et al., 2015). In our case this is crucial because the PCR assay has detected *cdh11* in the endoderm, but *cdh11* has not been observed in this tissue in the WISH assays, nor in the KV (Silva 2017; Figure 12 and 16).

We could also generate a new double-coloured transgenic line that would allow us to detect the KV structure. A strong candidate for this new transgenic line would have *sox17* promoter driving a reporter GFP protein, and the reporter RFP driven by the *foxj1a* promoter. Throughout development *foxj1a* is expressed in the KV and also the DFC, floor plate, IM, the pronephric duct and spinal cord (Caron et al., 2012; Hellman et al., 2010). The *sox17* it also expressed in the DFC as well as endodermal cells, pancreas and liver (Sakaguchi et al., 2006; Sampaio et al., 2014). The KV would be the only structure that is common in both expression patterns. This would allow us to clearly identify the KV cells under FACS. However, a Tg(*foxj1a*:RFP) line does not exist and would have to be generated as well.

4.4 – Cdh11 involved in both pathways of the relay of the LR information to the LPM

Starting at 5ss, *spaw* is expressed around the KV (Long et al., 2003) and by 10ss its expression is detected in the left LPM (Grimes & Burdine, 2016), meaning that the asymmetric information is transferred through Spaw itself or other intermediary between these stages. Initially we showed that *cdh11* is expressed in the IM at 8ss, which is localized between the KV and the LPM (Figure 12). We observed that Cdh11 knockdown alters the expression pattern of *spaw* and *pitx2* in the LPM, at 20ss and 24ss, respectively, indicating that Cdh11 is acting upstream of the Nodal cascade (Figure 11). This suggests that the IM could be involved in the transfer of the asymmetric signal from the KV to the LPM, either facilitating or hindering the passage of Spaw through the action of Cdh11.

However, further experiments showed that Cdh11 could also be present in the endodermal cells at this stage (Figure 18). While the mechanism of transfer of information from the LR organizer to the LPM in vertebrates is still relatively unknown, previous findings in mouse and frog embryos have raised two complementing hypotheses for this process involving the endoderm. Independent experiments in

the mouse and frog suggest that the Ca2+ signal starting from the KV spreads through gap junctions in the endodermal cells towards the LPM (Figure 3) (Beyer et al. 2012; Saund et al. 2012; Viotti et al. 2012). Additionally, some have suggested that in both mouse and frog the Nodal protein itself can be transferred along sGAGs located in a basement membrane between the endoderm and the mesoderm (Marjoram & Wright, 2011; Oki et al., 2007). Therefore, we have a model where calcium signalling in the endoderm might influence the underlying cell matrix, enhancing the secretion of sGAGs and so assisting the transfer of the Nodal protein from the organizer to the LPM (Figure 22) (Grimes & Burdine, 2017; Norris, 2012).

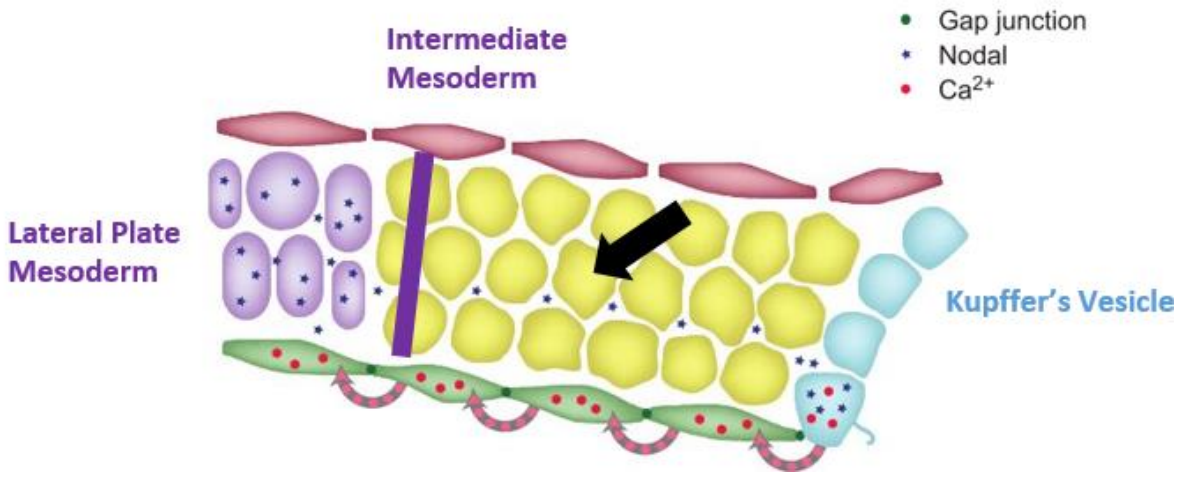

Figure 22 - Representation of the two hypotheses for the transfer of LR information from the LRO to the left LPM. Calcium signal is carried via gap junctions from the KV to the left LPM through the endoderm, and Spaw itself travels leftwards through an extracellular route directly to the LPM, crossing the IM. Blue – KV, Green – Endoderm, Red – Ectoderm, Yellow – Paraxial mesoderm, Purple – Lateral plate/intermediate mesoderm. Adapted from Norris 2012.

In the zebrafish, several experiments have shown that, starting at 10 hpf, fast Ca2+ waves with a velocity of approximately 5 um/s are generated with increased frequency (11 to 12 waves per hour) that propagate from the tail bud throughout the caudal half of the embryo (Figure 23). (Gilland et al., 1999; Webb & Miller, 2000; Webb & Miller, 2007). These might propagate through gap junctions, possibly mediated by the diffusion of either Ca2+ itself or IP_3 (Berridge et al. 2003)
A later experiment observed the occurrence of Intraciliary Calcium Oscillations (ICO) in the KV (Yuan et al. 2015). While these waves peaked on the left side of the organizer at 1ss to 4ss, they also detected asymmetric intracellular calcium waves at the LRO that peaked from 5ss to 9ss, which had also been observed in the mouse (Blum & Vick, 2015; Takao et al., 2013; Yuan et al., 2015)

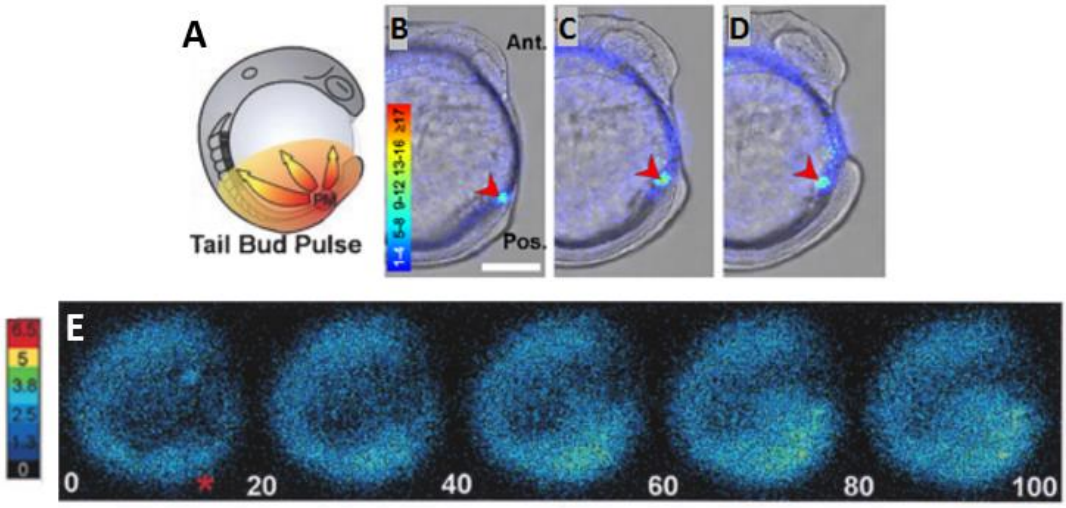

Figure 23 – Luminescent imaging showing calcium release and spatial waves in the developing embryo
Embryos were injected with aequorin and luminescent data were acquired with a photon imaging microscope**. A** – Representation of the calcium wave spread in zebrafish. **B-D** - Images representing 1 min of accumulated light, superimposed on the corresponding bright-field image at 3ss (**B**), 7ss (**C**) and 8ss (**D**). Colour scale indicates luminescence flux in photons/pixel. All scale bars are 200 um. Red arrow – transient Ca2+. Adapted from Webb 2007. **E** – Each section represents 20-second frames of signal at the 10-somite stage. Colour scale indicates luminescent flux in [(photons per pixel per sec) x 10^{-2}]. Red asterisk indicates wave initiating site. All scale bars are 200 μm. Adapted from Gilland 1999.

Other experiments have described that Spaw itself is transferred from the KV to the LPM. Some propose that Dvr1/Gdf3 (a member of the TGFβ family) facilitates the transfer of the LR signal from KV to the LPM (Peterson et al., 2013). Knockdown of Gdf3 prevents *spaw* expression from occurring in the LPM even in the absence of Nodal inhibitors Dand5 and Lefty1 (Pelliccia et al., 2017). Even though Nodal from the organizer is required for the expression of Nodal in the LPM in mouse (Brennan et al., 2002), this does not seem to be the case in zebrafish since mutants lacking either LRO-*spaw* expression or *spaw* mutants themselves still express *spaw* in the LPM (Burdine et al., 2016; Noel et al., 2013)

In light of the findings described above, Cadherin 11 could be involved in both steps of this hypothesis. In one hand, it has been suggested that the Ca2+ waves might be detected by the Ca2+ sensitive cadherins (Tada & Concha, 2001; Wallingford et al., 2001). Furthermore, cadherins are not only required for cell adhesion but also in the assembly of gap junctions (Wei et al., 2005, Govindarajan et al., 2010). Therefore, if Cdh11 is disrupted or absent, the calcium signal might not be able to transfer from the KV to the LPM through the endoderm.

We could test this by inhibiting the function of gap junctions in the zebrafish during this interval and observing the expression of Nodal cascade genes in the LPM. This can be done through the 18 alpha-Glycyrrhetinic acid, a general gap junction blocker (Davidson & Baumgarten, 1988). When added in mice, the expression of *lefty1/2* in the LPM was absent or severely reduced (Viotti et al., 2012). This drug could be added to zebrafish embryos starting at 5/8ss, and then we could observe the expression of *spaw* and *pitx2* in the LPM by WISH. In zebrafish, Connexin 43.4 (Cx43.4) is required for LR patterning. However, it was found to be expressed in the KV and involved in the morphogenesis of this organ (Hatler et al., 2009).

On the other hand, Cdh11 in the IM can also be involved in the passage of Spaw from the KV to the LPM. Previously in this investigation we observed by WISH that the expression of pax2a, a marker for the IM, was not altered after *cdh11* knockdown (Silva 2017). Our hypothesis states that Nodal reaches the LPM by the extracellular matrix (Marjoram & Wright, 2011; Oki et al., 2007) crossing

the IM. We also know that cadherins are a key component of adherens junctions between cells (Malinova & Huveneers, 2017; Takeichi, 2014). Therefore, we could observe how the knockdown or knockout of *cdh11* affects the adhesions between cells in the IM and consequently the passage of Spaw to the LPM. This could be done by observing sections of *cdh11* mutants and/or morphants of the Tg(*pax2a*:GFP) transgenic line (Picker et al., 2002), identifying the IM cells, and performing an immunohistochemistry assay with ZO-1, to observe the polarity of the cells, between 8ss and 14ss. Thus we can discern if the junctions between the cells are disrupted in the IM after knockdown or knockout of *cdh11*.

4.5 – Is Cdh11 in the anterior LPM affecting organogenesis?

We have seen that *cdh11* knockdown affects the looping of the gut and the heart by 50 hpf. However, in altered embryos, the conformation of the gut is predominantly inversed (Figure 9), while most of the morphant embryos display a "No-loop" heart phenotype (Figure 10). Previous experiments have already described a lack of concordance between the heart and gut during development (Ji et al., 2015; Lopes et al., 2010; Noel et al., 2013). It is possible to see that, in *pitx2* mutants, the asymmetric looping of the heart and the gut was normal, but in *spaw* mutants, where *pitx2* was absent from the LPM, embryos showed mostly normal heart looping while the gut laterality was completely randomized (Ji et al., 2015; Noel et al., 2013). In mutants for *deltaD*, a Notch ligand, the normal heart looping and randomized gut phenotypes were also observed. However, in this case, the expression of *spaw* and *pitx2* in the LPM is, in most cases, confined to the left side or bilateral (Lopes et al., 2010).

4.5.1 – Cdh11 might affect the heart primordia, disrupting the intrinsic chirality of the heart

In morphant embryos, the expression of both *spaw* and *pitx2* in the LPM at 20ss and 24ss, respectively, becomes randomized, being mostly restricted to the right side (Shiratori & Hamada, 2014). In our case, while the expression of *spaw* and *pitx2* in the right LPM can explain the inverted conformation in the gut, it does not explain the symmetric heart phenotypes. This suggests that *cdh11* should be acting upstream from *spaw* and *pitx2* (Silva 2017).

Initially we thought that these results meant that the *cdh11* knockdown could affect the development of the heart by preventing *spaw* from reaching the prospective heart region (Silva 2017). However, the detection of *cdh11* in the anterior LPM at 20ss using a different chromogenic substrate (NBT/BCIP) suggests that Cdh11 could be directly influencing the development of the heart in this region (Figure 21). To address this question, we could perform a double WISH with *cdh11* and a marker for the heart progenitors in the anterior lateral plate mesoderm, like *nkx2.5, myl7, lefty2* or starting at 20ss, to observe if the expression patterns of both genes coincide in WT embryos. Additionally, we could also analyse the expression of these markers for the heart progenitors after injection with a *cdh11*^{MO} or in a new *cdh11* mutant line.

As mentioned above, it has been shown that in *spaw* mutants the brain and gut laterality is randomized, but not the laterality of the heart (Noel et al., 2013). In this study they showed that the looping of the heart is intrinsic, and that disrupting actomyosin activity leads to mostly "No-loop" phenotype, even in the presence of asymmetric Nodal signal (Noel et al., 2013). Other studies have described that actin cytoskeleton self-organization allows cells to develop left–right asymmetry (Tee et al., 2015; Wan et al., 2011) and that asymmetrical cell behaviour has been shown to drive asymmetrical morphogenesis through regulation of adhesion–cytoskeletal interactions (Welsh et al., 2013). It is known that Cdh11 is a transmembrane protein that mediates cell-cell adhesion (Takeichi, 2014). Its cytoplasmic domain is associated with the cytoplasmic proteins catenins, which serve as intermediate linkers between the

cadherin and actin filaments (Ivanov et al., 2001). Therefore, we suggest that disruption of the Cdh11 protein could affect both the cohesion between migrating heart primordia, and their LR identity by disrupting the actin cytoskeleton organization.

In order to test this hypothesis we could perform immunohistochemistry assays on embryo sections, looking at the progression of the heart primordia. This can be done by using the Tg(*cmlc2*:GFP) transgenic line, expressing GFP under the control of the myocardial-specific *cmlc2* promoter (Rohr et al., 2008) and immunostaining with ZO-1 to reveal the polarity of the cells.
This could be performed in *cdh11* morphant and mutant embryos, starting at 18ss, which is just before the myocardial and endocardial progenitors migrate to the midline and fuse to create the cardiac cone, until 30 hpf when the heart tube is already formed (Staudt & Stainier, 2012).

4.5.2 – Gut looping affected by the disruption of the Nodal cascade

Previously in this work, we proposed that the abnormal expression of *spaw* and *pitx2* in the right LPM could affect the asymmetric migration of this tissue that induces the looping of the gut. This could happen if, for example, abnormal LR signalling leads to the right LPM acquiring the identity of the left LPM (Horne-Badovinac, 2003). The expression of *cdh11* in the LPM at 20ss suggests that this cadherin might directly influence the epithelial nature of the migrating LPM (Figure 21). However, the pattern of expression of *cdh11* is more anterior that the gut looping region and does not overlap with that area (Figure 19). These new findings indicate that the knockdown of *cdh11* might affect the structure of the anterior LPM, but may not affect the migrating region.

In conclusion, we saw that after injection with the MO, the organogenesis of the heart and the gut was altered. However they were not concordant: most of the affected embryos showed a symmetric heart while most of the affected embryos showed a reversed gut phenotype. This suggest that the morphogenesis of the heart and the gut might be uncoupled, that is, a certain moment their development occurs through different pathways. In the case of the gut, the reversion of the Nodal cascade genes *spaw* and *pitx2* might explain the reversion in its conformation. This means that *cdh11* would have to be acting upstream of the Nodal cascade: Cdh11 could be affecting the passage of the LR signal from the KV to the LPM, although we still do not know exactly how this might happen. It could might also be directly affecting the activity of Spaw in the KV, or around it. However, our results could not confirm whether it is present in the KV or not. In the case of the heart, the reversion of the Nodal cascade does not explain the predominantly symmetric phenotype of this organ. However, the expression of *cdh11* in the ALPM at the start of the heart organogenesis suggests that it might directly influence the morphogenesis of this organ. Consequently Cdh11 might have a double role in the establishment of laterality: Upstream of the Nodal cascade affecting the development of the gut, and later, in the anterior lateral plate mesoderm, directly influencing the morphogenesis of the heart (Figure 24).

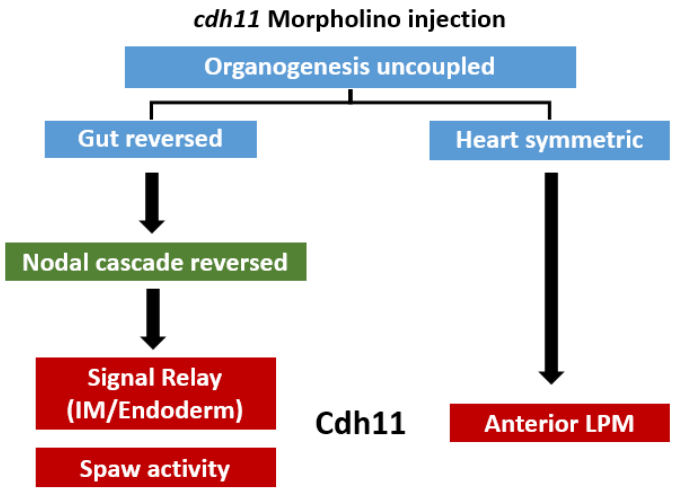

Figure 24 – Summary of the main results and hypotheses

Chapter 5 – Bibliography

Adachi, H., Saijoh, Y., Mochida, K., Ohishi, S., Hashiguchi, H., Hirao, A., & Hamada, H. (1999). Determination of left/right asymmetric expression of nodal by a left side-specific enhancer with sequence similarity to a lefty-2 enhancer. *Genes and Development*, *13*(12), 1589–1600.

Alimperti, S., & Andreadis, S. T. (2015). CDH2 and CDH11 act as regulators of stem cell fate decisions. *Stem Cell Research*, *14*(3), 270–282. http://doi.org/10.1016/j.scr.2015.02.002

Baker, K., Holtzman, N. G., & Burdine, R. D. (2008). Direct and indirect roles for Nodal signalling in two axis conversions during asymmetric morphogenesis of the zebrafish heart. *Proceedings of the National Academy of Sciences of the United States of America*, *105*(37), 13924–9.

Bakkers, J. (2011). Zebrafish as a model to study cardiac development and human cardiac disease. *Cardiovascular Research*, *91*(2), 279–288. http://doi.org/10.1093/cvr/cvr098

Bakkers, J., Verhoeven, M. C., & Abdelilah-Seyfried, S. (2009). Shaping the zebrafish heart: From left-right axis specification to epithelial tissue morphogenesis. *Developmental Biology*, *330*(2), 213–220.

Berridge, M. J., Bootman, M. D., & Roderick, H. L. (2003). Calcium signalling: Dynamics, homeostasis and remodelling. Nature Reviews Molecular Cell Biology, 4(7), 517–529.

Beyer, T., Thumberger, T., Schweickert, A., & Blum, M. (2012). Connexin26 -mediated transfer of laterality cues in Xenopus.

Blum, M., Feistel, K., Thumberger, T., & Schweickert, A. (2014). The evolution and conservation of left-right patterning mechanisms. *Development (Cambridge, England)*, *141*(8), 1603–13.

Blum, M., & Vick, P. (2015). Left-right asymmetry: Cilia and calcium revisited. *Current Biology*, *25*(5), R205–R207.

Bill, B. R., Petzold, A. M., Clark, K. J., Schimmenti, L. a, & Ekker, S. C. (2009). A primer for morpholino use in zebrafish. Zebrafish, 6(1), 69–77.

Brennan, J., Norris, D. P., & Robertson, E. J. (2002). Nodal activity in the node governs left-right asymmetry. *Genes and Development*, *16*(18), 2339–2344.

Burdine, R. D., Grimes, D. T., & Burdine, R. D. (2016). Antagonistic interactions in the zebrafish midline prior to the emergence of asymmetric gene expression are important for left – right patterning.

Burger, A., Lindsay, H., Felker, A., Hess, C., Anders, C., Chiavacci, E., … Mosimann, C. (2016). Maximizing mutagenesis with solubilized CRISPR-Cas9 ribonucleoprotein complexes. Development, 143(11), 2025–2037.

Campione, M., & Franco, D. (2016). Current Perspectives in Cardiac Laterality.

Caron, A., Xu, X., & Lin, X. (2012). Wnt/ -catenin signaling directly regulates Foxj1 expression and ciliogenesis in zebrafish Kupffer's vesicle. Development, 139(3), 514–524.

Chen, Y., Zeng, S., Hu, R., Wang, X., Huang, W., Liu, J., … Zhang, Y. (2017). Using local chromatin structure to improve CRISPR / Cas9 efficiency in zebrafish, 0, 1–19.Cayuso, J., Dzementsei, A., Fischer, J. C., Karemore, G., Caviglia, S., Bartholdson, J., … Ober, E. A. (2016). EphrinB1/EphB3b Coordinate Bidirectional Epithelial-Mesenchymal Interactions Controlling Liver Morphogenesis and Laterality. *Developmental Cell*, *39*(3), 316–328.

Chu, K., Cheng, C., Ye, X., Lee, Y., Zurita, A. J., Zhang, S., … Lin, S. (2009). Cadherin-11 Promotes the Metastasis of Prostate Cancer Cells to Bone. NIH Public Access, *6*(8), 1259–1267.

Clark, K. J., Balciunas, D., Pogoda, H. M., Ding, Y., Westcot, S. E., Bedell, V. M., … Ekker, S. C. (2011). In vivo protein trapping produces a functional expression codex of the vertebrate proteome. *Nature Methods*, *8*(6), 506–512.

Clendenon, S. G., Sarmah, S., Shah, B., Liu, Q., & Marrs, J. A. (2012). Zebrafish cadherin-11 participates in retinal differentiation and retinotectal axon projection during visual system development. *Developmental Dynamics*, *241*(3), 442–454.

Clendenon, S. G., Shah, B., Miller, C. A., Schmeisser, G., Walter, A., Gattone, V. H., … Marrs, J. A. (2009). Cadherin-11 controls otolith assembly: Evidence for extracellular cadherin activity. *Developmental Dynamics*, *238*(8), 1909–1922.

Collins, M. M., & Ryan, A. K. (2014). Are there conserved roles for the extracellular matrix, cilia, and junctional complexes in left-right patterning? *Genesis*, *52*(6), 488–502.

D'Amico, L. a, & Cooper, M. S. (1997). Spatially distinct domains of cell behavior in the zebrafish organizer region. *Biochemistry and Cell Biology = Biochimie et Biologie Cellulaire*, *75*(5), 563–77.

Davidson, J. S., & Baumgarten, I. M. (1988). James s. Davidson and Ingrid m. Baumgarten Departmentof Chemical Pathology,University of Cape Town Medical School, Observatory7925, South Africa. Observatory.

Doench, J. G., Hartenian, E., Graham, D. B., Tothova, Z., Hegde, M., Smith, I., … Root, D. E. (2014). Rational design of highly active sgRNAs for CRISPR-Cas9- mediated gene inactivation. Nature Biotechnology, 32(12), 1262–1267.

Kurpios, N. A., Sun, X., Gros, J., Martin, J. F., & Tabin, C. J. (2008). Article The Chirality of Gut Rotation Derives from Left-Right Asymmetric Changes in the Architecture of the Dorsal Mesentery, *2*.

Drummond, I. A., & Davidson, A. J. (2016). *Zebrafish kidney development*. *Methods in Cell Biology* (Vol. 134). Elsevier Ltd.

Eisen, J. S., & Smith, J. C. (2008). Controlling morpholino experiments: don't stop making antisense. Development, 135(10), 1735–1743.

Ekker, S. C. (2000). Morphants: a new systematic vertebrate functional genomics approach. Yeast (Chichester, England), 17(4), 302–306.

El-Brolosy, M. A., & Stainier, D. Y. R. (2017). Genetic compensation: A phenomenon in search of mechanisms. PLoS Genetics, 13(7), 1–17.

Essner, J. J., Amack, J. D., Nyholm, M. K., Harris, E. B., & Yost, H. J. (2005). Kupffer's vesicle is a ciliated organ of asymmetry in the zebrafish embryo that initiates left-right development of the brain, heart and gut. *Development (Cambridge, England)*, *132*(6), 1247–1260.

Ferreira, R. R., Vilfan, A., Jülicher, F., Supatto, W., & Vermot, J. (2017). Physical limits of flow sensing in the left-right organizer. *eLife*, *6*, 1–27.

Franklin, J. L., & Sargent, T. D. (1996). Ventral neural cadherin, a novel cadherin expressed in a subset of neural tissues in the zebrafish embryo. *Developmental Dynamics*, *206*(2), 121–130.

Fukumoto, T., Blakely, R., & Levin, M. (2005). Serotonin transporter function is an early step in left-right patterning in chick and frog embryos. Developmental Neuroscience, 27(6), 349–363.

Fukumoto, T., Kema, I. P., & Levin, M. (2005). Serotonin signaling is a very early step in patterning of the left-right axis in chick and frog embryos. Current Biology, 15(9), 794–803.

Gagnon, J. A., Valen, E., Thyme, S. B., Huang, P., Ahkmetova, L., Pauli, A., … Schier, A. F. (2014). Efficient mutagenesis by Cas9 protein-mediated oligonucleotide insertion and large-scale assessment of single-guide RNAs. PLoS ONE, 9(5), 5–12.

García-Castro, M. I., Vielmetter, E., & Bronner-Fraser, M. (2000). N-cadherin, a cell adhesion molecule involved in establishment of embryonic left-right asymmetry. *Science*, *288*(5468), 1047–1051.

Gilland, E., Miller, A. L., Karplus, E., Baker, R., & Webb, S. E. (1999). Imaging of multicellular large-scale rhythmic calcium waves during zebrafish gastrulation. Proc. Natl. Acad. Sci., 96(January), 157–161. http://doi.org/10.1073/pnas.96.1.157Gokey, J. J., Ji, Y., Tay, H. G., Litts, B., Amack, J. D., & Medical, U. (2017). HHS Public Access, *245*(1), 22–33.

González-Morales, N., Géminard, C., Lebreton, G., Cerezo, D., Coutelis, J. B., & Noselli, S. (2015). The atypical cadherin dachsous controls left-right asymmetry in Drosophila. *Developmental cell*, *33*(6), 675-689.Govindarajan, R., Chakraborty, S., Johnson, K. E., Falk, M. M., Wheelock, M. J., Johnson, K. R., & Mehta, P. P. (2010). Assembly of connexin43 into gap junctions is regulated differentially by E-cadherin and N-cadherin in rat liver epithelial cells. *Molecular biology of the cell*, *21*(23), 4089-4107.Grimes, D. T., & Burdine, R. D. (2017). Left – Right Patterning : Breaking Symmetry to Asymmetric Morphogenesis. *Trends in Genetics*, *xx*, 1–13.

Guschin, D. Y., Waite, A. J., Katibah, G. E., Miller, J. C., Holmes, M. C., & Rebar, E. J. (2010). Engineered Zinc Finger Proteins, 649, 247–256.

Hamada, H., Meno, C., Watanabe, D., & Saijoh, Y. (2002). Establishment of Vertebrate Left–Right Asymmetry. *Nature Reviews Genetics*, *3*(2), 103–113.

Harrington, M. J., Chalasani, K., & Brewster, R. (2010). Cellular mechanisms of posterior neural tube morphogenesis in the zebrafish. Developmental Dynamics, 239(3), 747–762.

Hashimoto, H., Rebagliati, M., Ahmad, N., Muraoka, O., Kurokawa, T., Hibi, M., & Suzuki, T.

(2004). The Cerberus/Dan-family protein Charon is a negative regulator of Nodal signaling during left-right patterning in zebrafish. *Development (Cambridge, England)*, *131*(8), 1741–53.
Hatler, J. M., Essner, J. J., & Johnson, R. G. (2009). A gap junction connexin is required in the vertebrate left-right organizer. Developmental Biology, 336(2), 183–191.
Heasman, J., Kofron, M., & Wylie, C. (2000). β-catenin signaling activity dissected in the early Xenopus embryo: A novel antisense approach. Developmental Biology, 222(1), 124–134.
Hellman, N. E., Liu, Y., Merkel, E., Austin, C., Le Corre, S., Beier, D. R., … Drummond, I. A. (2010). The zebrafish foxj1a transcription factor regulates cilia function in response to injury and epithelial stretch. Proceedings of the National Academy of Sciences, 107(43), 18499–18504.
Hochgreb-Hägele, T., Yin, C., Koo, D. E. S., Bronner, M. E., & Stainier, D. Y. R. (2013). Laminin β1a controls distinct steps during the establishment of digestive organ laterality. *Development (Cambridge, England)*, *140*(13), 2734–45.
Horne-Badovinac, S. (2003). A Cellular Framework for Gut-Looping Morphogenesis in Zebrafish. *Science*, *302*(5645), 662–665.
Horsfield, J., Ramachandran, A., Reuter, K., LaVallie, E., Collins-Racie, L., Crosier, K., & Crosier, P. (2002). Cadherin-17 is required to maintain pronephric duct integrity during zebrafish development. Mechanisms of Development, 115(1–2), 15–26.
Huang, H., Ruan, H., Aw, M. Y., Hussain, A., Guo, L., Gao, C., … Peng, J. (2008). Mypt1-mediated spatial positioning of Bmp2-producing cells is essential for liver organogenesis. Development, 135(19), 3209–3218.
Huang, C., Lira, C., Chu, K., Bilen, M. A., Lee, Y., Ye, X., … Lin, S. (2011). Cadherin-11 increases migration and invasion of prostate cancer cells and enhances their interaction with osteoblasts. NIH Public Access, *70*(11), 4580–4589.
Hwang, W. Y., Fu, Y., Reyon, D., Maeder, M. L., Kaini, P., Sander, J. D., … Yeh, J. R. J. (2013). Heritable and Precise Zebrafish Genome Editing Using a CRISPR-Cas System. PLoS ONE, 8(7), 1–9.
Ivanov, D. B., Philippova, M. P., & Tkachuk, V. A. (2001). Structure and functions of classical cadherins. Biochemistry (Moscow), 66(10), 1174–1186.
Jao, L.-E., Wente, S. R., & Chen, W. (2013). Efficient multiplex biallelic zebrafish genome editing using a CRISPR nuclease system. Proceedings of the National Academy of Sciences of the United States of America, 110(34), 13904–9.
Jensen, E. (2014). Technical Review: in situ hybridization. Anatomical Record (Hoboken, N.J. : 2007), 0, 1349–1353.
Ji, Y., Buel, S. M., & Amack, J. D. (2015). Mutations in zebrafish pitx2 model congenital malformations in Axenfeld-Rieger syndrome but do not disrupt left-right placement of visceral organs. *Developmental Biology*, *416*(1), 69–81. http://doi.org/10.1016/j.ydbio.2016.06.010
Kawakami, Y., Koth, C. M., Itoh, T., Morita, M., Raya, R. M., Dubova, I., … Izpisu, J. C. (2003). Notch activity induces Nodal expression and mediates the establishment of left – right asymmetry in vertebrate embryos, (858), 1213–1218.
Kimmel, C. B. C. B., Ballard, W. W., Kimmel, S. R., Ullmann, B., & Schilling, T. F. (1995). Stages of embryonic development of the zebrafish. *Developmental …*, *10*(3), 253–310.
Kok, F. O., Shin, M., Ni, C. W., Gupta, A., Grosse, A. S., vanImpel, A., … Lawson, N. D. (2015). Reverse genetic screening reveals poor correlation between morpholino-induced and mutant phenotypes in zebrafish. Developmental Cell, 32(1), 97–108.
Kramer-Zucker, A. G. (2005). Cilia-driven fluid flow in the zebrafish pronephros, brain and Kupffer's vesicle is required for normal organogenesis. *Development*, *132*(8), 1907–1921.
Kubota, F., Murakami, T., Mogi, K., & Yorifuji, H. (2007). Cadherin-6 is required for zebrafish nephrogenesis during early development. International Journal of Developmental Biology, 51(2), 123–129.
Kurpios, N. A., Ibañes, M., Davis, N. M., Lui, W., Katz, T., Martin, J. F., … Tabin, C. J. (2008). The direction of gut looping is established by changes in the extracellular matrix and in cell:cell adhesion. *Proceedings of the National Academy of Sciences of the United States of America*, *105*(25), 8499–506.
Law, S. H. W., & Sargent, T. D. (2014). The serine-threonine protein kinase PAK4 is dispensable in zebrafish: Identification of a morpholino-generated pseudophenotype. PLoS ONE, 9(6).

Lenhart, K. F., Lin, S.-Y., Titus, T. A., Postlethwait, J. H., & Burdine, R. D. (2011). Two additional midline barriers function with midline lefty1 expression to maintain asymmetric Nodal signaling during left-right axis specification in zebrafish. *Development*, *138*(20), 4405–4410.

Long, S., Ahmad, N., & Rebagliati, M. (2003). The zebrafish nodal-related gene southpaw is required for visceral and diencephalic left-right asymmetry. *Development (Cambridge, England)*, *130*(11), 2303–2316.

Lopes, S. S., Lourenco, R., Pacheco, L., Moreno, N., Kreiling, J., & Saude, L. (2010). Notch signalling regulates left-right asymmetry through ciliary length control. *Development*, *137*(21), 3625–3632.

Malinova, T. S., & Huveneers, S. (2017). Sensing of Cytoskeletal Forces by Asymmetric Adherens Junctions. Trends in Cell Biology, xx, 1–14.

Marjoram, L., & Wright, C. (2011). Rapid differential transport of Nodal and Lefty on sulfated proteoglycan-rich extracellular matrix regulates left-right asymmetry in Xenopus. Development, 138(3), 475–485.

Marra, A. N., & Wingert, R. A. (2014). Roles of Iroquois transcription factors in kidney development. *Cell & developmental biology*, *3*(1), 1000131.Matsui, T., Ishikawa, H., & Bessho, Y. (2015). Cell collectivity regulation within migrating cell cluster during Kupffer ' s vesicle formation in zebrafish, *3*(May).

Matsui, T., Thitamadee, S., Murata, T., Kakinuma, H., Nabetani, T., Hirabayashi, Y., … Bessho, Y. (2011). Canopy1, a positive feedback regulator of FGF signaling, controls progenitor cell clustering during Kupffer's vesicle organogenesis. *Proceedings of the National Academy of Sciences*, *108*(24), 9881–9886.

McGrath, J., Somlo, S., Makova, S., Tian, X., & Brueckner, M. (2003). Two populations of node monocilia initiate left-right asymmetry in the mouse. *Cell*, *114*(1), 61–73.

Meeker, N. D., Hutchinson, S. A., Ho, L., & Trede, N. S. (2007). Method for isolation of PCR-ready genomic DNA from zebrafish tissues. BioTechniques, 43(5), 610–614. http://doi.org/10.2144/000112619Marques, S., Borges, A. C., Silva, A. C., Freitas, S., & Cordenonsi, M. (2004). The activity of the Nodal antagonist. *Genes & Development*, 2342–2347.

Mendes, R. V., Martins, G. G., Cristovão, A. M., & Saúde, L. (2014). N-cadherin locks left-right asymmetry by ending the leftward movement of hensen's node cells. *Developmental Cell*, *30*(3), 353–360.

Moens, C. B., Donn, T. M., Wolf-Saxon, E. R., & Ma, T. P. (2008). Reverse genetics in zebrafish by TILLING. *Briefings in Functional Genomics and Proteomics*, *7*(6), 454–459.

Moreno-Mateos, M. A., Vejnar, C. E., Beaudoin, J. D., Fernandez, J. P., Mis, E. K., Khokha, M. K., & Giraldez, A. J. (2015). CRISPRscan: Designing highly efficient sgRNAs for CRISPR-Cas9 targeting in vivo. Nature Methods, 12(10), 982–988. http://doi.org/10.1038/nmeth.3543Matsui, T., & Bessho, Y. (2012). Left-right asymmetry in zebrafish. *Cellular and Molecular Life Sciences*, *69*(18), 3069–3077.

Nasevicius, A., & Ekker, S. C. (2000). Effective targeted gene "knockdown" in zebrafish. Nature Genetics, 26(2), 216–220. http://doi.org/10.1038/79951Noel, E. S., Verhoeven, M., Lagendijk, A. K., Tessadori, F., Smith, K., Choorapoikayil, S., … Bakkers, J. (2013). A Nodal-independent and tissue-intrinsic mechanism controls heart-looping chirality. *Nature Communications*, *4*, 1–9.

Nonaka, S., , Y., Okada, Y., Takeda, S., Harada, A., Kanai, Y., … Hirokawa, N. (1998). Randomization of left-right asymmetry due to loss of nodal cilia generating leftward flow of extraembryonic fluid in mice lacking KIF3B motor protein. *Cell*, *95*(6), 829–837.

Norris, D. P. (2012). Cilia , calcium and the basis of left-right asymmetry. BMC Biology

Norris, D. P., & Robertson, E. J. (1999). controlled by two distinct cis -acting regulatory elements Asymmetric and node-specific nodal expression patterns are controlled by two distinct cis -acting regulatory elements. *Genes & Development*, *13*(12), 1575–1588.

Okabe, N., Xu, B., & Burdine, R. D. (2008). Fluid dynamics in zebrafish Kupffer's vesicle. *Developmental Dynamics*, *237*(12), 3602–3612.

Okada, Y., Takeda, S., Tanaka, Y., Belmonte, J. C. I., & Hirokawa, N. (2005). Mechanism of nodal flow: A conserved symmetry breaking event in left-right axis determination. *Cell*, *121*(4), 633–644.

Oki, S., Hashimoto, R., Okui, Y., Shen, M. M., Mekada, E., Otani, H., … Hamada, H. (2007). Sulfated

glycosaminoglycans are necessary for Nodal signal transmission from the node to the left lateral plate in the mouse embryo. *Development*, *134*(21), 3893–3904.
Oteiza, P., Koppen, M., Concha, M. L., & Heisenberg, C.-P. (2008). Origin and shaping of the laterality organ in zebrafish. *Development*, *135*(16), 2807–2813.
Oteiza, P., Koppen, M., Krieg, M., Pulgar, E., Farias, C., Melo, C., … Concha, M. L. (2010). Planar cell polarity signalling regulates cell adhesion properties in progenitors of the zebrafish laterality organ. *Development*, *137*(20), 3459–3468.
Pegoraro, S., Ros, G., Piazza, S., Sommaggio, R., Ciani, Y., Rosato, A., … Manfioletti, G. (2013). HMGA1 promotes metastatic processes in basal-like breast cancer regulating EMT and stemness. *Oncotarget*, *4*(8), 1293–308.
Pelliccia, J. L., Jindal, G. A., & Burdine, R. D. (2017). Gdf3 is required for robust Nodal signaling during germ layer formation and left-right patterning. *eLife*, *6*, e28635.
Peterson, A. G., Wang, X., & Joseph Yost, H. (2013). Dvr1 transfers left-right asymmetric signals from Kupffer's vesicle to lateral plate mesoderm in zebrafish. *Developmental Biology*, *382*(1), 198–208.
Plageman, T. F., Zacharias, A. L., Gage, P. J., & Lang, R. A. (2011). Shroom3 and a Pitx2-N-cadherin pathway function cooperatively to generate asymmetric cell shape changes during gut morphogenesis. *Developmental Biology*, *357*(1), 227–234.
Renn, J., & Winkler, C. (2009). Osterix-mCherry transgenic medaka for in vivo imaging of bone formation. *Developmental Dynamics*, *238*(1), 241-248.Reyon, D., Tsai, S. Q., Khayter, C., Foden, J. A., Sander, J. D., & Joung, J. K. (2012). FLASH assembly of TALENs for high-throughput genome editing. Nature Biotechnology, 30(5), 460–465.
Ribeiro, A., Saúde, L., Monteiro, J. F., Certal, A. C., & Cristovão, A. M. (2017). Foxj1a is expressed in ependymal precursors, controls central canal position and is activated in new ependymal cells during regeneration in zebrafish. Retrieved from
Rossi, A., Kontarakis, Z., Gerri, C., Nolte, H., Hölper, S., Krüger, M., & Stainier, D. Y. R. (2015). Genetic compensation induced by deleterious mutations but not gene knockdowns. Nature, Aug 13(524), 230–3.
Saijoh, Y., Oki, S., Ohishi, S., & Hamada, H. (2003). Left-right patterning of the mouse lateral plate requires Nodal produced in the node. *Developmental Biology*, *256*(1), 160–172.
Saijoh, Y., Viotti, M., & Hadjantonakis, A. K. (2014). Follow your gut: Relaying information from the site of left-right symmetry breaking in the mouse. *Genesis*, *52*(6), 503–514.
Sakaguchi, T., Kikuchi, Y., Kuroiwa, A., Takeda, H., & Stainier, D. Y. R. (2006). The yolk syncytial layer regulates myocardial migration by influencing extracellular matrix assembly in zebrafish. *Development (Cambridge, England)*, *133*(20), 4063–72.
Sampaio, P., Ferreira, R. R., Guerrero, A., Pintado, P., Tavares, B., Amaro, J., … Lopes, S. S. (2014). Left-right organizer flow dynamics: How much cilia activity reliably yields laterality? *Developmental Cell*, *29*(6), 716–728.
Sanker, S., Cirio, M. C., Vollmer, L. L., Natasha, D., Mcdermott, L. A., Hukriede, N. A., & Vogt, A. (2013). Development of High-Content Assays for Kidney Progenitor Cell Expansion in Transgenic Zebrafish, (X).
Saund, R. S., Kanai-azuma, M., Kanai, Y., Kim, I., & Lucero, M. T. (2012). Gut endoderm is involved in the transfer of left-right asymmetry from the node to the lateral plate mesoderm in the mouse embryo, *2435*, 2426–2435.
Schulte-Merker, S., & Stainier, D. Y. R. (2014). Out with the old, in with the new: reassessing morpholino knockdowns in light of genome editing technology. Development, 141(16), 3103–3104.
Serluca, F. C., & Fishman, M. C. (2001). Pre-pattern in the pronephric kidney field of zebrafish. *Development (Cambridge, England)*, *128*, 2233–2241.
Shinohara, K., & Hamada, H. (2017). Cilia in left–right symmetry breaking. *Cold Spring Harbor Perspectives in Biology*, *9*(10), 1–10.
Shiratori, H. (2006). Conserved regulation and role of Pitx2 in situs-specific morphogenesis of visceral organs. *Development*, *133*(15), 3015–3025.
Shiratori, H., & Hamada, H. (2014). TGFβ signaling in establishing left-right asymmetry. Seminars in Cell and Developmental Biology, 32, 80–84.

Silva, D. M. N. (2017). The intermediate mesoderm, a new player in the establishment of organ laterality? (Master dissertation).
Simonneau, L., Kitagawa, M., Suzuki, S., & Thiery, J. P. (1995). Cadherin 11 expression marks the mesenchymal phenotype: Towards new functions for cadherins?? *Cell Communication and Adhesion*, *3*(2), 115–130.
Smith, D. J., Montenegro-Johnson, T. D., & Lopes, S. S. (2014). Organized chaos in Kupffer's vesicle: how a heterogeneous structure achieves consistent left-right patterning. *Bioarchitecture*, *4*(3), 119–125.
Stainier, D. Y. R., Kontarakis, Z., & Rossi, A. (2015). Making sense of anti-sense data. Developmental Cell, 32(1), 7–8.
Stainier, D. Y. R., Raz, E., Lawson, N. D., Ekker, S. C., Burdine, R. D., Eisen, J. S., … Moens, C. B. (2017). Guidelines for morpholino use in zebrafish. PLOS Genetics, 13(10), e1007000.
Staudt, D., & Stainier, D. (2012). Uncovering the Molecular and Cellular Mechanisms of Heart Development Using the Zebrafish. *Annual Review of Genetics*, *46*(1), 397–418.
Tabin, C. J., & Vogan, K. J. (2003). A two-cilia model for vertebrate left-right axis specification. *Genes and Development*, *17*(1), 1–6.
Tada, M., & Concha, M. L. (2001). Vertebrate gastrulation: Calcium waves orchestrate cell movements. Current Biology, 11(12), 470–472.
Takao, D., Nemoto, T., Abe, T., Kiyonari, H., Kajiura-Kobayashi, H., Shiratori, H., & Nonaka, S. (2013). Asymmetric distribution of dynamic calcium signals in the node of mouse embryo during left-right axis formation. Developmental Biology, 376(1), 23–30.
Talbot, J. C., & Amacher, S. L. (2014). A streamlined CRISPR pipeline to reliably generate zebrafish frameshifting alleles. *Zebrafish*, *11*(6), 583-585.Tanaka, Y., Okada, Y., & Hirokawa, N. (2005). FGF-induced vesicular release of Sonic hedgehog and retinoic acid in leftward nodal flow is critical for left-right determination. *Nature*, *435*(7039), 172–177.
Tavares, B., Jacinto, R., Sampaio, P., Pestana, S., Pinto, A., Vaz, A., … Lopes, S. S. (2017). Notch/Her12 signalling modulates, motile/immotile cilia ratio downstream of Foxj1a in zebrafish left-right organizer. *eLife*, *6*, e25165.
Tay, H. G., Schulze, S. K., Compagnon, J., Foley, F. C., Heisenberg, C.-P., Yost, H. J., … Amack, J. D. (2013). Lethal giant larvae 2 regulates development of the ciliated organ Kupffer's vesicle. *Development*, *140*(7), 1550–1559.
Tee, Y. H., Shemesh, T., Thiagarajan, V., Hariadi, R. F., Anderson, K. L., Page, C., … Bershadsky, A. D. (2015). Cellular chirality arising from the self-organization of the actin cytoskeleton. Nature Cell Biology, 17(4), 445–457. http://doi.org/10.1038/ncb3137Takeichi, M. (2014). Dynamic contacts: Rearranging adherens junctions to drive epithelial remodelling. Nature Reviews Molecular Cell Biology, 15(6), 397–410.
Vallin, J., Girault, J. M., Thiery, J. P., & Broders, F. (1998). Xenopus cadherin-11 is expressed in different populations of migrating neural crest cells. *Mechanisms of Development*, *75*(1–2), 171–174.
Vandenberg, L. N., & Levin, M. (2013). A unified model for left-right asymmetry? Comparison and synthesis of molecular models of embryonic laterality. Developmental Biology, 379(1), 1–15.
Viotti, M., Niu, L., Shi, S., & Hadjantonakis, A. (2012). Role of the Gut Endoderm in Relaying Left-Right Patterning in Mice, *10*(3).
Vouillot, L., Thélie, A., & Pollet, N. (2015). Comparison of T7E1 and Surveyor Mismatch Cleavage Assays to Detect Mutations Triggered by Engineered Nucleases. Genes| Genomes| Genetics, 5(3), 407–415.
Wallingford, J. B., Ewald, A. J., Harland, R. M., & Fraser, S. E. (2001). Calcium signaling during convergent extension in Xenopus. Current Biology, 11(9), 652–661.
Wan, L. Q., Ronaldson, K., Park, M., Taylor, G., Zhang, Y., Gimble, J. M., & Vunjak-Novakovic, G. (2011). Micropatterned mammalian cells exhibit phenotype-specific left-right asymmetry. Proceedings of the National Academy of Sciences, 108(30), 12295–12300.
Wang, T., Wei, J., Sabatini, D., & Lander, E. (2014). Genetic screens in human cells using the CRISPR/Cas9 system. Science, 343(6166), 80–84.
Wang, G., Manning, M. L., & Amack, J. D. (2012). Regional cell shape changes control form and function of Kupffer's vesicle in the zebrafish embryo. *Developmental Biology*, *370*(1), 52–62.

Wang, X., & Yost, H. J. (2008). Initiation and propagation of posterior to anterior (PA) waves in zebrafish left-right development. *Developmental Dynamics*, *237*(12), 3640–3647.
Warga, R. M., & Nüsslein-Volhard, C. (1999). Origin and development of the zebrafish endoderm. Development (Cambridge, England), 126(4), 827–838.
Webb, S. E., & Miller, A. L. (2007). Ca2+ signalling and early embryonic patterning during zebrafish development. Clinical and Experimental Pharmacology and Physiology, 34(9), 897–904.
Wei, C. J., Francis, R., Xu, X., & Lo, C. W. (2005). Connexin43 associated with an N-cadherin-containing multiprotein complex is required for gap junction formation in NIH3T3 cells. Journal of Biological Chemistry, 280(20), 19925–19936.
Weinberg, E. S., Allende, M. L., Kelly, C. S., Abdelhamid, a, Murakami, T., Andermann, P., … Riggleman, B. (1996). Developmental regulation of zebrafish MyoD in wild-type, no tail and spadetail embryos. Development (Cambridge, England), 122(1), 271–80. Retrieved from
Welsh, I. C., Thomsen, M., Gludish, D. W., Alfonso-parra, C., Bai, Y., & Martin, J. F. (2013). Article Integration of Left-Right Pitx2 Transcription and Wnt Signaling Drives Asymmetric Gut Morphogenesis via Daam2. *Developmental Cell*, *26*(6), 629–644.
Westerfield, M. The Zebrafish Book. A Guide for the Laboratory Use of Zebrafish (*Danio rerio*). University of Oregon Press, Eugene 4th Edition (2000).
Wingert, R. A., Selleck, R., Yu, J., Song, H. D., Chen, Z., Song, A., … Davidson, A. J. (2007). The cdx genes and retinoic acid control the positioning and segmentation of the zebrafish pronephros. PLoS Genetics, 3(10), 1922–1938.
Wu, X., Scott, D. A., Kriz, A. J., Chiu, A. C., Hsu, P. D., Dadon, D. B., … Sharp, P. A. (2015). HHS Public Access, 32(7), 670–676. http://doi.org/10.1038/nbt.2889.Genome-wideWang, G., Cadwallader, A. B., Jang, D. S., Tsang, M., Yost, H. J., & Amack, J. D. (2011). The Rho kinase Rock2b establishes anteroposterior asymmetry of the ciliated Kupffer's vesicle in zebrafish. *Development*, *138*(1), 45–54.
Yin, C., Kikuchi, K., Hochgreb, T., Poss, K. D., & Stainier, D. Y. R. (2010). Hand2 regulates extracellular matrix remodeling essential for gut-looping morphogenesis in zebrafish. *Developmental Cell*, *18*(6), 973–984.
Yoshiba, S., Shiratori, H., Kuo, I. Y., Kawasumi, A., Shinohara, K., Nonaka, S., ... & Nakai, J. (2012). Cilia at the node of mouse embryos sense fluid flow for left-right determination via Pkd2. *Science*, *338*(6104), 226-231.Yuan, S., Zhao, L., Brueckner, M., & Sun, Z. (2015). Intraciliary calcium oscillations initiate vertebrate left-right asymmetry. *Current Biology*, *25*(5), 556–567.
Zinski, J., Tajer, B., & Mullins, M. C. (2017). TGF- b Family Signaling in Early Vertebrate Development, 1–76.

Chapter 6 – Appendixes

1 - Solutions

25x Tricane (VF=1L)
- 2g Tricaine powder;
- 500mL milliQ Water;
- 10mL Tris 1M (pH 9);
- Adjust to pH 7.

Embryo medium 50x (VF=1L)
- 14,69g NaCl;
- 0,63g KCl;
- 2,43g CaCl2.2H2O;
- 4,07g MgSO4.7H2O;
- Up to 1L with osmosis reverse water.

Embryo medium 1x (VF=10L)
- 200mL 50X Embryo Medium;
- 1mL Methylene Blue Solution;
- Up to 10L with osmosis reverse water.

1x Tricane (VF=25mL)
- 24mL Embryo medium 1x;
- 1mL Tricane 25x.

PK (VF=1mL)
- 20mg PK;
- 1mL water.

Digestion buffer (VF=5mL)
- 125µL NaCl;
- 50µL EDTA;
- 50µL Tris;
- 0,25mL SDS;
- Up to 5mL with DNase-Free water.

20x SSC (VF=1L)
- 175.3g of NaCl;
- 88.23g of Tri-sodium citrate –dehydrate;
- In 800mL of distilled water;
- Adjust the pH to 7.0 with a few drops of 1M HCl;
- Adjust the volume to 1L with additional distilled water.

Pre-Hybridization Mix (VF=500mL)
- 250mL Formamide 100%;

- 125mL 20x SSC;
- 500µL Tween 20;
- 4,6 mL Citric Acid 1M (ajust to final pH 6.0);
- up to 500mL with milliQ water.

10x PBS (VF=2L)
- 160g NaCl;
- 4g KCl;
- 53,6g Na2HPO4-7H2O ;
- 4,8g KH2PO4;
- Adjust pH 7,4 with HCl;
- Up to 2L with milliQ water.

1x PBS (VF=1L)
- 100mL of PBS 10x;
- Adjust the volume to 900ml milliQ water.

4% PFA (VF=500mL)
- 50ml of PBS 1X;
- 20g of paraformaldehyde powder;
- Up to 500mL of PBS 1x.

2x SSC (VF=1L)
- 100mL 20x SSC;
- 900mL distilled water.

0,2x SSC (VF=1L)
- 10mL 20x SSC;
- 990mL distilled water.

Blocking solution for *in situ* (VF=10mL)
- 200µL sheep serum;
- 0.02g Bovine Serum Albumin (BSA);
- up to 10 mL with 0,1% PBT.

Staining Buffer (VF=50mL)
- 2,5mL Tris 2M pH 9,5;
- 1,25mL MgCl2 2M;
- 1mL NaCl 5M;
- 50µL Tween 20;
- up to 50mL with milliQ water.

NBT/BCIP (VF=10mL)
- 22,5µL NBT
- 35µL BCIP
- Staining buffer up to 10 mL

Blocking solution (VF=150mL)

- 1,5g BSA;
- 0,75mL Tween 20;
- 0,75mL Triton-X;
- 1,5mL Dimethyl sulfoxide (DMSO);
- Up to 150mL with 1x PBS.

Permeabilizant solution (VF=15mL)
- 0,075mL Tween 20;
- 0,075mL Triton-X;
- 0,11g Glycine;
- Up to 15mL with 1x PBS.

2% PFA (VF=20mL)
- 2,5mL 16% PFA
- 17,5mL 1x PBS

Dent's Fixative (VF=10mL)
- 8mL MetOH;
- 2mL DMSO.

TBS-T (VF=1L)
- 20mL TrisHCl 1M (pH 7.6);
- 27.5mL NaCl 5M;
- 1mL Tween 20;
- up to 1L milliQ water.

TBS (VF=1L)
- 20mL TrisHCl 1M (pH 7.6);
- 27.5mL NaCl 5M;
- up to 1L milliQ water.

50x TAE (VF=500mL)
- 121g TrisBase;
- 28,55mL Glacial acetic acid;
- 100mL EDTA 0,5M pH8;
- Up to 500mL with MilliQ water.

1x TAE (VF=2L)
- 40mL 50x TAE
- Up to 2L with milliQ water

Danieaus Solution (VF=1L)
- 11,5mL NaCl 5M
- 1,4mL KCl 0,5M
- 0,8mL $MgSO_4$ 0,5M
- 5mL HEPES 1M
- 1,2mL $Ca(NO_3)_2$ 0,5M
- H20 miliQ (up to 1L)

- Adjust to pH 7,6

CO2 independent medium complement with EDTA (VF=50 mL)
- 50 mL medium
- 500 µL 0,5M EDTA

2 –Supplementary Tables

Supplementary Table 1 – **List of tissues in which Cadherin-11 (transcript and protein) is known to be expressed during development in zebrafish.** ss – somite stage, hpf – hours post fertilization, Prim-5 – 24 hpf, Prim-15 – 30 hpf, Protruding-mouth – 72 hpf, Long pec- 48 hpf.

Organ/Tissue	**Developmental Stages**	**Reference**
Neural Keel, IM	5-ss	**[39]**
Mid brain, Diencephalon, otic vesicle, ventral neural tube, hindbrain, eye, tail bud	20-ss	
Cleithrum, pectoral fin bud proximal region	Prim-5 to Day 5	**[43]**
Inner ear	Prim-15	**[40]**
Otolith	Protruding-mouth	
Brain, inner ear, whole organism	Prim-5 to Adult	
Cranial nerve II, lens, optic tectum, optic vesicle, retinal, retinal ganglion cell	14-19-ss to Long pec	**[41]**
PN	Long pec	**[82]**

Supplementary Table 2 – **Primers used for PCR amplification**

Primer Name	**Sequence**	**Annealing Temperature**	**Product length**
Cdh_genot_Fw1	ACGTGGGAAATCAAATCCAGTGAGG	72°C	398bp
Cdh_genot_Rv1	GGGATCTGGGCCTGTGTACTCC	72°C	398bp
Cdh_genot_Fw2	GCCTGTGGACTTTGAGACTAAGCGA	72°C	334bp
Cdh_genot_Rv2	ACACTGCTGGACTGACAAGACAAA	72°C	334bp
Cdh_genot_Fw3	TACTGAATTTTCTTCTGTTGCTTTC	64,8°C	425bp
Cdh_genot_Rv3	AAAATAACTTCCCTCTGGTCTGGA	64,8°C	425bp
Dand5-Fw	CCGCAATCCTGACCCATAGCAA	72°C	200bp
Dand5-Rv	CTCCTCCGTTATGCGCTGTGTA	72°C	200bp

Supplementary Table 3 –Thermocycling protocol used for gRNA1, gRNA2 and Dand5 primer pairs

Cycle step	Temperature	Time	Cycles
Initial denaturation	98°C	30s	1
Denaturation	98 °C	7s	30
Annealing / Extension	72°C	15s	
Final extension	72°C	7 min	1
4°C		Hold	

Supplementary Table 4 –Thermocycling protocol used for gRNA3 primer pairs

Cycle step	Temperature	Time	Cycles
Initial denaturation	98°C	30s	1
Denaturation	98 °C	7s	30
Annealing	64,8°C	20s	
Extension	72°C	13s	
Final extension	72°C	7 min	1
4°C		Hold	

Supplementary Table 5 –Thermocycling protocol used for T7 Endonuclease assay

Step	Temperature	Time
Denaturation	95°C	5 min
Annealing	95 - 85 °C	-2 ºC/second
Annealing	85 - 25°C	-0.1 ºC/second
Hold	4°C	Hold

Supplementary Table 6 - Appropriate restriction enzyme and RNA polymerase for each probe.

Probe	Restriction Enzyme	Buffer	RNA polymerase	References
myl7	NotI (New England Biolabs, 10U/µL)	NEBuffer3.1	T3 (Roche Life Science)	L. Saúde's Laboratory
cdh11	HindIII (New England Biolabs, 20U/µL)	NEBuffer 2.1	T7	L. Saúde's Laboratory
cdh6	XhoI (Promega, 10U/µL)	BufferD	Sp6 (Roche Life Science)	S. Hans *et al* 2013

cdh17	NotI	NEBuffer3.1	Sp6	E. Butko *et al* 2015

3 - Supplementary figures

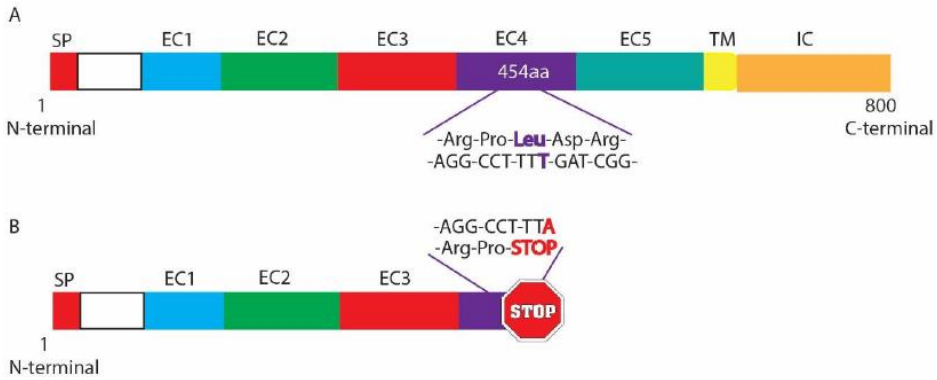

Supplementary Figure 1 - *cdh11* mutant line. A - WT Cdh11 protein structure, the 455th aa is a Leucine (Leu); B - Mutant Cdh11 truncated protein structure, with premature STOP codon. SP - signal peptide; EC1-5 - Extracellular Domain 1-5; TM - Transmembrane Domain; IC- Intracellular domain

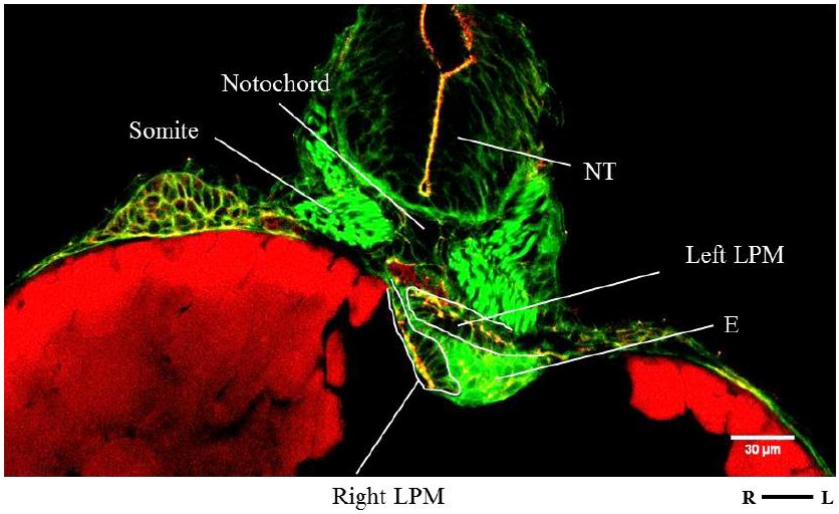

Supplementary Figure 2 – **Does the PN provide a stable structure for the asymmetric migration of the underlying LPM? - Protocol optimization.** Confocal Laser point-scanning image from Tg(*sox17*:EGFP) 20µm sections immunostained for ZO-1 (in red) and phalloidin 488 (in green) using 20x magnification. (scale – 30µm). LPM – lateral plate mesoderm, NT – neural tube, E – endoderm, L- left, R – Right.

Supplementary Figure 3 – **WT embryo injected with *cdh11*^{MO} in later assays**. Example of the side-effects caused on the embyos after injecting with the *cdh11*^{MO}, suggesting that it was no longer suitable for experiments.

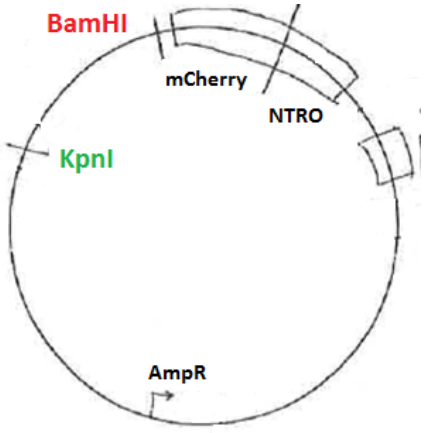

Supplementary Figure 4 - Representation of the Osx:mCherry-NTRO plasmid (Renn and Winkler 2008) with the localization of the restriction sites for the enzymes used in this investigation

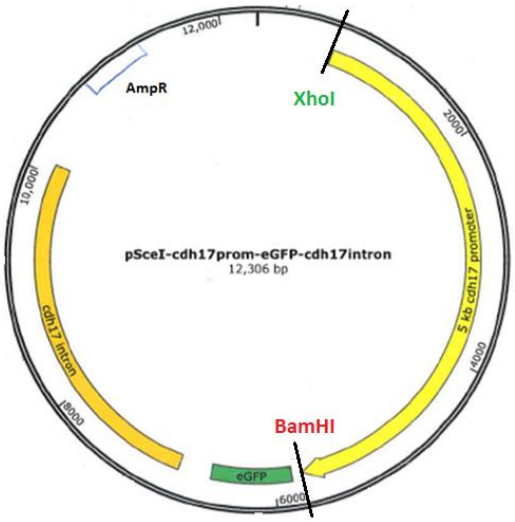

Supplementary Figure 5 – Representation of the pSceI-cdh17prom-eGFP-cdh17intron plasmid (Sanker 2013) with the localization of the restriction sites for the enzymes used in this investigation

Sequences recognized by the primers
Sequences targeted by the CRISPR
intronic regions
EXONIC REGIONS

A

acgtgggaaatcaaatccagtgaggtctcatcttgtccccattgacctctttagagaccgaaccattcagaggacgccctttgaaggattcctcctgga
ccttgatactcaccggaggggtgtgaacaggaaggtccagaggaagtggacagtttggcaggATGTGGGAGGGACTGAGATT
GCA**GGTGTTCTTCTTGTGTTTGG**GGGCTGCACTATGGAGTGCTGCAGCGGCAGCAACAC
ACAGGGGCTCAGGTCCACGGGAGCGTGGCCACCGGCGACATCTTTCTTTGCACAGACACA
GAGAGAGAGGCAAAGAGGGCCAGGTGCTTCACCGCTCCAAAAGAGGATGGGTCTGGAAC
CAGTTCTTTGTCATTGAGGAGTACACAGGCCCAGATCCC

B

gCCTGTGGACTTTGAGACTAAGCGATCGTACACACTCAAAGTAGAAGCCACCAACACACA
CGTGGACCC**ACGTTTCATCGCCTGGGGTC**CGTACAAAGATACAACCATTGTGAAAATAT
CAGTAGAAGATGCAGATGAGCCCCCGACCTTTATGGCTCCCAGCTACAACTTCGAGGTGG
AGGAAAACGCCCCAGCAGGCACACTGGTCGGCCGTGTGCATGCCAAAGACACCGACATG
ATGAACAACCCCATCAGgtagagtctgcttcctccaaaaatcatcagatctcatttgcatgggctgttttgttttgtcttgtcagtccagca
gtgt

C

tactgaattttcttctgttgctttcacagACAGCACTGCTAGCATCTTTGTGATCCGGAAGGGCTTCAGCAGA
ATGACCCAGGATATCTACCACCTTCCCATTGAGATCAATGACAACGGCGTACCCCCGATG
AGCAGCACCAATACCCTCATAATCCGCGTGTGTAGCTGCGACAGTAAAGACACCATCCTC
TCCTGCAACGTGGAGCCTTTCATCTTGACGGCTGGGCTTAGCACCGGAGCTCTGATTGCC
ATCTTGGCTTGCATTGTTATTCTACTGGgtgagcctaattatatttgtataagaatatacaagcagccatgtgtaaataatagg
ggtctagctcggttggtttaaacatcctatagggagccaaagcatgtcaatatttgcatttcactccagaccagagggaagttatttt
Primer – Sequence distance: 180/176 bp

Supplementary Figure 6 – **gRNA amplification primer pairs**.
A – Primer pair for gRNA1 (Site 1). Amplicon length: 298bp. Primer-Sequence distance: 159/172 bp. **B** - Primer pair for gRNA2 (Site 2). Amplicon length: 334bp. Primer-Sequence distance: 44/221 bp. **C** - Primer pair for gRNA3 (Site 3). Amplicon length: 425bp. Primer-Sequence distance: 180/176 bp

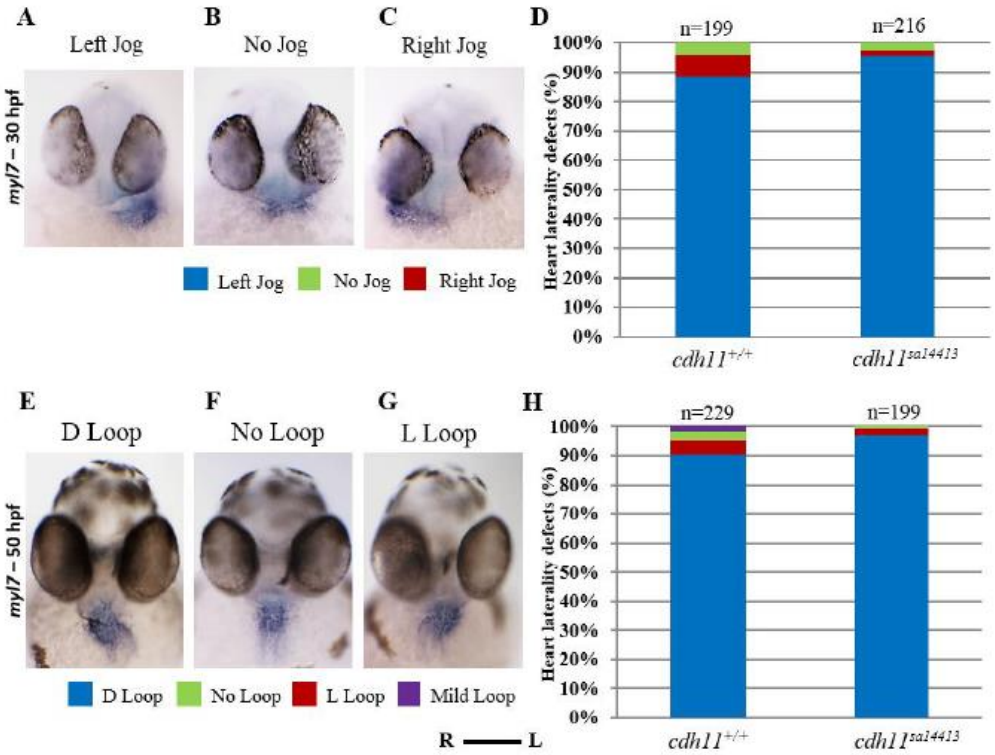

Supplementary Figure 7 – ***cdh11*^{sa14413} embryos do not exhibit heart jog or loop phenotype observed in morphants.** Ventral view of a *cdh11*+/+ or *cdh11*^{sa14413} embryos at 30 hpf (**A to C**) and at 50 hpf (**E to G**) after *WISH* for *myl7* (**A-** embryo with a WT conformation (Left Jog); **B-** Embryo with a centered heart (No Jog); **C-** embryo with inverted heart (Right Jog); **E-** embryo with a WT conformation (D Loop); **F-** Embryo with no heart Loop; **G-** embryo with L Loop; **D-** Percentages of Left Jog (blue), Right Jog (red) and No Jog (green) and in *cdh11*+/+ (n=199) and *cdh11*^{sa14413} (n=216) embryos. **H –** Quantifications of D Loop (blue), L Loop (red), No Loop (green) and Mild Loop (purple) in *cdh11*+/+ (n=229) and *cdh11*^{sa14413} (n=199) embryos. R-Right, L-Left. Taken from Dalila 2017

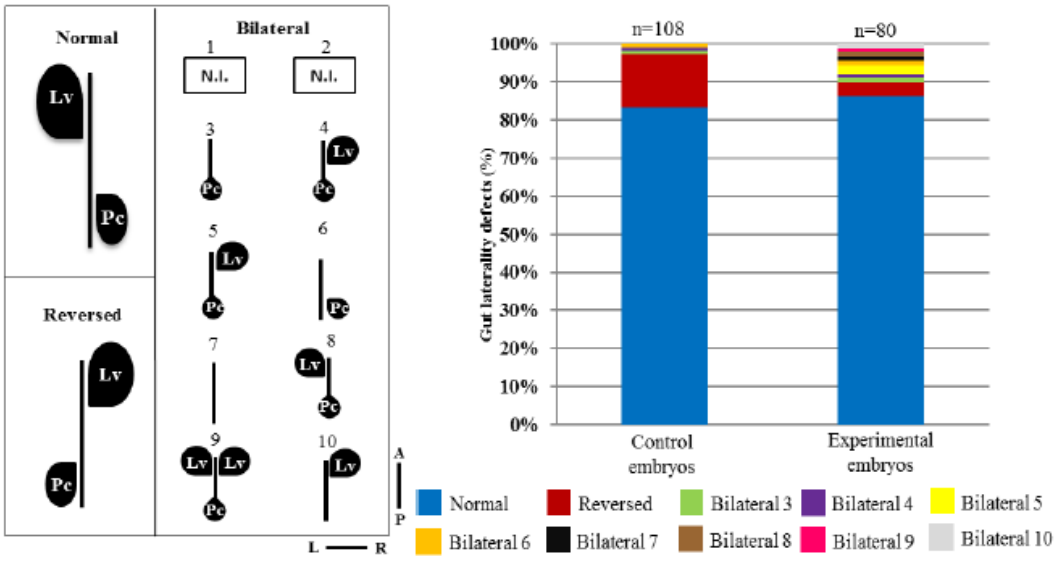

Supplementary Figure 8 – **Liver and pancreas placed in the normal configuration in Cdh11 mutants at 50 hpf.** Schematic representation of normal gut loop (Normal) and nine gut laterality

defects observed (Reversed, Bilateral 3, 4, 5, 7, 8, 9 and 10); Percentages of control (n=108) and experimental (n=80) embryos analyzed live at 50 hpf with normal (blue), reversed (red), bilateral 3 (green), bilateral 4 (purple), bilateral 5 (yellow), bilateral 6 (orange), bilateral 7 (black), bilateral 8 (Brown), bilateral 9 (pink) and bilateral 10 (gray). Blue arrow – progeny; Orange arrow- Sequencing results, green arrow- GFP Selecting GFP, yellow box- control embryos, purple box- experimental embryos, A– Anterior, P- Posterior, L- Left, R- Right, Lv- Liver, Pc- Pancreas, N.I.- Non identified. Taken from Dalila 2017

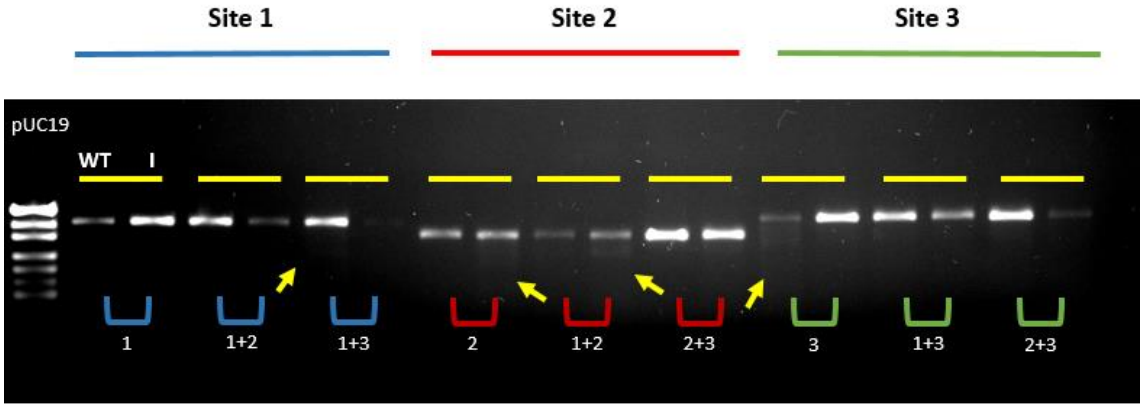

Supplementary Figure 9 – Level of gene modification after injection with different combinations of cdh11 gRNA. T7 Endonuclease assay was performed after injection of Cas9 protein with the following gRNA combinations: gRNAs 1, 2 and 3 individually, and gRNAs 1+2, 1+3, 2+3 (see Table 1). Each gRNA binding site was amplified using the corresponding pair of primers (Supplementary figure 6). Yellow arrows indicate digested fragments in the sample.